ALPHA FOUNDATION FOR THE IMPROVEMENT OF MINE SAFETY AND HEALTH

Final Technical Report

Project Title: Mine-Specific, Geology-Dependent Pillar and Standing-Support Design Tools

Grant Number: AFC719FO-101

Organization: West Virginia University, Morgantown, WV
886 Chestnut Ridge Road, PO Box 6845
Morgantown, WV 26506-6845

Principal Investigator: Ihsan (Berk) Tulu, Ph.D. (ME)
Phone: 304-293-3883, E-mail: itulu@mail.wvu.edu

Graduate Students: Deniz Tuncay, Ph.D.
Haochen Zhao, Ph.D.

Period of Performance: September 1, 2020 – April 30, 2023

1.0 Executive Summary:

Problem statement: In underground coal mines, pillar load, deformation and local ground response of the entries are affected by the local geology, in situ stress state and operational parameters of the mine, and can change drastically from one coal basin to another, or even within the same mine. Design software developed by the National Institute for Occupational Safety and Health (NIOSH) for global pillar stability, Analysis of Longwall Pillar Stability (ALPS) and Analysis of Retreat Mine Pillar Stability (ARMPS), and for local entry stability, the Support Technology Optimization Program (STOP), have improved the design of stable pillar layouts and successful standing support systems. These design tools have effectively incorporated the influence of operational parameters into the design. However, the mine-specific mechanical response of the rockmass due to the mine-specific geology is not included in the NIOSH design software.

Despite major progress in reducing ground control related fatalities and injuries between 2011 and 2019, fall of ground incidents still accounted for almost 30% of the occupational fatalities in underground coal mines (MSHA, 2020). Out of these ground control related fatal accidents, 25% of them were in longwall mines. Also, for fatalities related to ground control, 80% of them have occurred in areas with roof support (Sears et al., 2019). These statistics highlight the potential safety impact of fall of ground on underground coal miners.

Research approach: Safety in underground coal mines would be improved by enhancing ground control design software by incorporating mine-specific, geology-dependent, mechanical rockmass response into pillar and support design tools. This project developed a geology-dependent mechanical loading models to improve pillar design, and a geology-dependent Ground Reaction Curve (GRC) approach to improve longwall gateroad support design. The research accomplished in this project includes: (i) The development of a mine-specific, geology-dependent global loading model that can be applied to ALPS, ARMPS, and ARMPS-LAM approached. (ii) The development of a script program (beta version of ALPS-LAM) that runs LaModel program with ALPS input. (iii) The development of geology-dependent GRC design approach.

Accomplishments: During this research study, first, a new global loading model that is a function of the strength of overburden layers, thicknesses of strong beds, relative locations of the strong beds in the overburden, and the panel width and overburden depth was developed, and it was verified with field measurement case studies. This new method can be implemented into the Mine Safety and Health Administration (MSHA) recommended pillar design tools: LaModel, ALPS, ARMS and ARMPS-LAM, and a new script program version of ALPS-LAM that was developed in this research. In addition, in this research, to extend the GRC database and develop local geology and stress-dependent GRC for various geological and operational conditions, an entry-scale modeling methodology was developed for STOP.

Expected impact on mining health and safety: The practical design tool and methods developed during this research are immediately available to the mining industry, Mine Safety and Health Administration (MSHA) and National Institute for Occupational Safety and Health (NIOSH) to evaluate and consider for application in ground control analysis process. The research presented in this report has produced a number of practical outputs that would raise the quality of mine design in the United States in the future, particularly for deep cover, pillar retreat and longwall mines.

2.0 Problem Statement and Objective:

<u>The Research Focus Area</u>

The goal of this research is to reduce the exposure of underground coal mine workers to fall of ground through the (i) development and integration of mine-specific, geology-dependent global overburden loading model into the practical design tools, (ii) improvement of the longwall gateroad pillar design by incorporating the laminated overburden model in ALPS program, and (iii) development of local geology-dependent Ground Reaction Curve (GRC) approach and integration of this approach into the NIOSH design tool STOP. This project focused on the underground coal mining industry and addresses the Alpha Foundation Research Topical Area "*Health and Safety Interventions*" with a specific emphasis on "*prevention of unstable ground conditions that result in collapses and roof/rib falls*." *This work is directly relevant to Alpha Foundation Priority Area "Ground Control - Prevention of unstable ground conditions that result in collapses; roof and rib falls; and injuries due to insufficient support coverage.*"

<u>The Problem Statement</u>

In 2019, approximately 38% of the total coal production in the United States was by underground mining (MSHA, 2020a) and 60% of the underground coal production was performed by longwall coal mines. In underground coal mines, ground control plays a significant role in the safety of the operations, especially in high-extraction retreat mines (i.e., longwall and retreat room-and-pillar mines) due to higher mining-induced load concentrations in the vicinity of the gobs. Between 2011 and 2019, fall-of-ground incidents caused almost 30% of the occupational fatalities in underground coal mines, second only to fatalities caused by powered haulage (MSHA 2020b). Of these ground-control-related fatal accidents, 25% of them were in longwall mines. Also, for fatalities related to ground control in longwall mines, 80% of them have occurred even when there was roof support (Sears et al., 2019).

Design software developed by the NIOSH for global pillar stability, ALPS and ARMPS, and for local entry stability, STOP, have improved the design of stable pillar layouts and successful standing support systems. These design tools have successfully incorporated the influence of operational parameters into the design. However, the mine-specific mechanical response of the rockmass due to the mine-specific geology is not included in the NIOSH design software.

<u>Background</u>

<u>*Global Loading and pillar stability*</u>

Mining-induced stresses in underground coal mines play a significant role in pillar and support design, hence in the safety of mining operations. In the U.S., the Analysis of Coal Pillar Stability (ACPS) software is the most current tool used for designing longwall coal mine layouts (Mark and Agioutantis, 2019). ACPS software is the new pillar design software that integrates all three of its predecessor software applications namely Analysis of Longwall Pillar Stability (ALPS), Analysis of Retreat Mining Pillar Stability (ARMPS), and the Analysis of Multiple Seam Stability (AMSS) (Mark, 1992; Mark and Chase, 1997; Mark et al., 2007). The programs use "tributary area theory" or "pressure arch theory" for estimating development loads and the "abutment angle" concept together with the square decay stress distribution function to estimate the magnitude and distribution of the mining-induced loads. These design tools have successfully incorporated the influence of operational parameters into the design. In addition to panel width and overburden depth, site-specific overburden geology is known to have a considerable impact on the extent and magnitude of the abutment loads, although the pressure arch loading approach implemented in ARMPS2010 indirectly accounts for the generally stiffer overburden response of narrow and deep panels, it does not include the effect of mine-specific geology on the mechanics of the overburden (Mark, 2010).

The impact of overburden geology on surface subsidence has also been proven by various case studies and is included in different subsidence prediction tools such as the Comprehensive and Integrated Subsidence Prediction Model for Multiple Seam Mining (CISPM-MS) developed at West Virginia University (Luo and Qiu, 2012) and the Surface Deformation Prediction System (SDPS) software developed at Virginia Polytechnic Institute (Karmis et al., 1989; Agioutantis and Karmis, 2017). It can be reasoned that if overburden geology affects surface subsidence, then pillar stresses and deformations are also affected. Studies showed that while being mostly accurate for shallow mines, empirical methods have been less effective at estimating loads for deeper cover mines (Tulu and Heasley, 2012; Hill et al., 2015; Tuncay et al., 2020). These studies aimed to better estimate abutment loads for deeper cover mines by modifying the abutment angle calculation method to match the field measurements.

Past and recent research has suggested that very little attention is being paid to the effect of mine-specific overburden mechanics such as overburden stiffness and geology on pillar loads. A recent Alpha Foundation research project, AFC719-15, studied the effect of specific geology on pillar loads and concluded that the representation of the overburden with a simple factors like hard rock percentage (HR) resulted in similar overburden stiffnesses in the field cases from different coal regions and, due to this similarity, a statistically significant correlation between HR percentage and overburden loading is hard to be found. The mechanical response of the overburden strata for the case study mines was studied by the ground reaction curve (GRC) approach, and the results of GRC analysis indicated that quantifying the average strength and stiffness of the overburden needs to include, not only the thickness of the strong beds, but also the relative location of the strong bed in the overburden and the width of the panel.

Gateroad entry support

Longwall gateroad support systems are required to control the strata around the entry for maintaining safe access to the longwall face, provide a secondary escape way, and prevent any disruption to ventilation. Esterhuizen et al. (2021) stated that at present, gateroad support systems are designed based on historical experience in similar geological and operational settings and standing support selection usually facilitated by using the Support Technology Optimization Program (STOP) developed by Barczak (2000). Generally, a gateroad support system consists of the combination of the following support elements: primary bolts, secondary bolts (cable bolts), standing supports, rib bolts, truss bolts and strap and/or mesh. There are many research and case study papers published on the design and application of gateroad support systems in the US longwall mines, and the great majority of these papers were published in the International Conference on Ground Control in Mining (Peng, 2008). A full discussion of these publications isn't in the scope of this report, but a summary is provided that highlights the strengths and deficiencies of the current three practical design tools: 1) Analysis of Mine Roof Support (AMRS) developed by Mark et al. (2020), 2) gateroad support design tool developed by Esterhuizen et al., (2021) and 3) STOP developed by Barczak (2020).

AMRS is an empirical design methodology that starts by defining three modes of roof support based on the roof strength relative to the stress level (Mark et al., 2020). They defined that in suspension mode, roof bolts mainly provide skin control for strong roof geologies; in beam building mode, roof bolts alone can support moderate strength roof and in supplemental support mode, secondary (supplemental) supports are required to support the roof. Mark et al. (2020) used a large database of roof fall histories to estimate the boundaries of these three regimes based on Coal Mine Roof Rating (CMRR) and the depth of cover.

AMRS program provides a suggested primary roof support rating (PSUP) based on the successful and unsuccessful case histories, overburden depth and CMRR. Mark et al. (2020) stated that PSUP is a rough measure of the amount of steel installed in the roof and doesn't consider the type of bolt. PSUP rating can be used to assess the stability of the roof strata for suspension and beam building modes. For the supplemental support design (cable bolts, standing supports and etc.), program calculates the estimated weight of the detached roof and compared this with the total support capacity provided only by secondary support system, by calculating a safety factor. Again, program doesn't differentiate difference between the different type of standing supports or cable bolts. Furthermore, it is noted by that the support design does not consider failures above the bolted anchorage zone or the stiffness of the support. Finally, ARMS is suitable for development loading conditions and doesn't consider the influence of elevated stress conditions due to retreat mining in longwall mines.

Esterhuizen et al. (2020, 2021) recently developed a new procedure for assessing longwall gateroad ground response and stability. In this method, a conceptual model was developed by using the results of six field monitoring cases and numerical analysis of these cases. The conceptual model was used for developing a set of equations from the multivariable statistical analysis of the results from parametric studies with more than 2000 combination of parameters from calibrated numerical models.

Esterhuizen et al. (2021) stated that conceptual model was developed on the premise that the support system is required to control the detached roof strata that would collapse in the absence of any support. The conceptual model subdivides the roof strata into three categories: (i) intact strata that are not damaged by mining-induced stresses, (ii) failing strata that have been loaded beyond their peak strength, but have sufficient strength to remain self-supporting, and (iii) detached strata that would collapse in the absence of support (Esterhuizen et al., 2021). The set of equations used to assess the gateroad response and roof strata stability are relatively complex, but as a summary, this approach estimates the mining-induced roof sag and uses it as the main indicator of roof stability. The effect of primary bolting system and cable bolts on roof sag is estimated in the similar way to ARMS method. The standing support impact on roof sag is determined from a parameter called work capacity of the standing support system. Esterhuizen et al. defined the work capacity as the average work per cm of compression when compressing a standing support by 30 cm, and they state that this parameter allows for the peak and post-peak yield capacity of the support system to be considered. This approach can include the important factors like effect of geology and mining-induced stresses to the design explicitly, and account for the additional factors: bar failure, anchor failure and failures above the bolted anchorage zone that ARMS cannot account into the design. Esterhuizen et al. (2020) indicated that ground response curve (GRC) can be estimated from this method, but since the method only estimates the roof sag, floor heave must be assumed as a function of the roof sag. They then acknowledge that the STOP program can be used to evaluate the alternatives of the standing support systems.

Ground reaction curve (GRC) approach is one of the available design options in the Support Technology Optimization Program (STOP) developed by Barczak (2000) and has improved the tailgate/bleeder support design by facilitating the selection of the most effective of the available standing support systems. STOP is also used extensively by MSHA in the approval of new support applications. There are several loading design options in STOP but the most powerful is the Ground Reaction Curve (GRC) option. Although this option is available, the program is lacking ground reaction curve specifications for various mine geologies and stress conditions.

Specific Aims and Research Objectives

West Virginia University (WVU) Mining Engineering researchers performed a two-year study to develop a practical method to include the effect of overburden geology to estimated mining induced overburden load redistribution, the beta version of the ALPS-LAM program, and a local geology and stress-dependent GRC methodology for various geological and operational conditions. The following research specific aims and research objectives were undertaken:

Specific Aim 1: Develop a mine-specific, geology-dependent global loading model.

- *Research Objective 1.1:* To build a statistical model for estimating mining induced loading, and calibrating structural inputs for the laminated overburden model from mine-specific geology, in situ stress and operational parameters.
- *Research Objective 1.2:* To refine geology-dependent loading model for accurate 3D load concentration near the tailgate corner and Active Mining Zone (AMZ).

Specific Aim 2: Adapting practical mechanics-based design tool for longwall pillar design.

- *Research Objective 2.1:* To program and verify laminated overburden model longwall pillar stability approach.

Specific Aim 3: Develop a local geology-dependent GRC design option for STOP.

- *Research Objective 3.1:* To develop a suite of representative local geology-dependent ground reaction curves.

3.0 Research Approach:

The goal of the research is to improve safety in the underground coal mining industry through the (i) development of a practical mine-specific, geology-dependent global overburden loading model, (ii) improvement of the longwall gateroad pillar design by incorporating the laminated overburden model into the ALPS program, and (iii) development of local geology-dependent Ground Reaction Curve (GRC) approach and integration of this approach into the NIOSH design tool STOP. The following research specific aims were undertaken to achieve the research goal:

<u>Specific Aim 1:</u> Develop a mine-specific, geology-dependent global loading model.

In this section of the report, we describe the development of the mine-specific, geology-dependent, global loading model. In this research, to include the effect of geology in the overburden load estimations, a new parameter was defined as the *total strong layer thickness* (t_{str}) that represents the strength and stiffness of the overburden with a single value. This parameter is a function of the strength of overburden layers, thicknesses of strong beds, relative locations of the strong beds in the overburden, and the panel width and overburden depth. In this study, to develop a site-specific t_{str}, 13 field measurement case studies from 12 different U.S. longwall mines with different overburden geologies were used. Numerical models of the case studies were verified against the field measurements such as surface subsidence, and stress. After verifying the numerical models, parametric studies were performed to be able to assess the influence of panel dimensions on mining-induced stresses and to simulate different panel conditions such as critical, subcritical, and supercritical. Overburden stress redistribution on the pillar system, gob, and adjacent solid coal was estimated from the modeling results. Using these results, a regression analysis was conducted for a loading model with the t_{str} as a variable, and a method to estimate the percentages of loads carried by the gob was constructed.

<u>Research Objective 1.1:</u> To build a statistical model for estimating mining induced loading, and calibrating structural inputs for the laminated overburden model from mine-specific geology, in situ stress and operational parameters.

Task 1.1.1: *Database development.*

The database development task in this research consisted of gathering information on various field monitoring cases from mines operating in different physiographic provinces and geological formations. A database of 13 case studies from 12 different U.S. longwall mines was put together with information on overburden geology and with subsidence or stress measurements to verify the models. Detailed geologic core logs were available for all the mines. Figure 3.1 shows the generalized stratigraphic columns of the case study sites where adjacent thin layers of the same rock types were combined for easier representation. Table 3.1 shows a summary of the cases. The codes given to different mines (NA, CA, BW, W) represent different regions and basins the mines are located: Northern Appalachian, Central Appalachian, Black Warrior, and Western, respectively. Details of the database can be found in Tuncay (2021).

Table 3.1. *Summary of case study mines (Tuncay, 2021).*

Case	Seam Name	Seam Height	In situ Stress Region	Panel Width / Depth
NA-1	Pittsburgh	6.5 ft	Eastern U.S., Northern Appalachia	2.08
NA-2	Pittsburgh	7.5 ft	Eastern U.S., Northern Appalachia	1.67
NA-3	Middle Kittanning	7.0 ft	Eastern U.S., Northern Appalachia	2.27
NA-4	Lower Kittanning	7.0 ft	Eastern U.S., Northern Appalachia	0.91
NA-5	Pittsburgh	7.0 ft	Eastern U.S., Northern Appalachia	0.82
NA-6	Pittsburgh	6.5 ft	Eastern U.S., Northern Appalachia	1.45
CA-1	Pocahontas No.3	6.6 ft	Eastern U.S., Central App.	Case a: 0.34 Case b: 0.55
CA-2	Pocahontas No.3	4.2 ft	Eastern U.S., Central App.	1.64
CA-3	Pocahontas No.3	5.5 ft	Eastern U.S., Central App.	0.29
BW-1	Blue Creek.	7.9 ft	Eastern U.S., Eastern Mid-Continent	0.69
W-1	Hiawatha	8.0 ft	Western U.S. (Utah)	0.41
W-2	D coal seam	8.0 ft	Western U.S. (Colorado)	0.42

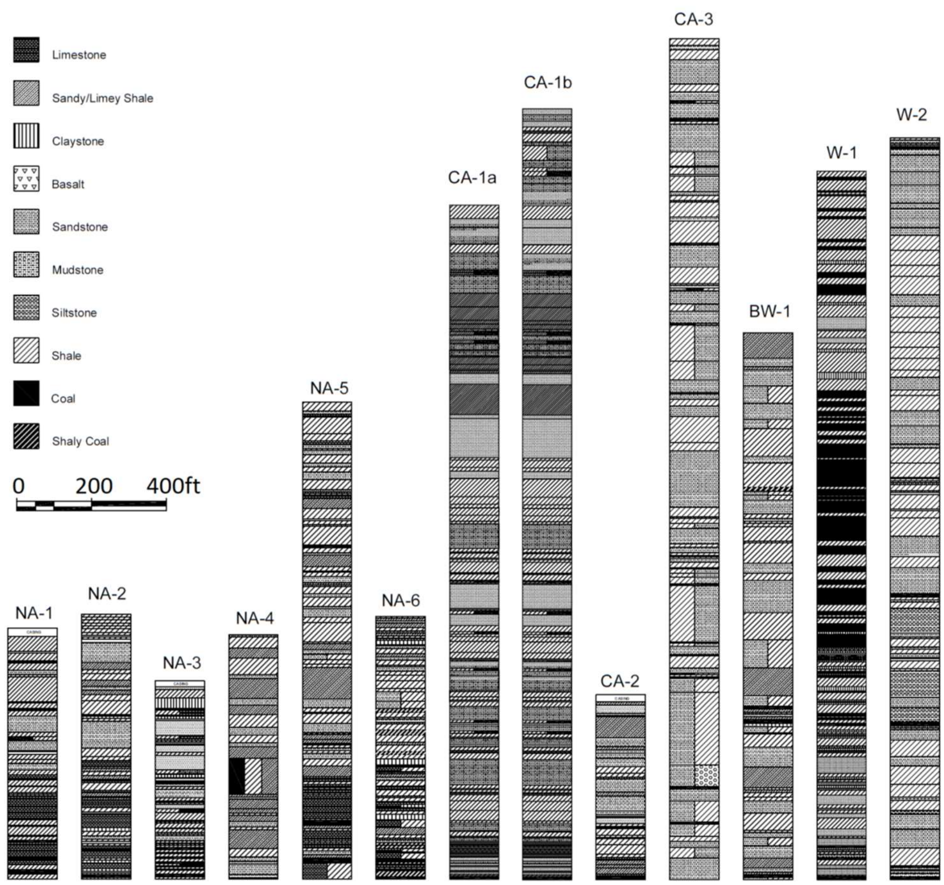

Figure 3.1. *Generalized stratigraphic column representation of the case study mines (Tuncay, 2021).*

Task 1.1.2: *Analysis of the database with the Finite Volume Modelling methodology*

For each case study, FLAC3D models were constructed and analyzed for a two-dimensional cross-section of the instrumented location of the mine. The overburden model for each mine was developed from actual stratigraphy, using all the geological layers with a minimum layer thickness of 1 ft, from a core hole near the instrumentation sites. The element sizes were selected as 3.28 ft (1 m) in x- and y-direction. The element sizes in z-direction were selected based on the layer thicknesses, keeping them less than 3.28 ft. The boundaries of the models were selected to be at least three times the depth on both sides of the outer panels. The side boundaries of the models were fixed on x- and y-directions and free on z-direction. Figure 3.2 visualizes the model geometry. Selection of the material model parameters can be found in the following publications: Esterhuizen et al. (2010), Tulu et al. (2017, 2018), Tuncay et al. (2021, 2022) and Tuncay (2021).

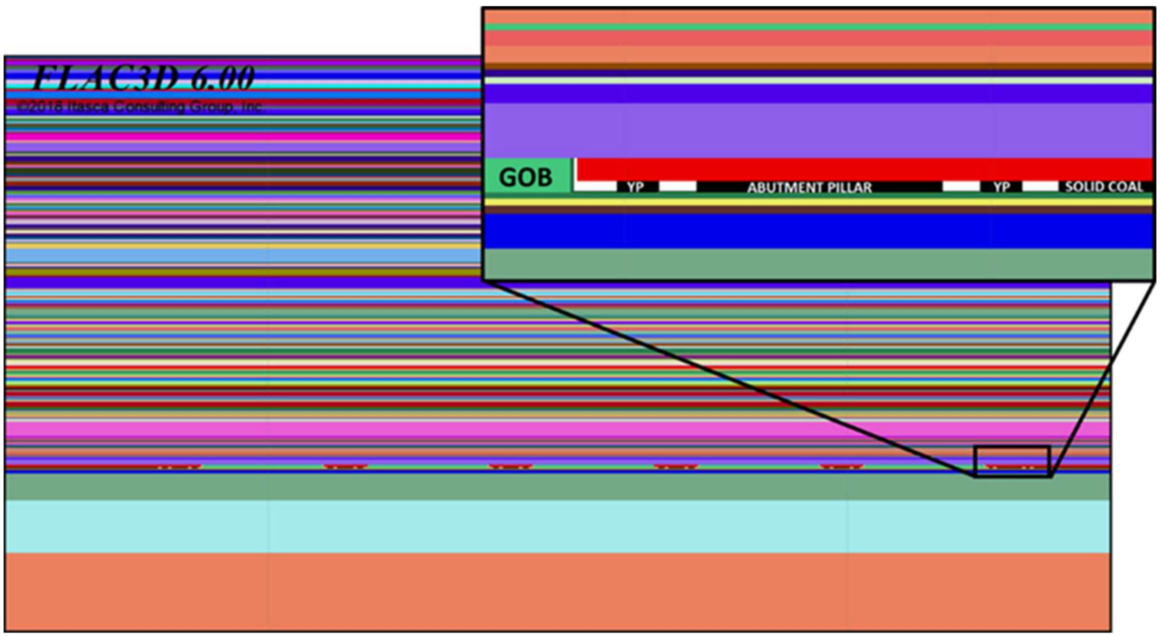

Figure 3.2. *Model geometry of a longwall mine with five consecutive panels (Tuncay, 2021).*

Each model was solved in successive loading stages, simulating different panels' mining relative to the instrumented site. For all the cases, the first stage was simply the development-mining scenario when all the model entries were mined, followed by the complete mining of consecutive panels on the next steps. The total number of panels to be mined for the consecutive panel models was determined uniquely for each case to simulate the influence of the consecutive panel mining on instrumented sections. The active panel represents the last panel being mined for each modeling step and the previous panel is the one before that. The shallow mines were modeled as one or two consecutive panel mining, whereas the deeper case studies were modeled with up to five consecutive panels to analyze the effect of the sub-critical loading condition on consecutive panels.

After each case study mine model was solved, stresses and displacements computed at the instrument locations were queried and compared with the field monitoring results for model verification. For cases where detailed measurements were not available, estimates about maximum subsidence and/or subsidence profiles obtained from SDPS and CISPM-MS were used (Luo, 1989; Luo and Qiu, 2012; Karmis et al., 1989; Agioutantis and Karmis, 2017). These empirical subsidence estimation tools are proven to be successful in predicting subsidence profiles for mines in the Appalachian region, where several cases in their database are located. Figure 3.3 shows the comparison of the surface subsidence results obtained from the models to the field measurements for case study mines: NA-1, NA-2, NA-3, NA-4, NA-6, and W-1. For mine NA-2 (Figure 3.3b), results from the empirical prediction tool, CISPM-MS, were used for the verification. For mine CA-2, the maximum possible subsidence value was compared with the results obtained from the model. The model approximated the maximum subsidence on the CA-2 mine panel to be 1.99 ft compared to the reported value of 2.04 ft. Numerical models for the mines NA-5, CA-1, and BW-1 were verified by the field measurements collected by NIOSH researchers. The results obtained from the study have been included in the publications (Klemetti et al., 2019a, 2019b; Van Dyke et al. 2020; Tuncay, 2021; Tuncay et al., 2022).

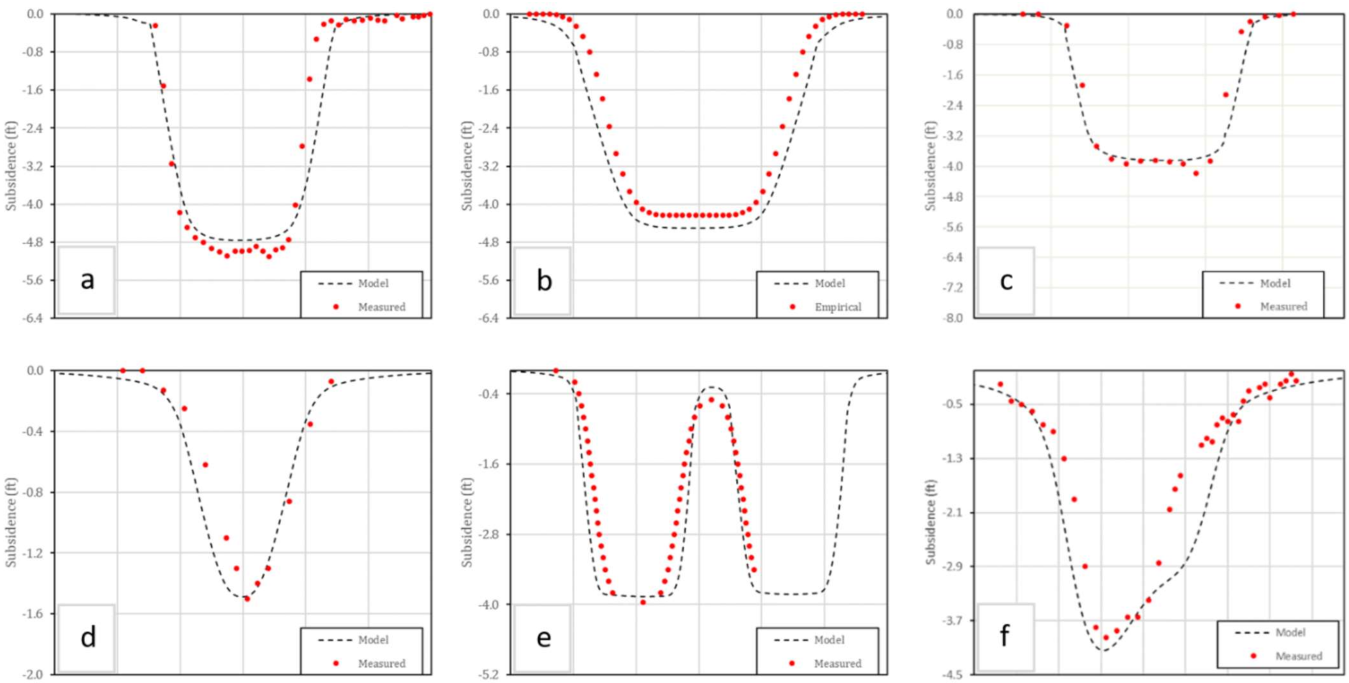

Figure 3.3. *Subsidence profiles obtained from the models compared to the field measurements for (a) Mine NA-1 (b) Mine NA-2 (c) Mine NA-3 (d) Mine NA-4 (e) Mine NA-6 (f) Mine W-1 (Tuncay, 2021).*

Following the verification of the models with field information, each case was re-run with different panel dimensions, keeping the overburden geology unchanged. The panel dimensions for the parametric runs were selected to test varying panel width-to-depth ratios, ideally sub-critical, critical, and super-critical. At least two additional parametric runs were conducted even when sub or super-critical conditions could not be achieved with plausible panel widths. Details of the model verification and parametric runs can be found in Tuncay (2021).

Every model run, including the parametric runs, was initially analyzed in terms of single panel abutment loading. The total abutment load percentages were calculated for each case. For the original cases with multi-panel runs, detailed analysis including mining-induced loads on the chain pillars and the solid coal of the next panel together with the gob loads were determined.

Using the 2D models; only the development, bleeder, and isolated loads can be simulated and estimated since the other loading conditions require a 3D model to simulate different locations of the panel face. For comparable abutment loads for various case studies, dimensionless (normalized) loads were calculated for analysis rather than absolute loads. The percentages of the total panel load transferred to the abutments and carried by the gob were determined using the method shown in Figure 3.4.

The normalized load percentages represent the ratio of the load (side abutment, inter-panel gateroad, or gob) to the single panel tributary area load (TAL). The percentages sum up to 200% in the case of the two-panel model, since it is the ratio of the total transferred load (2×TAL) to the single panel tributary area load (TAL).

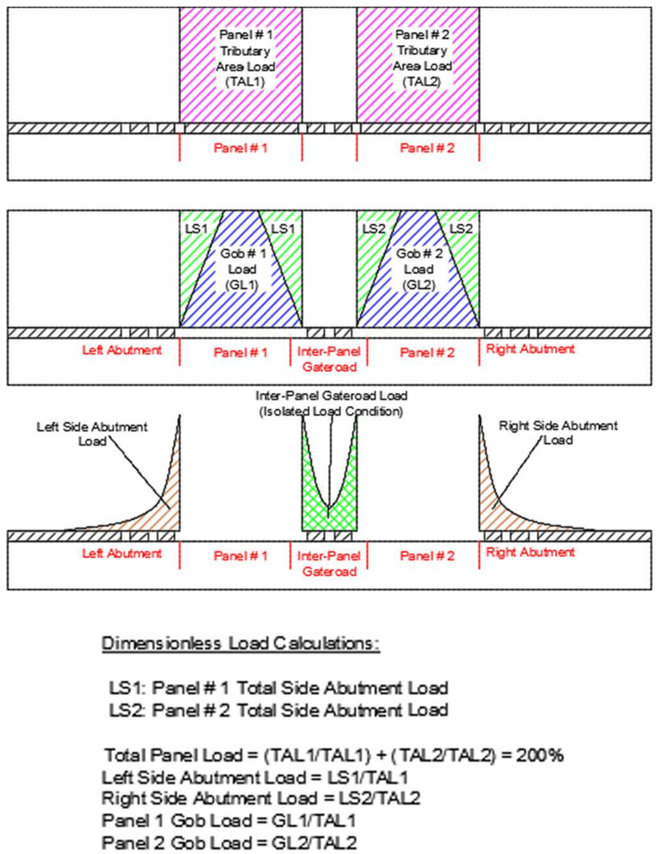

Figure 3.4. *Dimensionless (normalized) overburden load calculation for analyzing mining-induced loads for a two-panel model (Tuncay et al., 2021).*

Task 1.1.3: *Development of overburden Hard Rock Influence Factor (HRIF).*

To include the effect of geology in statistical modeling, a new parameter that represents the strength and stiffness of the overburden was proposed. This parameter is a function of the strength of the overburden layers, the thickness of strong beds, and the relative location of the strong beds in the overburden. The critical span, which is the self-supporting length of a rock layer, is the main strength component of the geological parameter.

For this study, the elastic thin plate model was selected due to its practicality of calculation compared to other iterative approaches such as the voussoir beam approach. There are also other non-iterative methods to calculate critical span lengths, but the theory of thin plates is also the basis of the laminated model that was used in this study. The elastic thin plate model, which is based on plate theory, was derived by Salamon et al. (1972) and later improved by Galvin (1981) to estimate the span required to break a dolerite sill in the overburden of the South African coal mines. This theory was used by Salamon et al. (1972) to calculate critical panel widths when a very strong geological unit, e.g., a dolerite sill, exists in the overburden. During the derivation of the equations, Salamon et al. (1972) assumed that an elastic thin plate is loaded uniformly with fixed boundary conditions at each side of the plate. According to this theory, the critical (maximum) stress in a sill can be calculated using Equation 3.1 if the critical span when collapse occurs (S) is known (Galvin, 1981).

$$\sigma_c = k_\gamma \frac{D_D S^2}{t_D^2} \tag{3.1}$$

where σ_c is the critical stress, k_γ is the specific weight of the overburden, D_D is the depth to the base of the sill, t_D is the thickness of the sill and S is the critical panel span. In Equation 3.1, the critical stress can be replaced with critical failure stress of the rock layer (f_c) to calculate the critical span for each rock layer on the overburden by using Equation 3.2.

$$S_i = t_i \sqrt{\frac{f_i^c}{k_\gamma D_i}} \tag{3.2}$$

where S_i is the critical span for a rock layer in the overburden, t_i is the thickness of the rock layer, f^c_i is critical failure stress or strength of the rock layer, k_γ is the specific weight of the overburden and D_i is the depth to the base of the rock layer. The estimation of the critical failure stress (f^c_i) values was done for the studied dolerite sills and was a function of k_γ and the sill's depth-to-thickness ratio (Galvin, 1981). The constants in the formula to estimate the critical failure stress were semi-empirically derived from observations of failed and intact sills. For this study, the critical failure stress (f^c_i) values were selected as the UCS values.

Task 1.1.4: *Statistical analysis and model development.*

The geology-dependent global loading model is a statistical model. The statistical relationships between the independent parameters: the geological parameter, overburden depth, and panel width, and the dependent parameter, gob load percentages, were tested. The load percentages carried by the gobs were used as the statistical model response since the pillar loads depend highly on the dimensions of the chain pillar systems. After estimating the gob loads, the pillar loads can easily be calculated using the empirical load distribution function in ACPS or the analytical functions in LaModel.

Mine W-1 was omitted at this stage of the analysis since that is the only mine that utilizes a 2-entry yield pillar system and requires further investigation. Assumed as the most influential parameters, overburden depth and panel width were the variables considered in the analysis together with the critical span (S_i) of the overburden layers. For each case study, the critical span of every geological layer was calculated using Equation 3.2.

<u>Research Objective 1.2:</u> To refine geology-dependent loading model for accurate 3D load concentration near the tailgate corner and Active Mining Zone (AMZ).

Task 1.2.1: *Analysis of field measurements with full 3D FVM to investigate the influence of strong units in the overburden on 3D stress concentration.*

Five case study mines were modeled in 3D using FLAC3D, and different stages of panel advancements were simulated. The models include the longwall panels, the adjacent chain pillar systems, and the different stratigraphic layers of the overburden. Using the 3D model, stress changes induced by an approaching longwall face were examined and verified against field stress measurements.

<u>Mine A:</u> Mine A is in Virginia and operates in the Pocahontas No.3 coal bed. The depth of cover throughout the mine ranges from 1200 to 2300 ft. The longwall panels are roughly 700 ft wide by 10000 ft long. The gateroad system is a four-entry with approximately center-to-center, 50-ft-wide yield pillars and 174-ft-wide abutment pillars with approximately 18 ft wide entries. The mining height is approximately 5.5 ft on average for the studied panel. The typical roof geology consists of silty to sandy shales, sandstones, and coal. Shales usually dominate the bolted horizon, followed by a sandstone with an inconsistent shale parting before reaching the Pocahontas No. 4 coal seam (Klemetti et al., 2019).

In the 3D model, the minimum size of elements on the overburden was selected as 16 ft (5.0 m). In order to generate a 3D model that can approximate stresses accurately with larger elements, overburden lithological layers with the same rock type with a thickness of less than 16 ft (5.0 m) were combined and represented with a transversely isotropic material model. The 3D model of the mine had 35 different layers and approximately 1.3 million elements. The stability mapping grid generator is used to generate the mine layout at the seam level (Wang and Heasley, 2005). The instrumented pillars, roof, and floor were simulated with 3.3 ft (1.0 m) elements for more detailed simulation. The geometry of the model with the representative geological sequence that was modeled is shown in Figure 3.5.

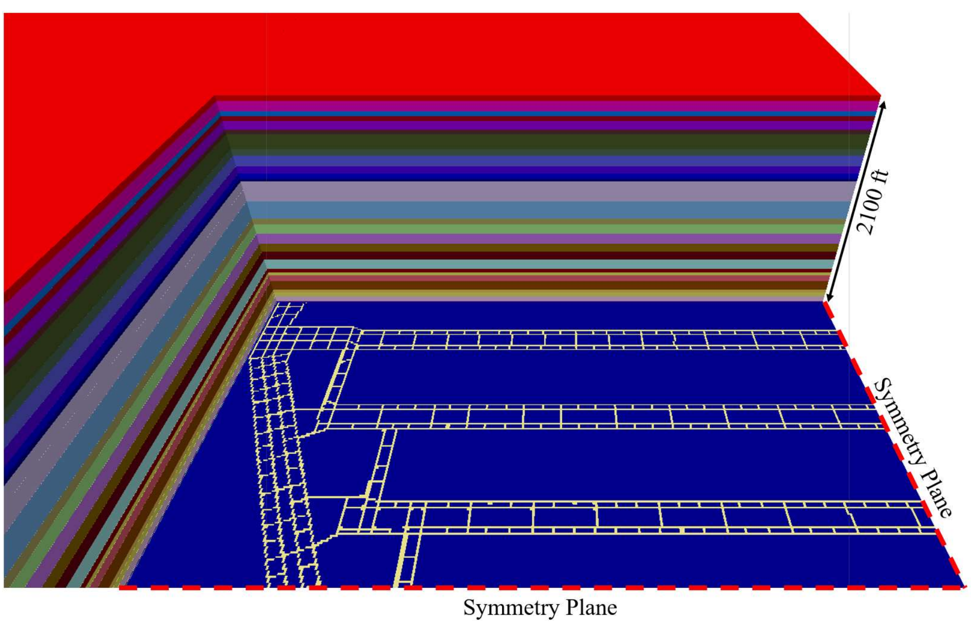

Figure 3.5. *Modeled area depicting the geological sequence and the mining geometry for Mine A (from Klemetti et al., 2019)*

The model was solved in five stages, simulating different face positions relative to the study site or references to specific dates based on face position, as seen in Figure 3.6. Stress analysis was done for the instrumented pillars, and the results were compared to the BPC measurements from the field.

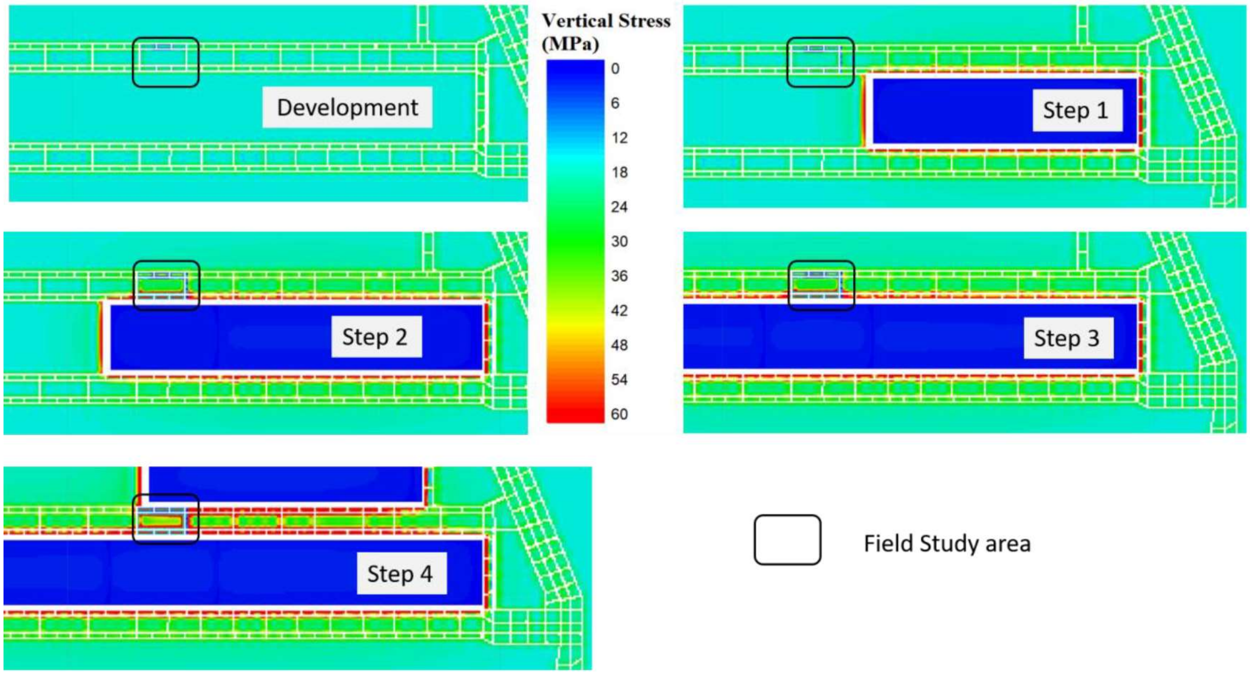

Figure 3.6. *Modeling steps with resulting vertical stress for Mine A (from Klemetti et al., 2019)*

Following the model verification, stresses on the bleeder entries (step 3) and the barrier pillar, and the tailgate T-junction were analyzed and compared to the empirical estimations used in the NIOSH pillar design tool, ALPS. For the comparison, percent increases from development stresses were used in an effort to normalize the results of different case study mines. Figure 3.7 shows the stress distribution obtained from the 3D model and how it is compared to the square decay function used in ALPS. The FLAC3D model is also able to model the yielding of the pillar ribs, where we observe negative stress change.

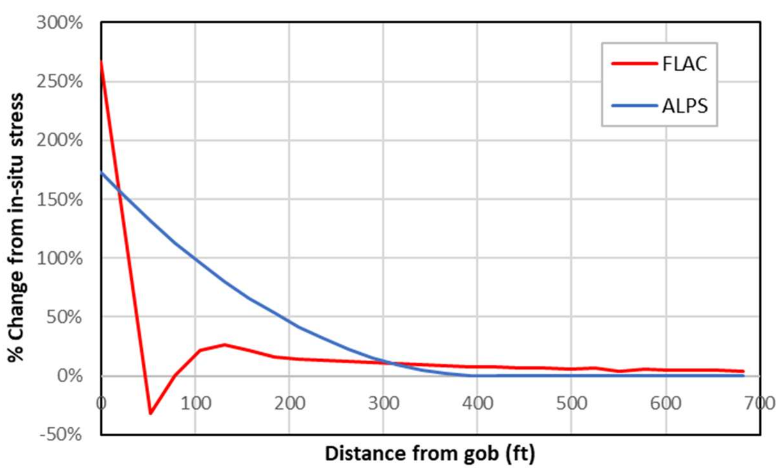

Figure 1.7. *Stress distribution on the bleeders after full panel extraction for Mine A.*

When we analyze the average stress increase within the abutment extent determined by the empirical abutment extent formula (426 ft), ALPS showed an average of 62% stress increase from development, whereas the 3D model showed a 33% increase. However, it was also observed that the abutment extent in the 3D model was also longer (Figure 3.7).

In the tailgate loading condition (step 4), stresses were analyzed around the T-junction. The results from ALPS indicated a 170% increase from development load for the tailgate loading. The 3D model showed an average of 104% increase from the development loading while also simulating the yield pillars. Figure 3.8 shows the percent stress increase around the tailgate T-junction for Mine A.

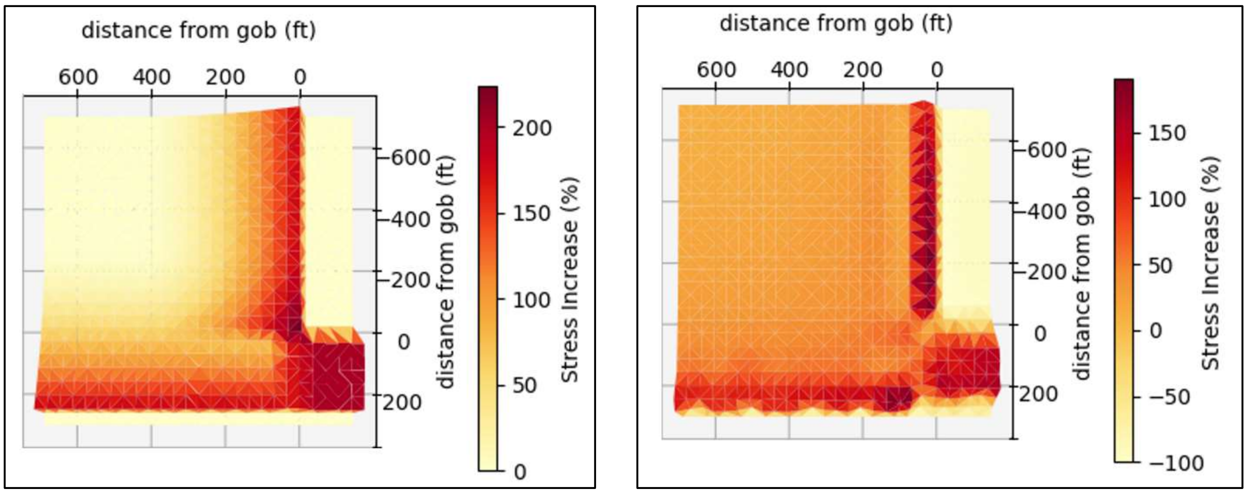

Figure 3.8. *Percent stress increase around the tailgate T-junction for Mine A (a) ALPS (b) FLAC3D*

Mine B: Mine B operates in the Black Warrior basin and mines the Blue Creek coal seam. It is a moderately deep mine with an average overburden depth of 1450 ft and panel width of 1000 ft. The depth of cover throughout the mine ranges from 1100 to 2200 ft. The longwall panels are roughly 1000 ft wide by 7000 ft long. The gateroad system is a four-entry with approximately center-to-center, 40-ft-wide yield pillars and 165-ft-wide abutment pillars with approximately 20 ft wide entries. The mining high is approximately 7.9 ft.

The Blue Creek seam that is mined is overlain by a shale parting that follows the Mary Lee seam. The two seams can be separated by as much as 25 ft, but when the Mary Lee seam is within 3 ft of the Blue Creek seam, both seams are mined simultaneously. The local roof geology consists of silty shale and sandstones. The sandstone is thinly bedded to laminated with shale, with shale and coal streaks in the upper and lower extents (Klemetti et al., 2020).

The 3D model of the mine had 30 different layers and approximately 1.16 million elements. In order to generate a 3D model that can run in a reasonable time frame, the minimum thickness of elements on the overburden was increased, and the overburden lithological layers with the same rock type with a thickness less than 23 ft (7 m) were combined and represented with a transversely isotropic material model. The instrumented pillars, roof, and floor were simulated with 3.3 ft elements in the detailed area. The geometry of the model with the representative geological sequence that was modeled can be seen in Figure 3.9.

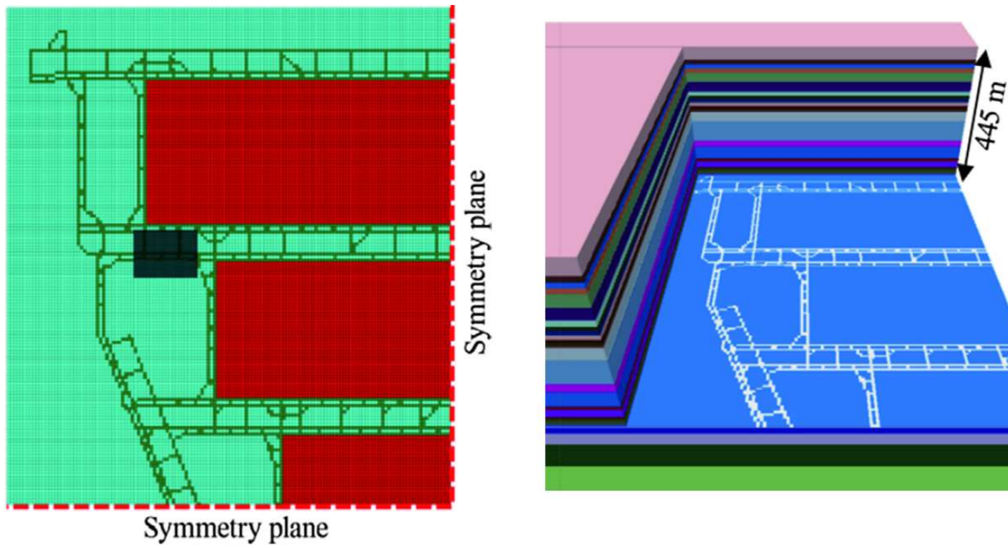

__Figure 3.9.__ The geological sequence and the mining geometry for Mine B (modified from Klemetti et al., 2020)

The model was solved in three stages simulating the development stage and the mining of two consecutive panels, as seen in Figure 3.10. Stress analysis was done for the instrumented pillars, and the results were compared to the field observations.

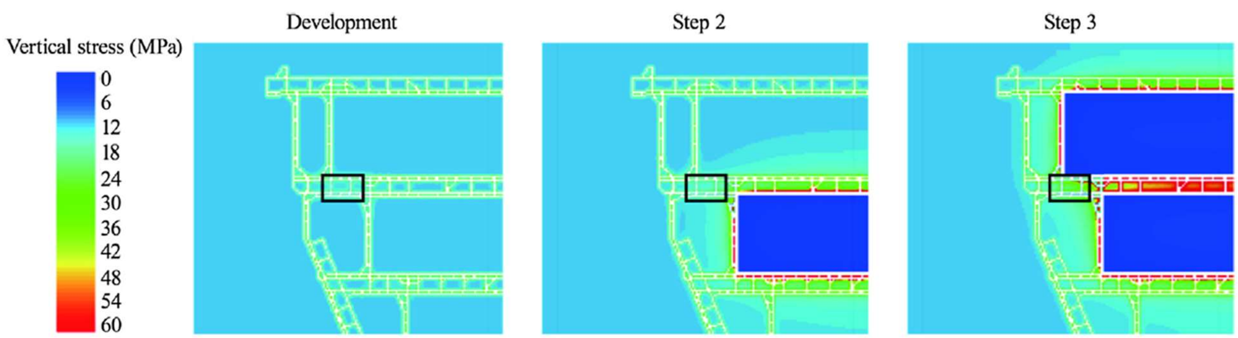

__Figure 3.10.__ Modeling steps with resulting vertical stress for Mine B (from Klemetti et al., 2020)

Following the model verification, stresses on the bleeder entries (step 2) and the barrier pillar were analyzed and compared to the empirical estimations used in ALPS. Similarly, percent increases from development stresses were used. Figure 3.11 shows the stress distribution obtained from the 3D model and how it is compared to the square decay function used in ALPS. When we analyze the average stress increase within the abutment extent determined (355 ft), ALPS showed an average of 78% stress increase from development, whereas the 3D model showed a 74% increase. It was also observed that the abutment extent in the 3D model was considerably larger (Figure 3.11). Due to the symmetry planes and mining sequence, tailgate loading was not simulated for this mine.

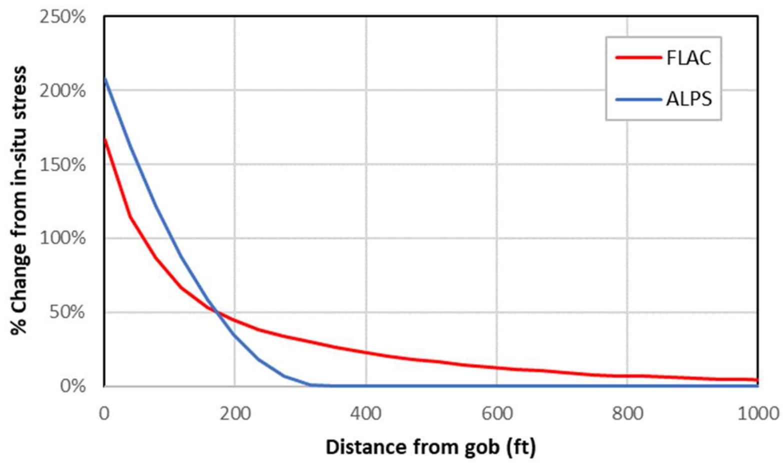

Figure 3.11. *Stress distribution on the bleeders after full panel extraction for Mine B.*

Mine C: Mine C is a northern Appalachian longwall mine, mining the Pittsburgh coal seam. The depth of cover at this mine ranges from 400 ft to about 1400 ft. The longwall panels near the study site were 1100-ft-wide and 12,000 ft long. The gateroad consisted of a small and a large pillar with center-to-center widths of 90 ft and 165-ft-wide. The entry and crosscuts in the gateroads were 18 ft wide, and the mining height was around 7 ft.

The 3D model of Mine C had 24 different overburden layers and approximately 1.1 million elements in total. The instrumented pillars, roof, and floor were simulated with 3.3 ft (1.0 m) elements with increasing element sizes away from the detailed area. The geometry of the model with the representative geological sequence that was modeled can be seen in Figure 3.12.

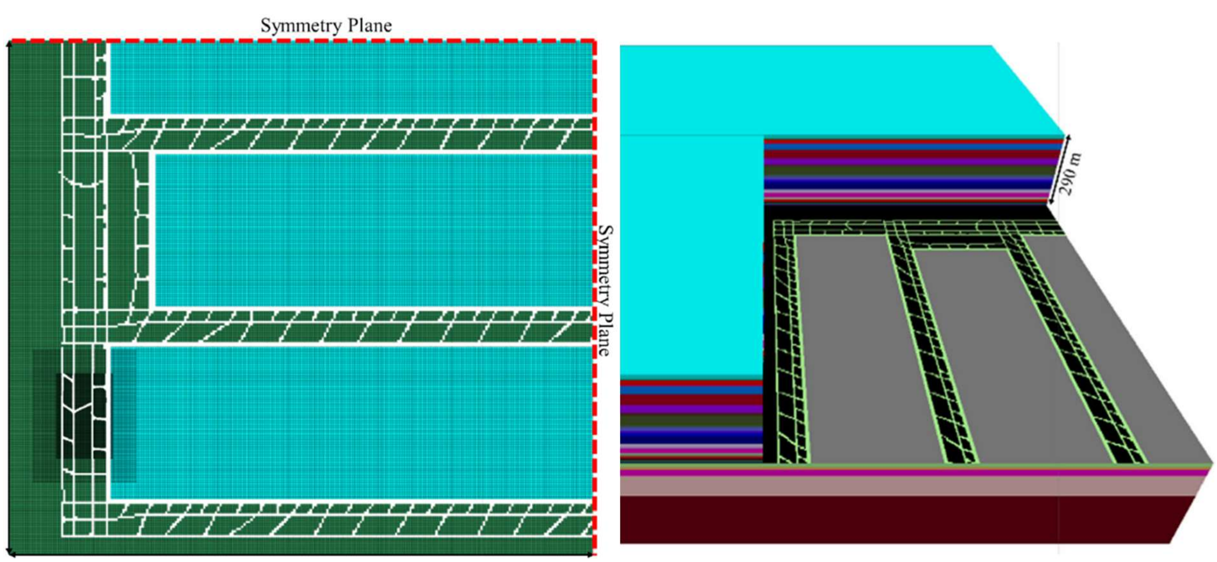

Figure 3.12. *The geological sequence and the mining geometry for Mine C (modified from Van Dyke et al., 2021).*

The numerical model was solved in five stages (Figure 3.13), the first being development. The second and third steps are the complete retreating of the second and third panels of the current district. The fourth stage is the first 330 ft of the fourth panel extracted, which is followed by the fifth stage being the complete retreat of the fourth panel. Stress analysis was done for the instrumented pillars, and the results were compared to the BPC measurements from the field. For the analysis of the tailgate loading condition, an additional step was simulated with the fourth panel mined for 2,200 ft (step TG).

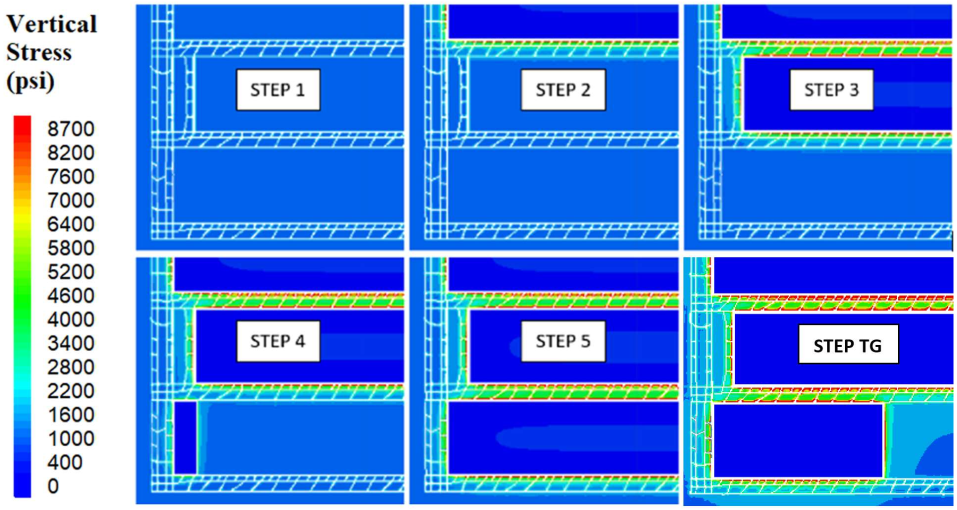

Figure 3.13. *Modeling steps with resulting vertical stress for Mine C (from Van Dyke et al., 2021).*

Following the model verification, stresses on the bleeder entries and the barrier pillar (step 5), and the tailgate T-junction (step TG) were analyzed and compared to the empirical estimations used in ALPS. Figure 3.14 shows the stress distribution obtained from the 3D model and how it is compared to the square decay function used in ALPS for the bleeder side. When we analyze the average stress increase within the abutment extent determined (325 ft), ALPS showed an average of 68% stress increase from development, whereas the 3D model showed an 84% increase. The FLAC3D model also showed a higher abutment extent (Figure 3.14).

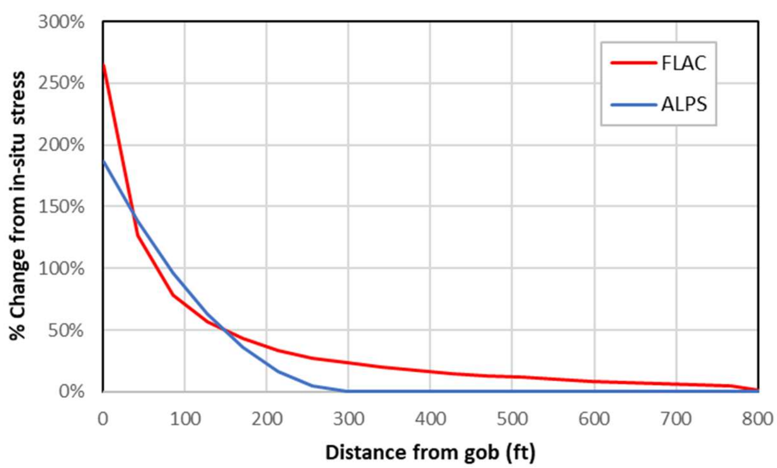

Figure 3.14. *Stress distribution on the bleeders after full panel extraction for Mine C.*

In the tailgate loading condition (step TG), stresses were analyzed around the T-junction. The results from ALPS indicated a 156% increase from the development load for the tailgate loading. The 3D model showed an average of 172% increase from the development loading. Figure 3.15 shows the percent stress increase around the tailgate T-junction for Mine C.

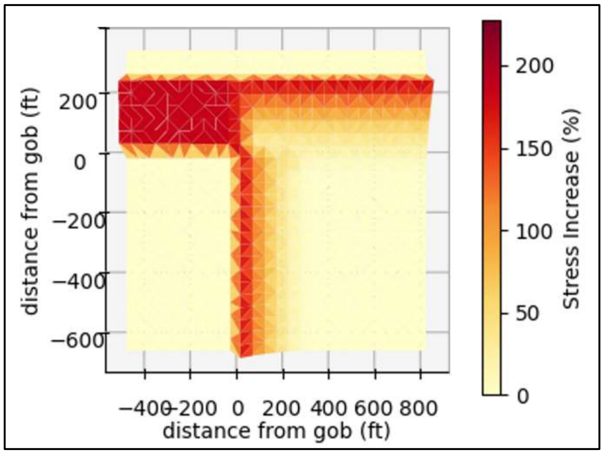

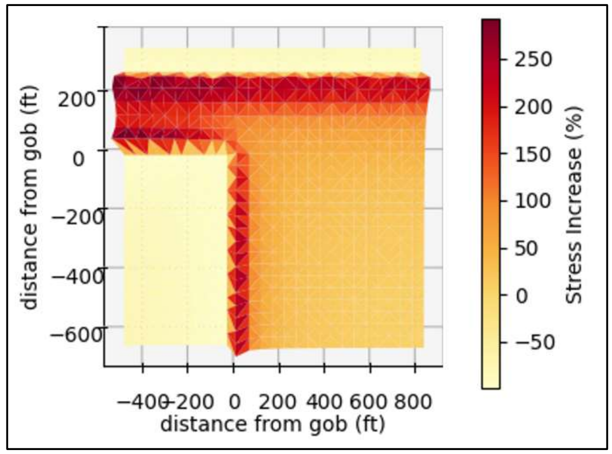

Figure 3.15. *Percent stress increase around the tailgate T-junction for Mine C (a) ALPS (b) FLAC3D.*

Mine D: Mine D is in Utah and operates in the Lila Canyon coal seam. The depth of cover around the instrumented area was 1,275 ft. The analyzed longwall panels were roughly 845 ft wide and 3500 ft long. The gateroad system is a two-entry yield pillar system with center-to-center, 50-ft-wide pillars, and 18 ft wide entries. The mining height was approximately 11.5 ft.

The largest grid size was selected as 20 ft (6 m), whereas the grid size for the detailed area around the measurement site was selected as 3.3 ft (1 m). Figure 3.16 represents the different consecutive modeling steps selected for the analysis and the resulting vertical stresses. Additional steps are added near the measurement site to plot and compare the stress changes more precisely.

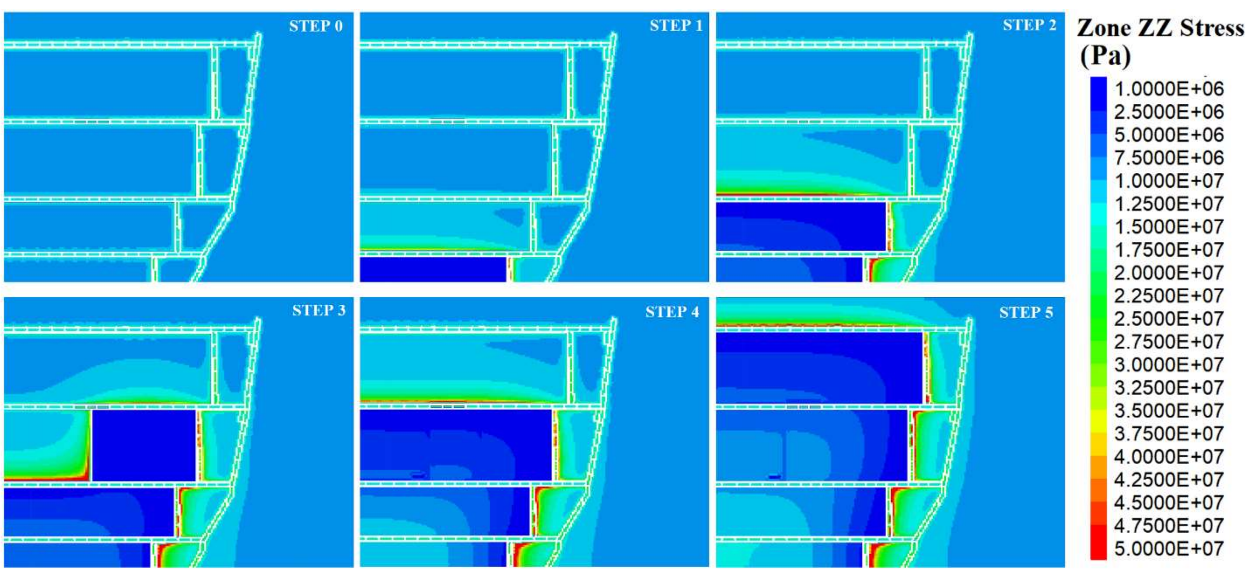

Figure 3.16. *Modeling steps with resulting vertical stress for Mine D.*

Following the model verification, stresses on the bleeder entries and the barrier pillar (step 4) were analyzed and compared to the empirical estimations used in ALPS. Figure 3.16 shows the stress distribution obtained from the 3D model and how it is compared to the square decay function used in

ALPS for the bleeder side. When we analyze the average stress increase within the abutment extent determined (332 ft), ALPS showed an average of 73% stress increase from development, whereas the 3D model showed a 97% increase. The FLAC3D model was also able to capture the yielding of the pillars and the stress transfer toward the barrier pillar. The FLAC3D model also showed a higher abutment extent (Figure 3.16). Due to the application of the yield pillar system in Mine D, tailgate loading was not analyzed.

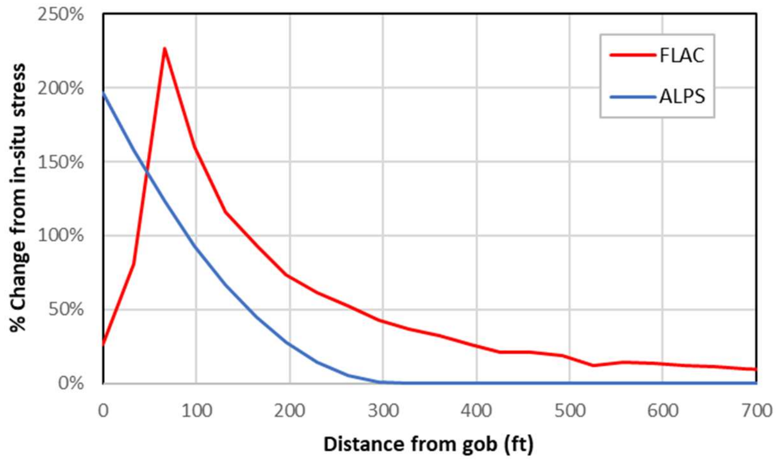

Figure 3.16. *Stress distribution on the bleeders after full panel extraction for Mine D.*

Mine E: Mine E is in Northern West Virginia and operates in the Middle Kittanning coal bed. The depth of cover throughout the mine ranges from 500 to 750 ft, and the typical depth is about 520 ft. The longwall panels are roughly 1200 ft wide by 8000 ft long. The gateroad system is a three-entry with approximately center-to-center, 100-ft-wide chain pillars with approximately 20 ft wide entries. The mining high is approximately 7 ft.

Based on the in-mine mapping, as well as available exploration drillhole data, the geologic conditions are typical for the Allegheny Formation. The Middle Kittanning coal bed that is mined is overlain by dark gray to carbonaceous clay shale. The clay shale grades upward to gray sandy shale, dark gray sandy shale, or gray sandstone. The gray sandy silt shale and dark gray sandy silt shale beds vary in grain size and sand content based on their proximity to the laterally correlative gray sandstone beds.

The 3D model of the mine had 29 different layers and approximately 1.3 million elements. The instrumented pillars, roof, and floor were simulated with 3.3 ft (1.0 m) elements with increasing element sizes away from the detailed area. The geometry of the model with the representative geological sequence that was modeled can be seen in Figure 3.17.

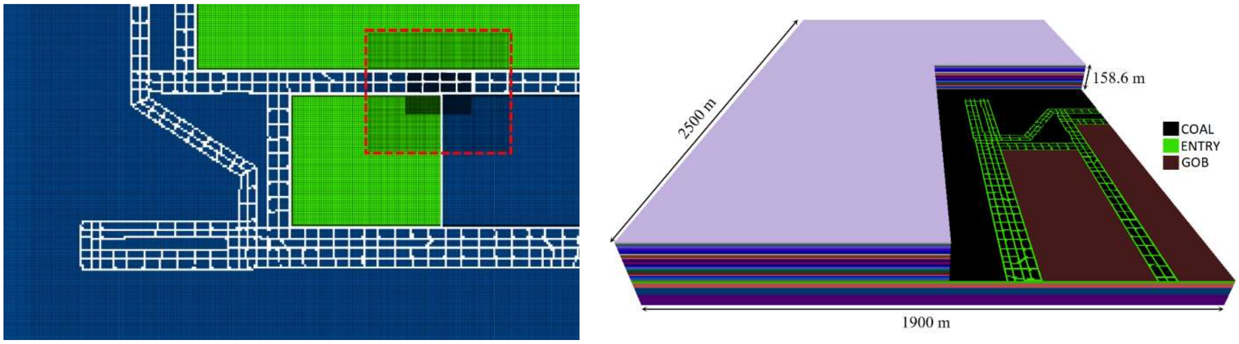

Figure 3.17. *The geological sequence and the mining geometry for Mine C (modified from Van Dyke et al., 2021).*

The model was solved in four stages to simulate different face positions relative to the study site to compare with field measurements. The first stage (development) was simply the development mining scenario when all the entries in the model were mined. The second stage (step 1) was the complete retreat of the first panel, and the third and fourth stages (steps 2-3) were the longwall face of the second panel being mined was about 65 ft outby and 85 ft inby (last available cell readings) the instrumentation site, respectively (Figure 3.18).

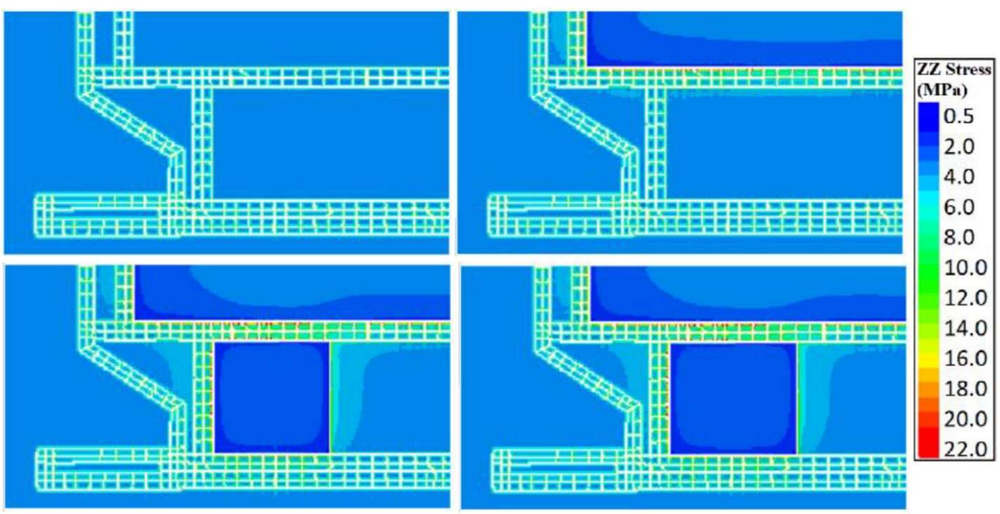

Figure 3.18. *Modeling steps with resulting vertical stress for Mine E (from Tuncay et al., 2020).*

Following the model verification, stresses on the bleeder entries and the barrier pillar (step 3), and the tailgate T-junction (step 3) were analyzed and compared to the empirical estimations used in ALPS. Figure 3.19 shows the stress distribution obtained from the 3D model and how it is compared to the square decay function used in ALPS for the bleeder side. Full panel extraction was not simulated for Mine E since supercritical loading was already achieved in steps 2 and 3. When we analyze the average stress increase within the abutment extent determined (212 ft), ALPS showed an average of 59% stress increase from development, whereas the 3D model showed a 49% increase. The FLAC3D model also showed a higher abutment extent (Figure 3.19).

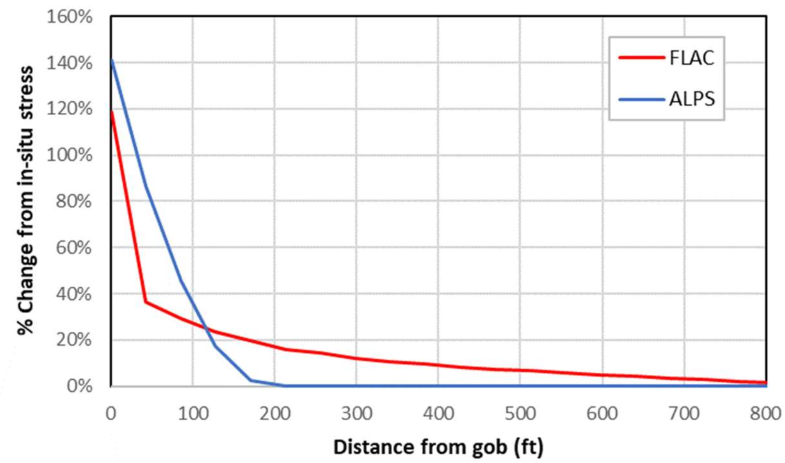

Figure 3.19. *Stress distribution on the bleeders after step 3 for Mine E.*

In the tailgate loading condition (step 3), stresses were analyzed around the T-junction. The results from ALPS indicated an 87% increase from the development load for the tailgate loading. The 3D model showed an average of 53% increase from the development loading. Figure 3.20 shows the percent stress increase around the tailgate T-junction for Mine E.

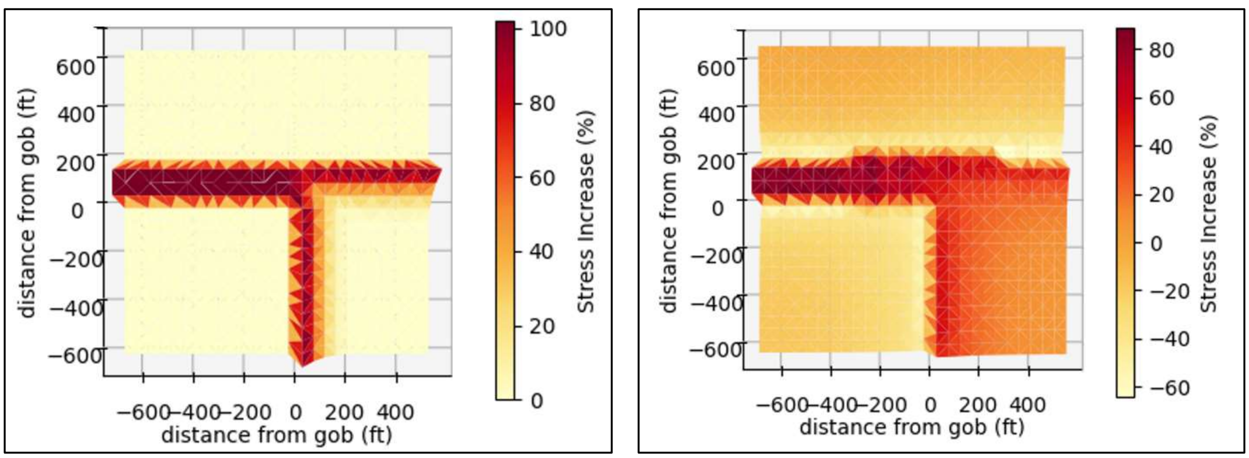

Figure 3.20. *Percent stress increase around the tailgate T-junction for Mine E (a) ALPS (b) FLAC3D.*

Task 1.2.2: *Test the effectiveness of the new mine-specific, geology-based mechanical loading model with the database.*

The new gob loading model can be easily implemented into LaModel through the gob wizard option in LaMPre 3.0. After de-selecting the "Use the Suggested Value" tick box and inputting the estimated gob load percentage into the gob wizard, the user can easily calculate and implement the appropriate final gob modulus that will match the estimated gob load percentage. This allows the practical implementation of the effect of overburden geology into a design tool capable of modeling complex mine geometries. By selecting at least two "Number of Gob Materials to be Defined" the user can input the estimated gob load percentages for both the active and previous panels and calculate and use the appropriate final gob moduli.

To check for its applicability, three cases that are not included in the original analyzed database were used for this verification. These case histories are obtained from personal communications with David Hill (formerly of Strata Engineering Australia, currently with Strata2 Pty Ltd). All three cases are from Australia with varying overburden depths between 1198 ft and 1683 ft. They utilize 2-entry chain pillar systems but instead of small yield pillars, they use large abutment pillars with similar widths ranging from 140 ft up to 150 ft. Table 3.2 shows the depths and the panel configurations for these cases.

Table 3.2. *Depths and Panel configurations for the Australian case studies.*

CASE	Depth of Cover (ft)	Panel Width (ft)	Entry Width (ft)	Pillar width (ft)
Mine AU-1	1198	820	16	140
Mine AU-2	1329	820	16	145
Mine AU-3	1683	745	16	150

Core logs from near the instrumentation sites were visualized and presented in Figure 3.21. Layers with more than one rock type represent interbedded or intermixed components, but the percentages may vary. Also, thick layers do not necessarily represent massive rock formations. Adjacent thin layers of the same rock types were combined for easier representation. Using the information from the core logs, the geological parameter t_{str} for each case was calculated.

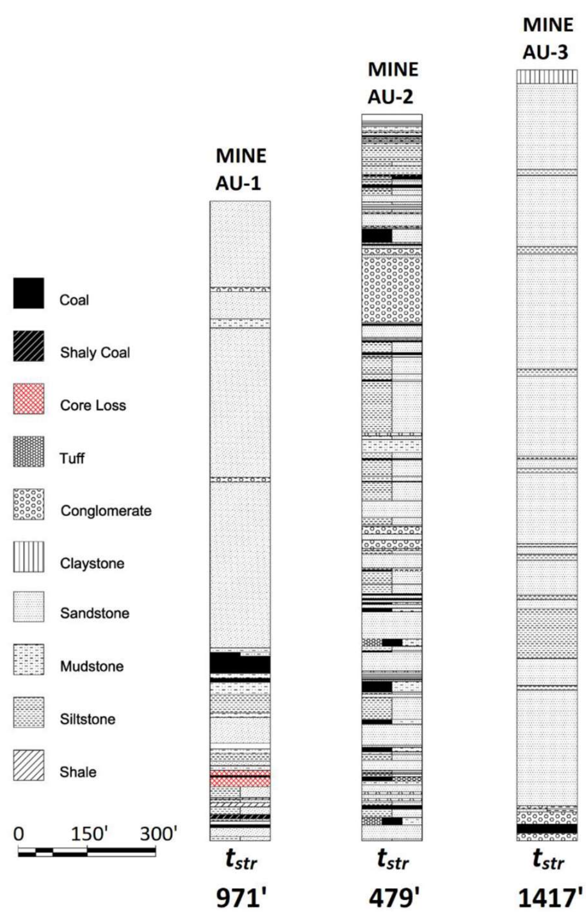

Figure 3.21. *Stratigraphic columns for the Australian case studies (Tuncay, 2021).*

<u>Specific Aim 2:</u> Adapting practical mechanics-based design tool for longwall pillar design.

<u>Research Objective 2.1:</u> To program and verify laminated overburden model longwall pillar stability approach.

This research objective entails the development of a python script program of ALPS-LAM, which uses the ALPS input and laminated overburden model to determine the distribution of the overburden loading on the longwall gateroad pillars and the resultant tailgate stability factor.

Task 2.1.1: Program the Python Script Program of ALPS-LAM.

A script version of the program that takes the basic ALPS geometric input for defining the mining plan and loading condition, and then automatically develop and analyze a complete LaModel file of the mining geometry to calculate the stability factor on the gateroad pillars were developed:

- Data Import: Program reads excel file containing the ALPS geometry data as an input.
- Property Calibration: Determine the appropriate properties for the structural inputs (lamination thickness, rockmass modulus and gob material model parameters) for the laminated overburden model.
- Calculate Stability Factors: From the LaModel output file, determine tailgate stability factors of the longwall gateroad pillar system.

Task 2.1.2: Verify the New Script Program.

This new script program discussed in this report is a research-oriented design that is capable of batch solving numerous longwall mine case histories. This new version of the program was validated against ALPS, using the longwall case histories detailed in specific aim 1, by manually performing the analysis and then comparing the results to the automated program results.

<u>Specific Aim 3:</u> Develop a local geology-dependent GRC design option for STOP.

Longwall gateroad entries are generally subjected to severe mining-induced stress changes and deformations; they are prone to large roof falls, floor heaves, and rib sloughing. The standing support system in underground mines needs to be carefully designed to compensate for the mining-induced deformation of the surrounding rock mass and consecutively protect the integrity of gateroad entries. Local geology, together with mining-induced stress redistribution, influences the ground response and plays a major role in the performance of a standing support design. In the US, Support Technology Optimization Program (STOP) and its Ground Reaction Curve (GRC) design criteria have been applied to evaluate the performance of the standing support systems. The ground reaction curve of a gateroad entry is a function of geology and stress states, and it can be used to assess the influence of local geology and stress states on standing support performance. However, at present, measuring GRC in an underground mine remains impractical, and only a few GRC samples are available in STOP.

In this research, to extend the GRC database and develop local geology and stress-dependent GRC for various geological and operational conditions, an entry-scale modeling methodology was developed. Four field measurement case studies in different underground mines were used for constructing and calibrating the modeling procedure. Two cases, which are not included in the previous database, were used to verify the modeling procedure. Then, the geology and stress-dependent GRC developed for different case study mines were integrated into STOP to evaluate standing support design and verify the approach.

***Research Objective 3.1*: To develop a suite of representative local geology-dependent ground reaction curves.**

Task 3.1.1: *Development of the ground reaction curve modelling approach*.

Barczak (2020) indicated that the ground reaction curve shows the relationship between the support load density required to maintain an open entry in equilibrium, and the roof-to-floor convergence of the opening after mining. Figure 3.22 shows the conceptual illustration of the GRC design criteria of the STOP.

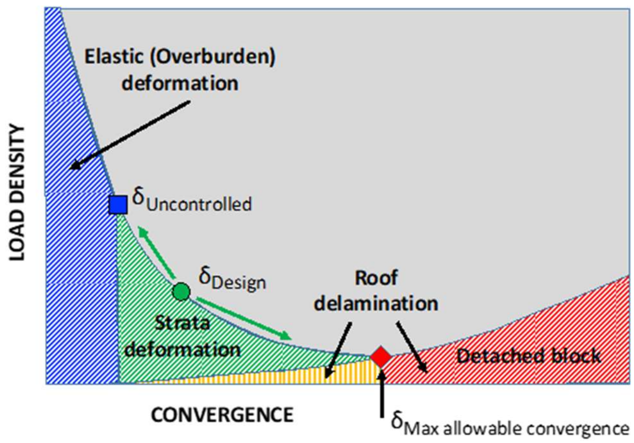

Figure 3.22. *Conceptual illustration of GRC approach in STOP (after, Barczak, 2020)*

Barczak et al. (2008) demonstrated the methodology to estimate the GRC for the longwall tailgate indirectly by using field measurements and calibrated numerical models. Esterhuizen et al. (2010) explains the difficulty in measuring the ground reaction curve in the field due to the significant loads that would have to be applied to balance the deformation of the roof and floor. They proposed to estimate the GRC indirectly through well-calibrated numerical models. In this task, the GRC modeling methodology was developed. During the development of the modeling methodology FLAC3D finite difference software was used and, the following studies were taken as a basis: Esterhuizen et al., (2008, 2017, 2020), Barczak et al., (2008) and Tulu and Esterhuizen (2016).

Model Geometry and Boundary Conditions: Figure 3.23 presents the front view of the constructed entry-scale model, including the rock mass strata and the applied roof bolt support system. To realistically reproduce the ground response in a gateroad entry, boundary conditions representing the stress state observed in the field needed to be applied to the model (Barczak, 2008 & Zhao et al., 2018). Since the constructed model represents a slice of the entry, displacement was fixed to zero at the base of the model, and roller boundary conditions were applied to the faces out of plane directions of the model. The same roller boundary condition was applied normal to horizontal for simulating the underground pillar system symmetrically. The top surface of the constructed model was set free in the z-axis direction (Figure 3 .23).

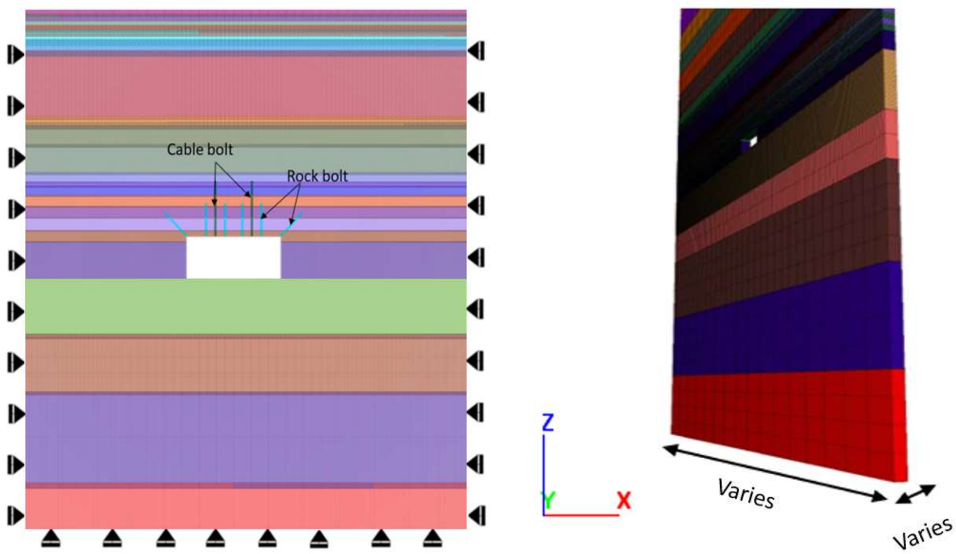

Figure 3.23. *Front and isometric views of the entry-scale model used to simulate gateroad entry and the applied boundary condition (Zhao, 2022).*

As shown in Figure 3.23, the constructed model only includes portions of the overburden strata. The gradient vertical stress was initialized in the model before excavating the gateroad to simulate the effect of the overburden stress. To implicitly simulate the vertical load induced on the excavation during the development and longwall retreats, a stress boundary condition was applied on the top of the model along the direction of gravity. Horizontal stresses were initialized at the development stage to simulate the in-situ horizontal stress, where their magnitudes are estimated by the equation from Dolinar et al., (2003). According to the relative locations between the longwall face and the monitoring site, an infinite number of stress states can be simulated with this approach. In this study, five distinct stress states are considered: development, front abutment, side abutment, tailgate and isolated.

Ground Reaction Curve Development: The goal of this research task is to develop the ground reaction curves for the gateroad under various stress states and geological conditions.

To generate GRC from the entry-scale model, the following steps are followed:

1) Before excavating the gateroad entry, a constant load should be applied on the top of the model to simulate the in-situ overburden loading. The model is solved to simulate the stress distribution around the gateroad. In the meantime, the reaction forces of all gridpoints around the entry are recorded (Figure 3.24a).
2) Then, the gateroad entry is excavated. The recorded reaction forces from the first step are applied in the opposite direction to balance the in situ ground pressure (Figure 3.24b).
3) Reaction forces on each gridpoint around the entry are reduced with small decrements to progressively relax the entry. Entry convergence is calculated simultaneously. There is no standard range for the reduction ratio; it normally ranges from 1% to 10%. A smaller reduction ratio can produce more numerically stable results and data monitoring points, which results in smoother GRC, but increases the simulation time.

4) The entry relaxation step is repeated until the magnitude of the applied reaction forces reaches zero. The total internal applied pressure and the resultant entry convergence for each step are recorded. Finally, GRC, internal pressure vs entry convergence, is plotted.

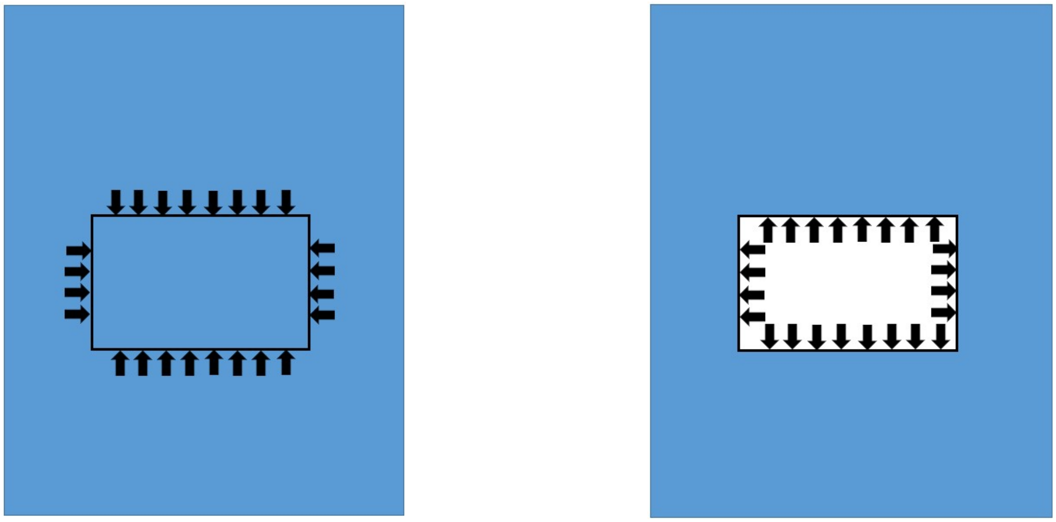
(a) (b)

Figure 3.24. *(a) Collection of reaction force of each gridpoint around the gateroad; (b) Balance resistant force application.*

Details of GRC development approach are explained in Zhao (2022), Zhao and Tulu (2021), and Batchler et al. (2021).

Primary and Cable Bolt Modeling: In U.S. underground coal mines, primary bolts and cable bolts are widely applied for reinforcing the gateroad roof. In this study, bolt model properties were calibrated to simulate the response of the roof bolts in the field. Pile element, which is available in FLAC3D, was used for modeling the primary and cable bolts. The mechanical properties of the fully grouted bolt were calibrated through a trial-and-error approach. Pull-out tests performed by Serbousek et al., (1987), Short Encapsulation Pull Test (SEPT) performed by Mark et al. (2002), and cable bolt tests conducted by Tadolini (2012) were used in calibration. Details of primary and cable bolt modelling are explained in Zhao (2022).

Coal Measure Rock Mass Modeling: In his study, the coal measure rock mass was classified into several groups according to their laboratory-tested UCS magnitude and rock type (Tables 3.3 and 3.4). A detailed discussion about the rock mass material properties selection and determination can be found in Esterhuizen et al., (2010), Tulu et al., (2018), and Zhao (2022). UCS values in Tables 3.3 and 3.4 are laboratory-scale values. The field value of the UCS is estimated by multiplying the laboratory value by 0.58 (Esterhuizen et al., 2010; Hoek and Brown, 1980). The rock strength, deformation properties, and bedding strength properties suggested for modeling coal measure rocks in the United States are presented in Tables 3.3 and 3.4.

Table 3.3 *Suggested intact rock properties after Esterhuizen et al. (2010).*

Type	**UCS (MPa)**	**E (GPa)**	**ν**	**Friction Angle (°)**	**Cohesion (MPa)**	**Tensile Strength (MPa)**
Limestone	140	24.675	0.2	42	18.93	8.12
	100	21.98	0.2	42	15.10	5.80
	80	20.632	0.2	40	13.39	4.64
Sandstone	120	16.113	0.2	42	16.23	6.96
	100	14.454	0.2	40	13.52	5.80
	80	12.795	0.2	37	12.08	4.64
	60	11.136	0.2	35	9.06	3.48
	40	9.4776	0.2	30	6.70	2.32
Shale	80	12.795	0.2	32	14.78	4.64
	60	11.136	0.2	30	12.18	3.48
	40	9.4776	0.2	25	8.90	2.32
	30	8.6468	0.2	20	7.30	1.74
	20	7.8188	0.2	20	4.87	1.16
	10	6.9894	0.2	20	2.66	0.58
	5	6.5747	0.2	20	1.35	0.29
Coal/Entry	11	2	0.2	35	1.66	0.63

Table 3.4 *Suggested material bedding strength properties after Esterhuizen et al. (2010).*

Type	**UCS (MPa)**	**Bedding Cohesion (MPa)**	**Bedding Friction Angle (deg.)**	**Bedding Tensile Strength (MPa)**
Limestone	140	9.47	32	6.50
	100	7.55	30	4.64
	80	6.70	28	3.71
Sandstone	120	8.11	30	5.57
	100	6.76	30	4.64
	80	6.04	27	0.46
	60	4.53	25	0.35
	40	3.35	20	0.23
Shale	80	2.96	10	0.46
	60	2.44	7	0.35
	40	1.78	7	0.23
	30	0.50	7	0.17
	20	0.30	5	0.12
	10	0.20	5	0.06
	5	0.10	5	0.03

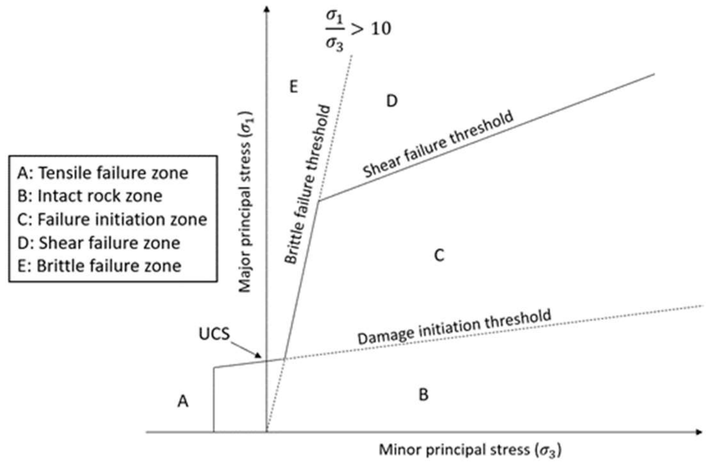

Figure 3.25 *Conceptual brittle rock mass failure criteria, after Kaiser et al. (2010).*

In this study, the strain softening ubiquitous criterion, which is available in FLAC3D, was used for modeling the rock strata. The rock element size in the model typically varied between 0.1 m to 2.0 m in the vertical (z-direction). Model element thickness was set as 0.1m in the proximity of the coal seam to accurately simulate the ground response and monitor the rock behavior along the gateroad. The rock strata away from the gateroad were modeled by the large size element to increase the modeling efficiency. In this study, the model only extended up to 30 m to 50 m above the roofline, and the thickness of rock layering was modeled between 0.2 m to 3.0 m to approximate the local geology effect on the ground response accurately. Any rock stratum with a thickness of less than 0.2 m was combined with other rock strata to improve the model run-time efficiency. In this model, the interface mechanical properties between each stratum were derived from Su et al., (1991), Lu et al., (2008), Esterhuizen et al., (2010), and Itasca (2022). Details of material model and interface properties are explained in Zhao (2022) and Zhao and Tulu (2021).

In this study, the CWFS (Cohesion Weakening Friction Strengthening) approach is used for simulating the brittle extensional rock failure around the gateroad entries (Esterhuizen et al., 2016). In this approach, for the rock blocks, which are identified as brittle rock, their vertical cohesive strength is set according to Table 3.3. Their horizontal cohesive strength is calculated by using the strength anisotropy ratio factor. In this approach, rock strata, which are not identified as brittle rock, follow the shear strength criteria and the same anisotropy approach is applied to calculate horizontal strength. Figure 3.25 represents a conceptual rock mass failure criterion employed in this study, which is based on the S-shaped rock failure criterion from Kaiser et al., (2010). As shown in Figure 3.25, the ratio of major principal stress to minor principal stress is taken as the boundary to separate the standard shear-based failure criterion and brittle rock failure criterion. In FLAC3D, the built-in programming language (FISH) is used to identify the brittle rock zones. The details of the logic of brittle zone identification are explained in Zhao (2022).

Task 3.1.2: *Development of database of local roof/floor geologies and field measurements from different U.S. coal fields.*

The ground response under a variety of loading conditions and geologic conditions that extend beyond the range of the limited field monitoring case history sites can be investigated with numerical models. However, it is necessary to have a model calibrated against actual field data to ensure that the model provides realistic results. We used the modeling methodology that is presented in Task 3.1.1, and verify the methodology with field measurements of 6 case studies from 4 different U.S. longwall mines. All these case study mines are from the Eastern U.S. coalfields, and their approximate locations are shown in Figure 3.26.

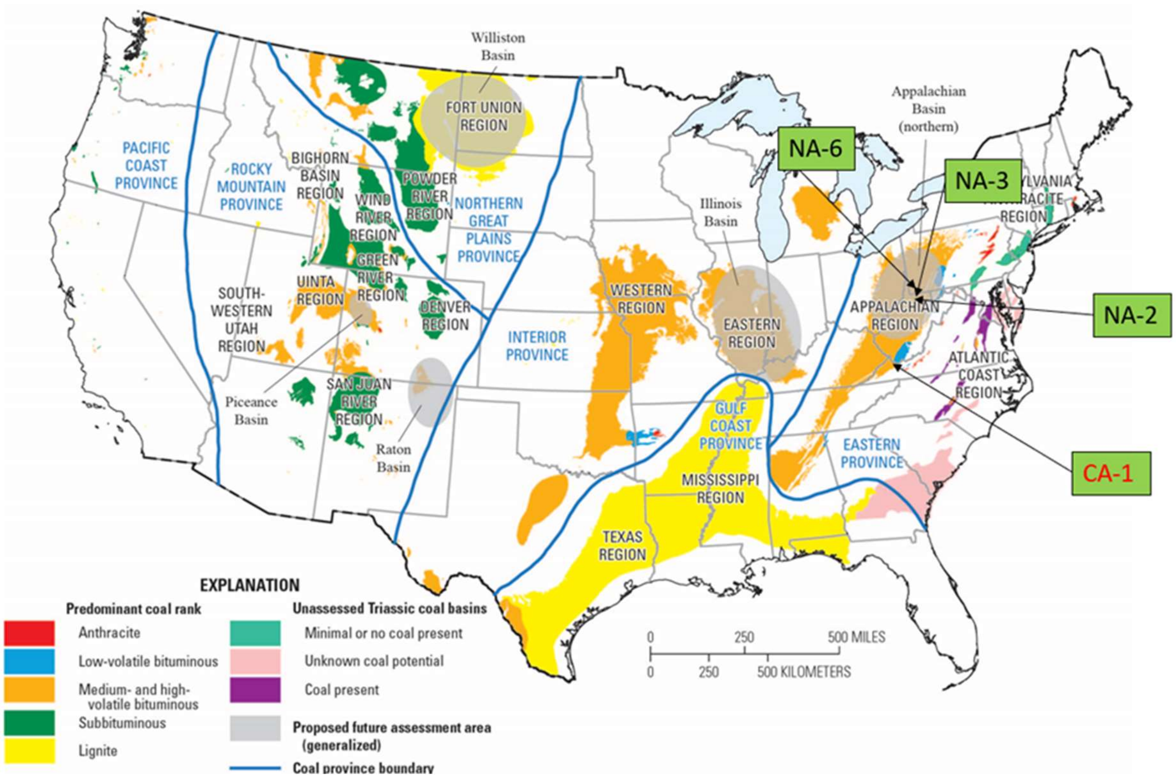

Figure 3.26. *Coal fields of the conterminous United States and the locations of Case Study Mines (After USGS 2022).*

Among these six study sites, four cases were used for calibrating the entry scale model. The remaining two case studies, which are from CA-1 mine, were used to verify the modeling methodology. Table 3.5 shows the summary of the case study mines, and Table 3.6 presents the operational parameters of each case study mine. The abbreviated codes (NA & CA) were assigned to each case study to represent the coal regions they come from: NA for North Appalachia and CA for Central Appalachia. The constructed database contains information about the immediate roof/floor geology, roof rock movement, stress distribution, and bolt performance for model calibration and validation purposes. Detailed geological core logs are available for all the case studies, and Figure 3.26 shows the portions of immediate roof/floor strata of the case studies.

Table 3.5 *Summary of case study mines (Zhao, 2022).*

Case	Seam Name	Seam Height	In situ Stress Region
NA-2	Pittsburgh	2.3 m	Eastern U.S., Northern Appalachia
NA-3	Middle Kittanning	2.1 m	Eastern U.S., Northern Appalachia
NA-6	Pittsburgh	2 m	Eastern U.S., Northern Appalachia
CA-1	Pocahontas No.3	2.3 m	Eastern U.S., Central Appalachia

** NA = North Appalachia; CA = Central Appalachia*

Table 3.6 *Basic characteristics of case study mines (Zhao, 2022).*

Case	Depth (m)	Panel width (m)	Entry system	Pillar size (m)	Support system
NA-2	213	357	Three entries gateroad	42 - 30.5	Three 2.7-m long combined bolts on 1.2 m spacing and a single row of nine-point wood cribs with 2.4 m spacing.
NA-3	180	366	Three entries gateroad	30	Four 1.8-m long primary rock bolts with 1.2 m spacing; Four 3-m long cable bolts with 2.4 m spacing, and two rows of nine-point wood cribs.
NA-6	200	N/A	Three entries gateroad	33	Three 2.4-m long two pieces combined bolt with 1.2 m spacing
CA-1	410-730	214	Four entries gateroad	15-53-15	Four 1.8-m long fully grouted roof bolt and two 3.6-m long cable bolt

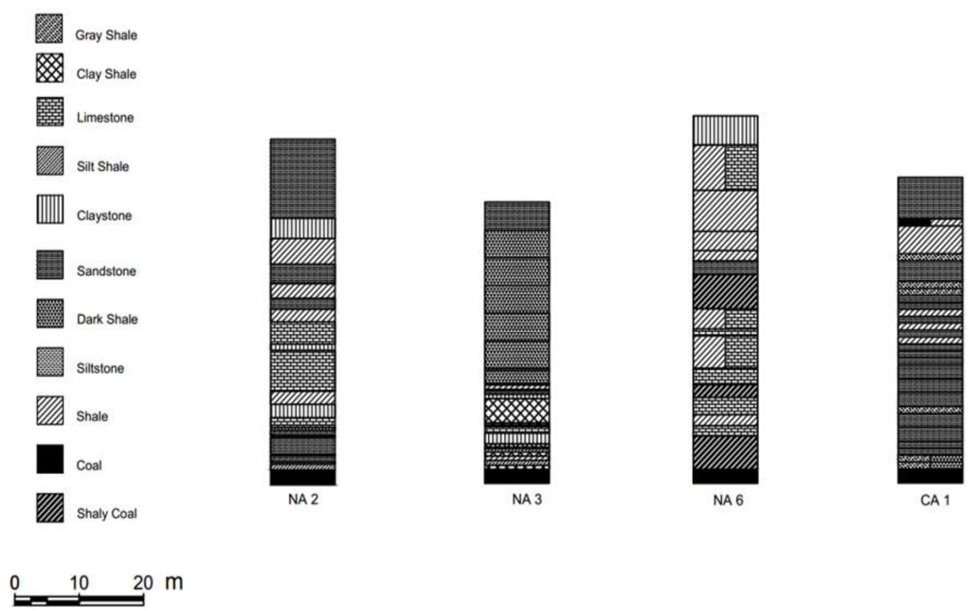

Figure 3.26. *Generalized stratigraphic column representation of the case study mines for model construction (Zhao, 2022).*

Task 3.1.2: *Develop local geology-dependent ground reaction curves for STOP.*

The objective of this study is to develop a methodology to allow generation of ground reaction curves (GRC) for various mining conditions and add them to STOP as references for the potential user. To realize this goal, GRC developed with the proposed modelling methodology should be in the correct format to be able to be integrated into STOP. In order to apply GRC design criteria of STOP, uncontrolled convergence and maximum allowable convergence design parameters need to be selected (Barczak, 2020). Therefore, together with the GRC, these two important design parameters must be computed from the model results.

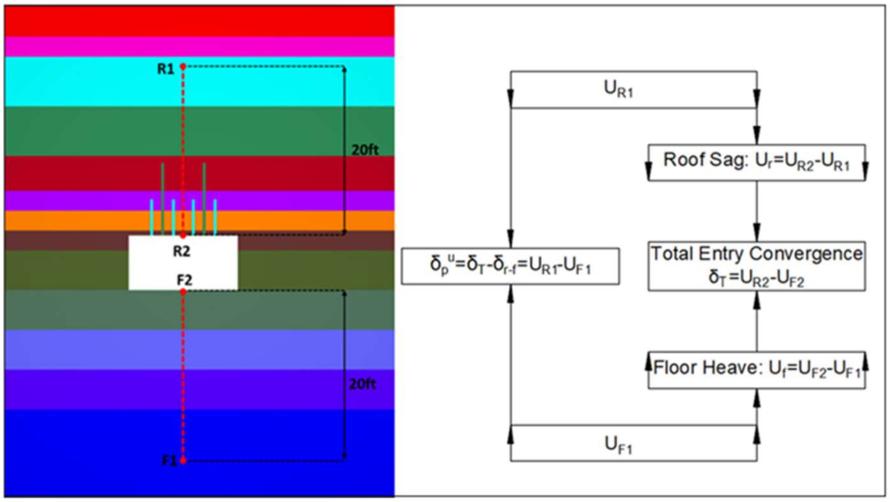

Figure 3.27*. Entry scale model and deformation computations (after, Batchler et al., 2021).*

GRC parameter computations from model results: The uncontrollable convergence refers to the deformations mainly produced by the elastic response of the overburden and pillar deformations. Figure 3.27 and Equations 3.3 to 3.8 show how to estimate it from the model results (Batchler et al., 2021).

As shown in Figure 3.27, roof deformation (u_r) and floor deformation (u_f) can be calculated using Equations 3.3 and 3.4.

$$u_r = u_{R2} - u_{R1} \tag{3.3}$$

$$u_f = u_{F2} - u_{F1} \tag{3.4}$$

Where: u_{R1} & u_{R2} represents the vertical displacement of "R1 and "R2" and u_{F1} & u_{F2} represents the vertical displacement of "F1" and "F2."

The total entry convergence "δ_T" was calculated by using Equation 3.5

$$\delta_T = u_{R2} - u_{F2} \tag{3.5}$$

Entry deformation due to the roof and floor deformations (δ_{r-f}) was calculated by Equation 3.6.

$$\delta_{r-f} = u_r - u_f \tag{3.6}$$

Uncontrollable convergence due to the pillar deformation (δ_p^u) was calculated by Equation 3.7.

$$\delta_p^u = \delta_T - \delta_{r-f} \tag{3.7}$$

The uncontrollable convergence (δ_{r-f}^u) due to the roof and floor elastic deformation cannot be simply estimated. It can be estimated by querying the bedding plane separation and slip. Finally, the total uncontrollable convergence (δ^u) can be calculated by Equation 3.8.

$$\delta^u = \delta_p^u - \delta_{r-f}^u \tag{3.8}$$

In STOP, the maximum allowable convergence refers to the gateroad deformation when the failure height exceeds the primary bolt horizon. In this study, the detached condition of the roof rock strata is determined by checking if roof strata sag is greater than 2.54 cm or not (Esterhuizen et al., 2020). And the roof detachment height is approximated by summarizing the thickness of all the detached rock layers.

Task 3.1.4: *Test reliability of STOP program with the new mine-specific, geology-dependent local GRC approach.*

After deriving the ground reaction curve from the model results, the developed GRC were manually input to STOP. STOP contains most of the applied standing support systems in the U.S. Any number of support system alternatives can be compared side-by-side to evaluate their relative performance under a common set of roof loading and convergence criteria. The STOP program with the new mine-specific, geology-dependent local GRC approach was tested and verified with the roof deformation and standing support measurements from verification case studies from CA-1 mine.

4.0 Research Findings and Accomplishments:

Our research findings and accomplishments are summarized by classifying them into the following categories: (i) development of a practical mine-specific, geology-dependent overburden loading model, (ii) development of ALPS-LAM script program, and (iii) development of local geology-dependent Ground Reaction Curve (GRC) approach for STOP.

Mine-specific, geology-dependent overburden loading model:

Below the statistical loading model and its verification are reported from Tuncay (2021) and Tuncay et al. (2022).

Statistical Loading Model

For each of the 13 field measurement case studies, at least four numerical models were constructed: three single panel models (with the original panel width, plus two parametric panel widths) and a model of consecutive panel (original panel width) mining. Depending on the depth of the mine, the number of panels for the consecutive panel mining models ranged between two and five. For shallow super-critical panels, two panels were modeled since the effect of consecutive panels was found to be negligible. For deeper mines, at least three panels were modeled to investigate the influence of consecutive panels on overburden stress distribution. For all numerical models, total load transfers to the pillar system, the gob, and the adjacent coal were calculated.

The statistical relationships between the independent parameters: the geological parameter, overburden depth, and panel width, and the dependent parameter, gob load percentages, were tested. The load percentages carried by the gobs were used as the statistical model response since the pillar loads depend highly on the dimensions of the chain pillar systems. After estimating the gob loads, the pillar loads can easily be calculated using the empirical load distribution function in ACPS or the analytical functions in LaModel.

Mine W-1 was omitted at this stage of the analysis since that is the only mine that utilizes a 2-entry yield pillar system and requires further investigation. Assumed as the most influential parameters, overburden depth and panel width were the variables considered in the analysis together with the critical span (S_i) of the overburden layers. For each case study, the critical span of every geological layer was calculated using Equation 3.2 mentioned in research task 1.1.3.

After examining various plots with different possible geological parameters, a new parameter called the total strong layer thickness (t_{str}) was introduced. The t_{str} parameter is the sum of the thickness of all layers with S_i/pw values larger than 0.1, where pw is panel width.

The cut-off value of 0.1 was initially selected as the best-fit value considering an exponential relationship between the parameter and gob load percentages. Later, the cut-off value of 0.1 was investigated for individual cases considering available geological information. This cut-off allowed us to distinguish known weak overburden mines from the mines with known competent overburden. Mines with thick and strong layers near the seam where those layers are known to withstand the mining-induced loads were also influential in verifying the cut-off value. The layers closer to the surface intrinsically show higher Si/pw since the span length calculation considers the weight above the layers. These layers might still deform or break, but the cut-off value was mainly selected to better differentiate the layers closer to the seam.

Figure 4.1 shows the calculated S_i/pw values for each stratigraphic layer for Mines NA-3, and CA-1 and the dashed red lines represent the selected cut-off value of 0.1. Mine NA-3 is an example of a supercritical panel with a known weak overburden. The sandstone layers in the overburden are known to cave due to the large panel width. For mine CA-1, there are strong and thick sandstone layers which are known to withstand mining of the panels. The panel widths are designed narrower for deeper mines, to ensure the stability of the strong layers.

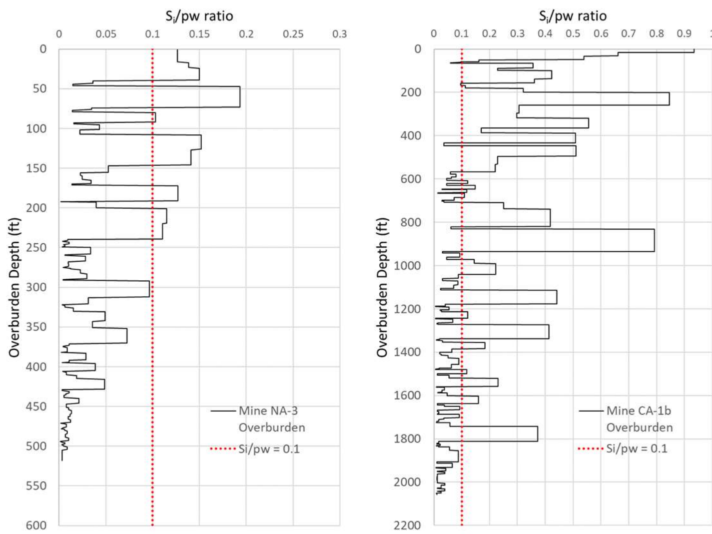

Figure 4.1. *Calculated Si/pw ratios for the overburden layers of mines NA-3 and CA-1 (Tuncay, 2021).*

In the statistical analysis, the ratio "t_{str}/pw" was found to exhibit a trend with the gob load percentage. It can be seen in Figure 4.2, there is an inverse relationship between the load transferred to the gob and the t_{str}/pw ratio and this ratio is selected to be used for the statistical analysis. In Figure 4.3, the exponential trend of the single-panel gob loads calculated from the field studies and the parametric runs with their respective t_{str}/pw ratios can be seen.

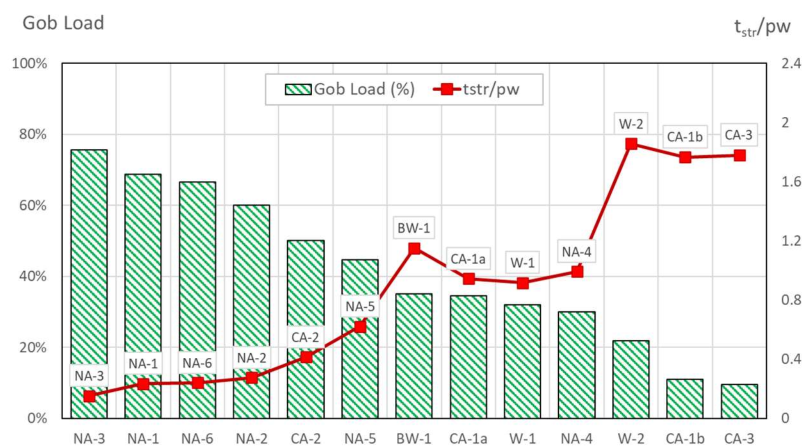

Figure 4.2. *Relationship between the tstr/pw parameter and the transferred gob load percentage (Tuncay, 2021).*

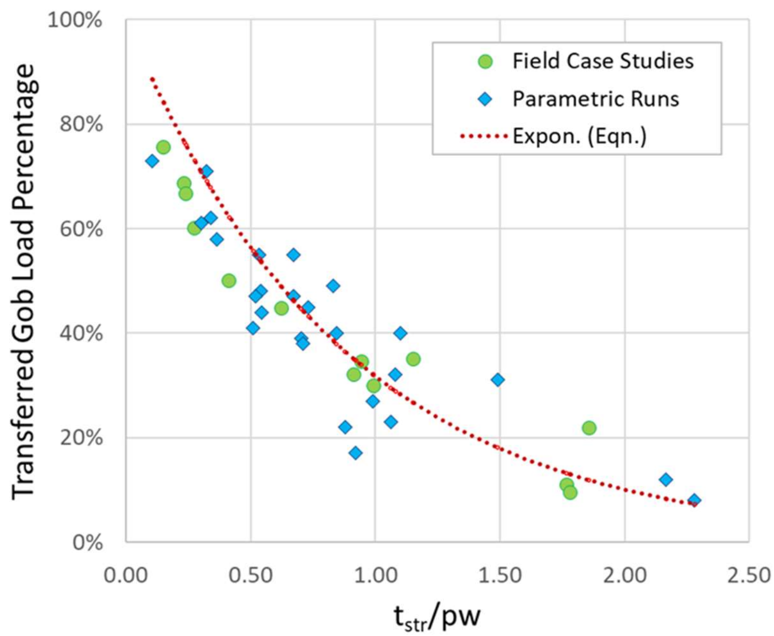

Figure 4.3. *Single-panel gob loads with respect to geological parameter t_{str}/pw (Tuncay, 2021).*

The gob load percentage for single-panel mining was selected as the basis of the estimation methodology. Since single-panel models also included the parametric models, there were more data points from single-panel model results. The load estimation for consecutive panels was built on top of the single panel estimations calculated by the exponential function presented in Equation 4.1 which was determined using the least squared error fit. The comparison of estimated single panel gob loads with the case study and parametric model results can be seen in Figure 4.4. The coefficient of determination (R2) was found to be 78.5%.

$$GOB(\%)_{single} = e^{-1.15\times\left({t_{str}}/{pw}\right)} \tag{4.1}$$

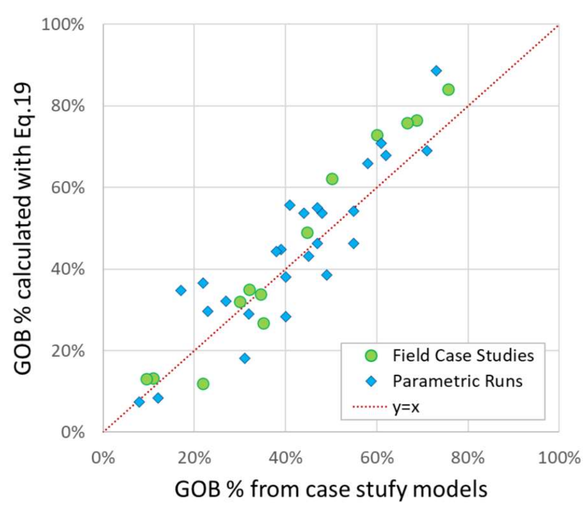

Figure 4.4. *Comparison of estimated single panel gob loads with the case study model results (Tuncay, 2021).*

Table 4.1. *Active panel and previous panel gob load percentages for deep cover consecutive panel models (Tuncay, 2021).*

	Panel 1	**Panel 2**		**Panel 3**		**Panel 4**		**Panel 5**	
	Single Panel	previous	active	previous	active	previous	active	previous	active
NA-5	44.7%	50.6%	46.3%	52.6%	46.2%	-	-	-	-
CA-1a	11.0%	54.8%	34.2%	56.0%	35.2%	57.4%	36.7%	-	-
CA-1b	34.5%	28.8%	20.9%	32.5%	20.0%	31.6%	20.7%	32.6%	20.6%
CA-3	9.5%	18.0%	15.4%	27.0%	17.3%	27.4%	16.6%	27.9%	18.7%
BW-1	35.1%	48.2%	34.8%	47.6%	35.5%	-	-	-	-
W-2	21.9%	31.6%	26.6%	31.5%	26.3%	31.1%	26.2%	-	-

As seen in Table 4.1, the gob load on the active panel increases when there is a previous panel mined. However, this increase is not dependent on the number of panels before the active panel, the increase in the gob load is only observed going from a single panel to the second-panel mining. To estimate the active panel gob loads, a consecutive panel factor (F_{cons}) to be multiplied with the single panel estimation is analyzed. Sum of squared error fit with the t_{str}/pw ratio was used to construct Equation 4.2 which can be used to calculate the consecutive panel factor. The factor can be assumed as 1 when the t_{str}/pw ratio is less than 0.87. This factor can then be introduced into Equation 4.3 to estimate the active panel gob percentage.

$$F_{cons} = 1.1\left({}^{t_{str}}/_{pw}\right)^{0.7} \qquad \text{for } {}^{t_{str}}/_{pw} > 0.87$$
$$F_{cons} = 1 \qquad \text{for } {}^{t_{str}}/_{pw} \leq 0.87 \tag{4.2}$$

$$GOB(\%)_{cons} = F_{cons} \times GOB(\%)_{single} \tag{4.3}$$

The gob loads of the active panels estimated with the new method compared to the results obtained from the case studies and the parametric runs showed a coefficient of determination (R^2) of 86.1% (Figure 4.5).

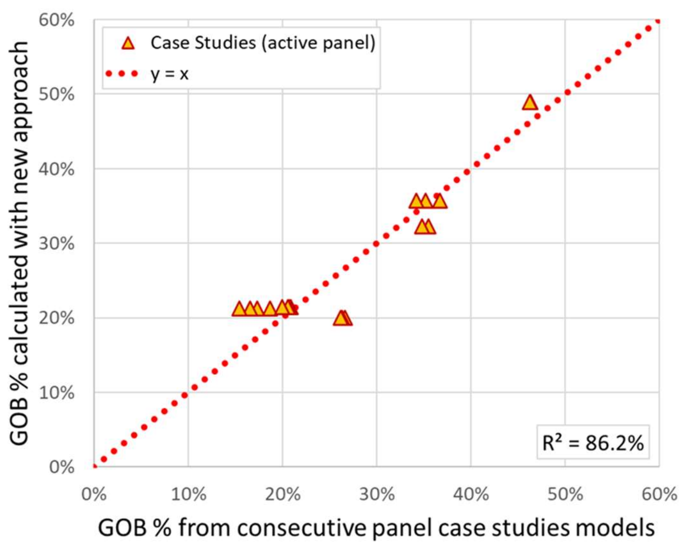

Figure 4.5. *Comparison of estimated active panel gob loads with the consecutive panel (Tuncay, 2021).*

After constructing the method for active panel gob load estimation, the next analysis was performed for the gob load percentages of the panel previous to the active one. The calculated gob load percentages for the panels on the tailgate side (Table 4.1) of the active panels were used to construct the equation. The calculated results showed that the major load increase on the gob occurred when the second panel was extracted. The increase in the gob load with consecutive panels after the second panel (3rd, 4th, and 5th panels) was found to be negligible (Tuncay, 2021). Equation 4.4 was found to be the most practical way to calculate the previous panel gob load percentage with an R^2 of 86.4% where the $GOB(\%)_{cons}$ value is calculated using Equations 4.2 and 4.3. The comparison of estimated previous panel gob loads with the case study and parametric model results can be seen in Figure 4.6.

$$GOB(\%)_{prev} = 1.35 \times GOB(\%)_{cons} \tag{4.4}$$

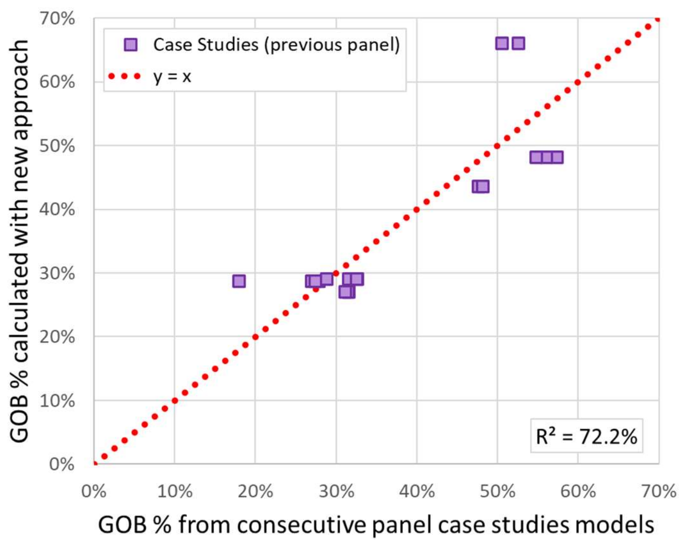

Figure 4.6. *Comparison of estimated previous panel gob loads with consecutive case study model results (Tuncay, 2021).*

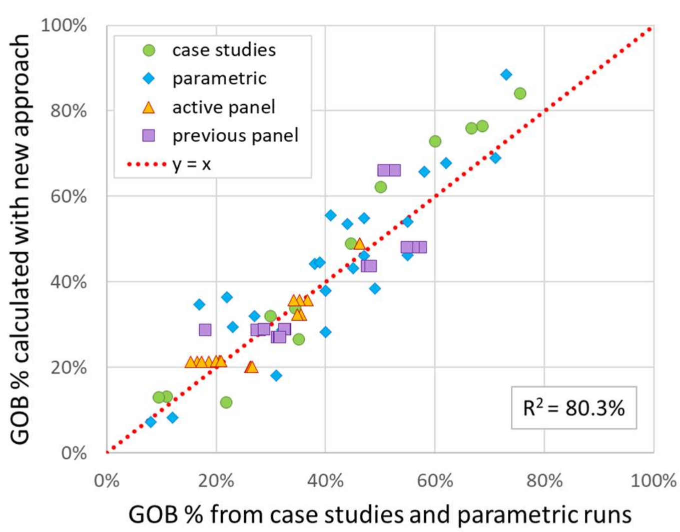

Figure 4.7. *Comparison of estimated gob load percentages (Tuncay, 2021).*

Figure 4.7 further shows all the available data points including the field case studies, parametric models, and consecutive models (both active panel and previous panel). The gob load percentages estimated using the new method were compared against the results calculated from the field measurements and the model runs. The coefficient of determination (R^2) was found to be 80.3%.

Special consideration was given to Mine W-1 as a 2-entry yield pillar system was utilized that affected the gob load percentages significantly. Most of the load transferred to the yield pillars is shed to the adjacent gob or solid coal because of the yield pillar design. To take the effect of yield pillars on the load transfer to the gob into account, additional factors are introduced to the Equations 4.1 through 4.4.

For the single panel condition, the calculated gob load for Mine W-1 did not exhibit a significant difference compared to the value estimated using Equation 4.1. The major difference in load re-distribution was observed for the consecutive panel models compared to other mines that utilize larger pillars. To estimate the active panel and previous panel load distributions, simple multipliers were selected using the least squared error fit method. Equations 4.5 and 4.6 where the F_{cons} parameter is still calculated using Equation 4.2 can be used to estimate the consecutive active and previous panel gob percentages for these cases.

$$GOB_{yp}(\%)_{cons} = F_{cons} \times GOB(\%)_{single} \times 1.5 \tag{4.5}$$

$$GOB_{yp}(\%)_{prev} = 1.6 \times GOB_{yp}(\%)_{cons} \tag{4.6}$$

The estimated gob loads for Mine W-1 were re-plotted into Figure 4.6 and Figure 4.7, and they are presented in Figure 4.8. Figure 4.9 shows all available data points including Mine W-1 and its parametric runs.

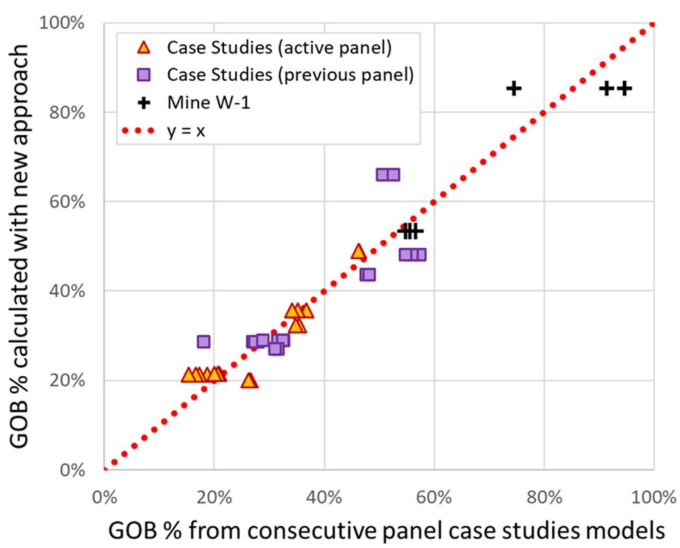

Figure 4.8. *Comparison of estimated active and previous gob load percentages with the consecutive case study model results including Mine W-1 (Tuncay, 2021).*

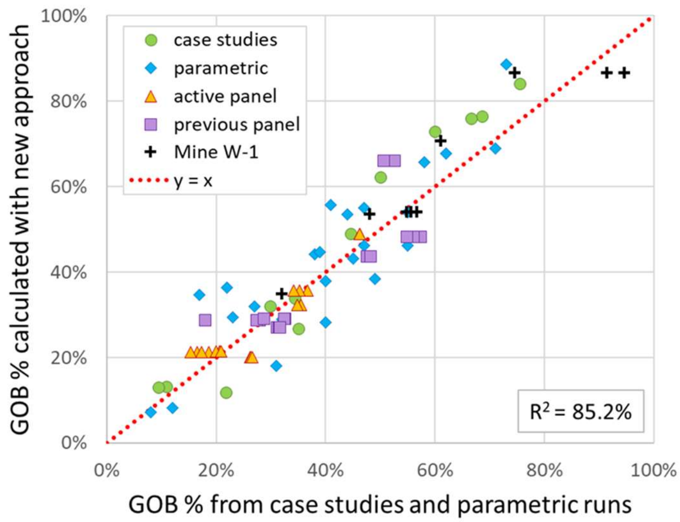

Figure 4.9. *Comparison of estimated gob load percentages with the case study and parametric model results including Mine W-1 (Tuncay, 2021).*

Statistical Loading Model Verification

This new method of gob load estimation can be easily implemented into LaModel through the gob wizard option in LaMPre 3.0. After de-selecting the "Use the Suggested Value" tick box and inputting the estimated gob load percentage into the gob wizard, the user can easily calculate and implement the appropriate final gob modulus that will match the estimated gob load percentage. This allows the practical implementation of the effect of overburden geology into a design tool capable of modeling complex mine geometries. By selecting at least two "Number of Gob Materials to be Defined" the user can input the estimated gob load percentages for both the active and previous panels and calculate and use the appropriate final gob moduli. To verify the loading model, field studies from Australia were modeled using LaModel and the stress measurements on the pillars and the adjacent coal were compared with LaModel results.

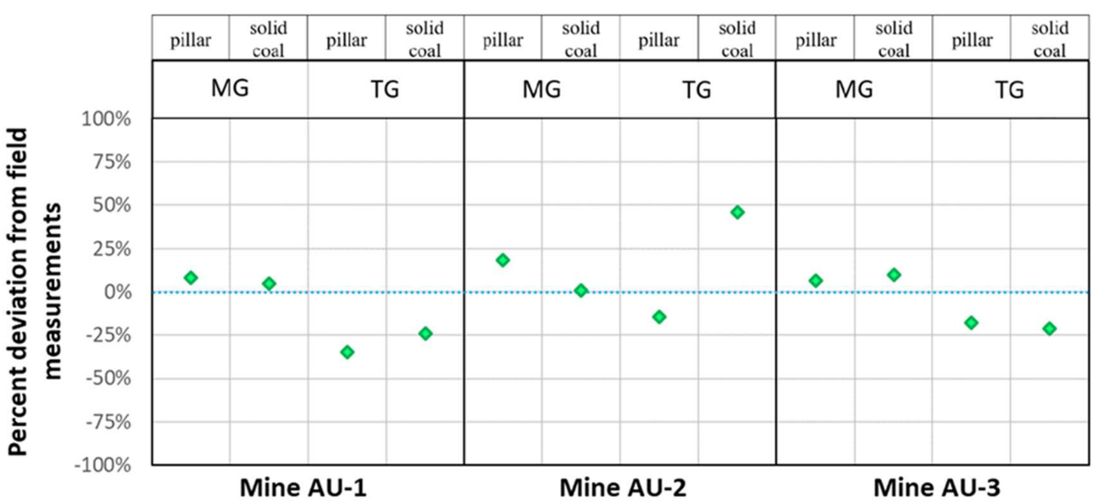

Figure 4.10. Comparison of LaModel results with the field measurements (Tuncay, 2021).

The comparison of stress measurements with the LaModel results was achieved by assessing the "area under the curve" for field measured and LaModel calculated stress profiles which gives the total load within that distance. The load increase on the pillars and the load increase on the solid coal were compared separately for both the maingate and tailgate loading conditions (Figure 4.10). The R^2 value was computed as 89.7% when we compare the estimated results with the measured values.

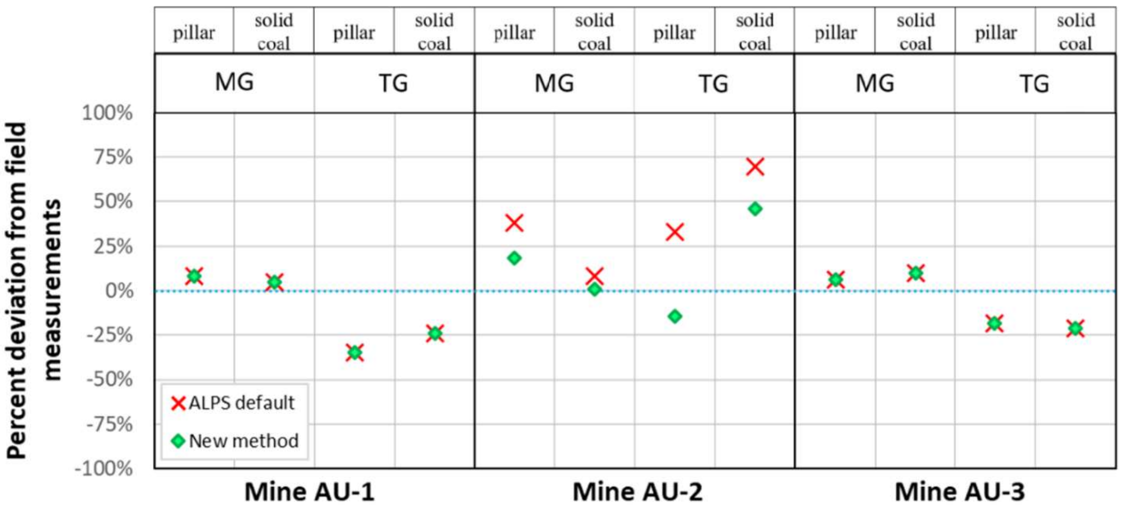

Figure 4.11. *Comparison of LaModel results with the field measurements, ALPS method of gob modulus calculation included (Tuncay, 2021).*

The next step was to compare the new method against the default ALPS method already implemented in LaModel. The models were re-run with the default gob percentages calculated by the LaMPre 3.0 and the areas under the stress profiles were calculated for the loads on the pillars and the solid coal. The R^2 was calculated as 82.8% and the percentage deviations from the field measurements are plotted in Figure 4.11. No difference was observed when the coal failed at the measurement points since both methods use the same coal properties with the same post-peak behavior.

ALPS-LAM script program:

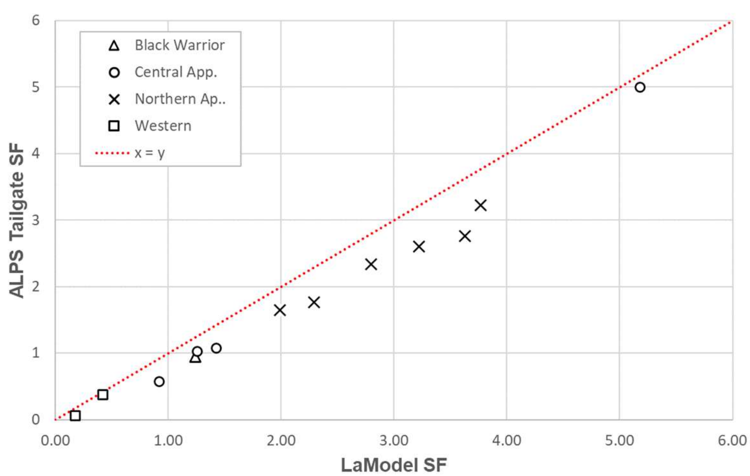

Figure 4.12. Comparison of ALPS-LAM results with ALPS method.

Figure 4.12 shows the comparison of the tailgate safety factors calculated by ALPS and new ALPS-LAM script program using the 13 longwall gateroad cases listed in section 3, task 1.1.1. Results indicate that overburden loads on the tailgate pillar system calculated by the laminated model is lower than the one estimated by ALPS tailgate loading factor. In this study default lamination thickness calibration approach developed by Heasley et al. (2010) was used in the analysis.

Development of Local Geology-Dependent Ground Reaction Curves (GRC):

Due to the limitation of the field measurements, six field measurement case studies from four underground coal mines in Eastern U.S. were used to develop and verify the modeling methodology discussed in task 3.1.2. All the case study mines are from the Appalachia coal basin. Four case studies were used for calibrating the model and developing the methodology. After completing the model calibration exercise, these four case studies that were used for calibration were re-evaluated to assess support performance using the final set of input parameters and modeling technique (Zhao, 2022). The remaining two cases were used to verify the modeling approach at different sites within the same mines (Zhao, 2022 and Zhao et al., 2022).

GRC Modeling Approach Calibration Results

Case study 1 – NA-3 Mine: NA-3 is located in Northern West Virginia and extracts the Middle Kittanning coal bed. The overburden depth ranges from 150 to 240 m with an average depth of approximately 180 m. Detailed discussions of the field instrumentation and monitoring results at NA-3 mine were published by Esterhuizen et al., (2017&2018), Gearhart et al., (2017), Tulu et al., (2017), and Zhao (2022).

The longwall panels in NA-3 mine are approximately 366 m wide, and length of the panels range from 1500 m to 2100 m. The mining height is typically 2.1 m, and the gateroad entry height is about 2.4 m at the monitoring site. The monitoring site was part of a three-entry gateroad system (Figure 4.13-right). It was located at the tailgate of Panel 2C, which is located at the mid-pillar site shown in Figure 4.13-left. Field instruments were installed a few days after the development of the gateroad (Tulu et al., 2018).

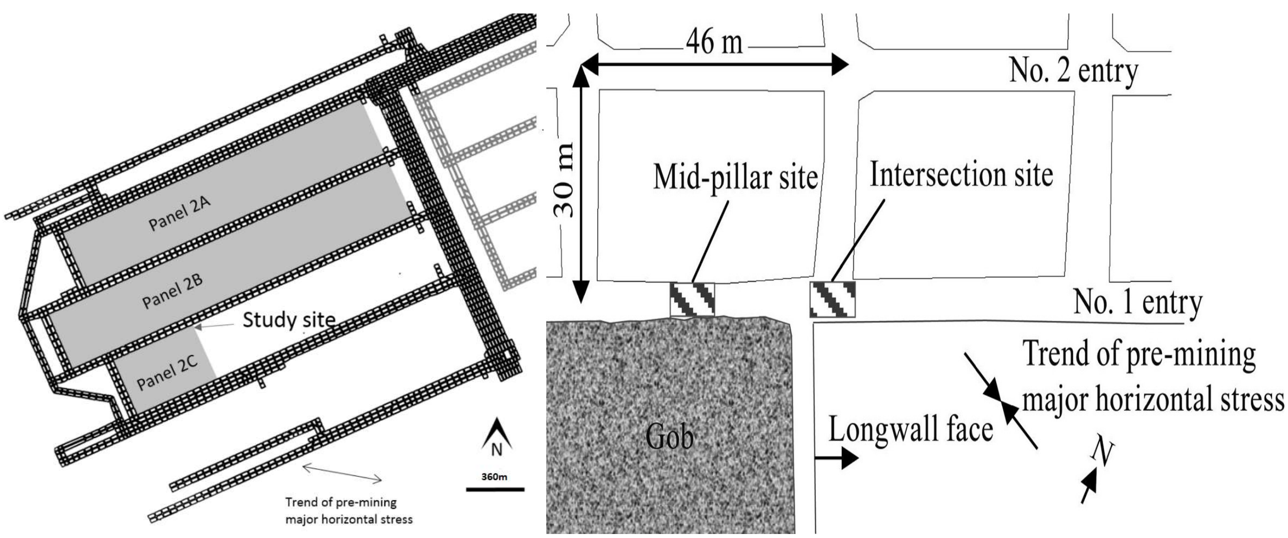

Figure 4.13. *Longwall panels layout and location of the study site, and plan view of the monitoring site (after, Esterhuizen et al., 2017).*

Mine NA-3 portrays the typical geologic features of the Allegheny Formation based on the geologic analysis and observations from exploratory drill core data. The immediate roof of the Lower Kittanning coalbed consists of dark gray to carbonaceous clay shale. Johnstown limestone layer is located above the carbonaceous clay shale layer. The overburden strata mainly consist of alternating sandstone and shale beds, and their thickness range from 6 m to 20 m (Zhao, 2022). To gather geotechnical parameters at the study site, rock core test was carried in the NIOSH Pittsburgh Mining Research Division (PMRD) rock mechanics laboratory (Esterhuizen et al., 2017). Tests were performed on the cores, which were taken from the vertical holes in the gateroad entry's roof and floor. The summary of material properties of the immediate roof/floor rocks are presented in Appendices, Table A.1.

In NA-3 mine, hollow inclusion cells were used for measuring the stress changes and in situ stresses. Three hollow inclusion cells (HI-cells) were installed over the panel, and the other three were installed over the pillar. The holes for the hollow inclusion cells were drilled at 30°, 45°, and 60° from the horizontal and each were approximately 9 m deep (Tulu et al., 2018). The HI-cell in the 60° hole over the panel was overcored to obtain the in-situ stress in the rock, and the major horizontal stress was measured as 7.58 MPa and the minor horizontal stress was measured as 5.86 MPa (Tulu et al., 2018). In addition to in situ stress and stress change measurements by HI-cells, various instruments were installed at the monitoring site to monitor the mining induced ground response. The instruments and their locations at the mid-pillar site are explained in Zhao (2022) and Tulu et al. (2018). There were: (i) cable bolt load cells, (ii) four hydraulic load cells installed on four wooden cribs, (iii) one 2.4 m long extensometer, and (iv) one 6.1 m extensometer. Therefore, in NA-3 mine, roof sag, cable bolt loads, and wooden crib loads were monitored and recorded by the dataloggers, until the panel face reached the monitoring site (Tulu et al., 2018).

The entry-scale model of the measurement site was generated and used to derive the ground reaction curve (GRC) under the changing stress states. The model can approximate ground response close to the field observation only if the behavior of roof strata is modeled with sufficient realism. Roof strata behaviors, including roof rock deformation, stress distribution measurement and support loading measurement shown in Figure 4.14 were re-evaluated by the calibrated model and compared with the field measurements. Figure 4.14-right shows the comparison of the cable bolt loads measured in the field and calculated by the model. The roof deformation and bolt loads approximated by the model were within the range of the field measurements. Zhao (2022) and Zhao and Tulu (2021) discussed the model calibration and results of NA-3 case study in detail.

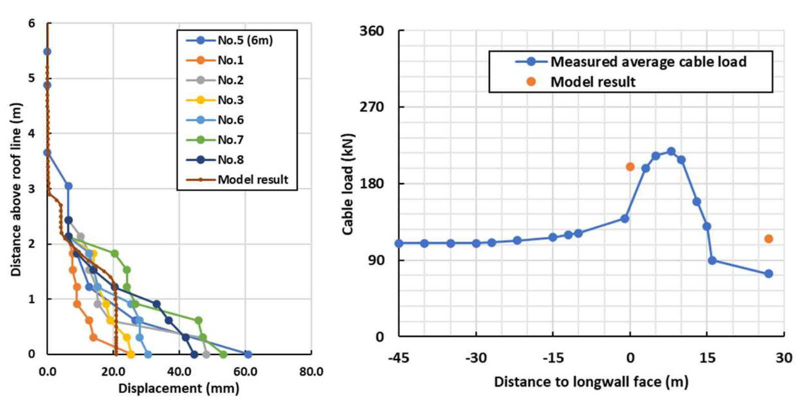

Figure 4.14. *Comparison between model calculated roof deformation and field measurement, and cable bolt loads (After Esterhuizen et al., 2017) (tailgate stress state).*

For NA-3 mine, ground reaction curves for different loading conditions were developed. Figure 4.15-left shows GRCs developed from the model results under different stress states. Figure 4.15-right illustrates the Support Response Curve (SRC) of the standing support system used in NA-3 mine, and the GRC derived from the entry-scale model (Tailgate stress state). The loading pressure applied on standing supports and the resultant entry convergence can be evaluated by finding the intersection point between the ground reaction curve and the support response curve. This mine used 9-point wood cribs spaced on a 122-cm center to center spacing for standing support at the instrumentation location. Due to erratic crib loading measurements taken in the mine, a supply of timber blocks from the mine were used to construct comparable cribs for testing in the NIOSH Mine Roof Simulator to measure the load-displacement characteristics. The support timbers were of poor quality and did not represent a well-constructed quality wood crib. The response of the three cribs varied significantly with the gray line representing the average performance that was used to approximate the standing support performance at the monitoring site (Figure 4.14-right). The field measured support loading density was 370 kN/m (as indicated by the dashed red line) when the longwall panel face reached the monitoring site, and the average crib loading of 320 kN/m at the intersection of the GRC (Figure 4.15-right) indicates that the model closely approximated the actual support loading density. It can be concluded that the model results fit reasonably well with the field measurement.

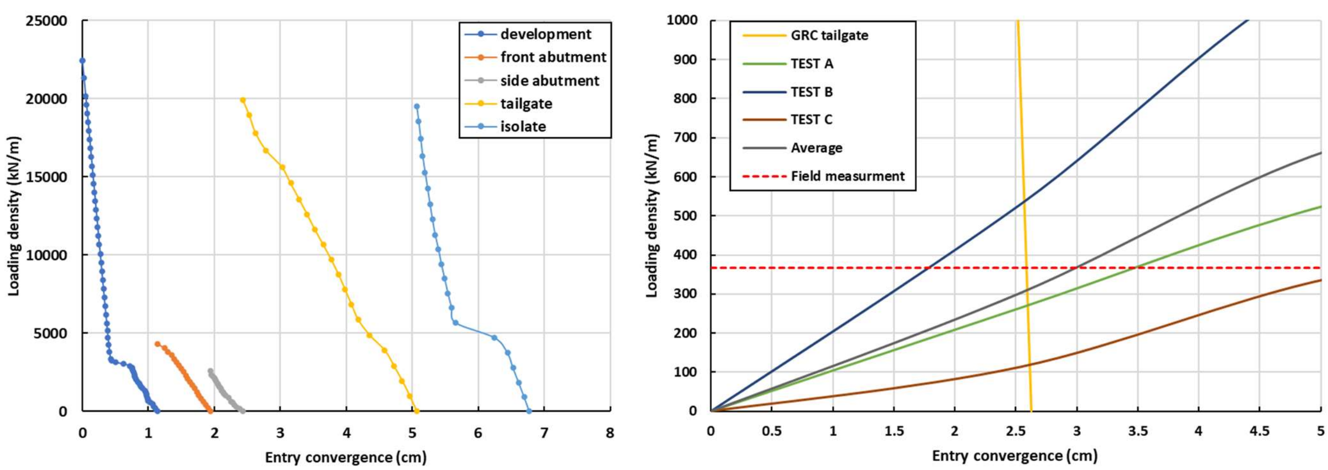

Figure 4.15. *GRCs under various stress states in mine NA-3, and wood crib performance evaluation (after, Zhao, 2022).*

<u>*Case study 2 – NA-2 Mine:*</u> NA-2 is located in Northern West Virginia and extracts the Pittsburgh coal seam. Detailed discussions of the monitoring results and the background information related to NA-3 mine can be found in Zhao (2022), Gearhart et al., (2017) and Zhang et al., (2018). The longwall panels in NA-2 mine are approximately 356.7 m wide, and the length of the panel is about 1220 m. The coal seam is approximately 2 m thick. There is a claystone layer, which was about 0.3 m thick, above the top of the coal seam. During the development stress state, the weak claystone was mined, and the entry height was increased to 2.3 m (Zhang et al., 2018). The panel configuration of NA-2 mine was right-handed, and the three-entry gateroad system was employed between two longwall panels (Figure 4.16-left).

The immediate roof generally consisted of shale, rider coal, claystone, and sandstone or limestone rock layers. A dark shale layer, which is always interbedded with some thin coal streaks, is located above the weak claystone layer (Figure 4.16-right). The thickness of the dark shale layer normally ranges from 2 m to 3 m. Then, a laminated sandstone layer was observed on the top of the dark shale rock and followed by an approximately 2.5 m thick claystone rock strata. At the end of the scope hole, a strong limestone rock layer was reported (Zhang et al., 2018). Thick claystone and shale rock layers were also observed in the floor of NA-2 mine. Because the laboratory test results for mechanical rock properties are not available in NA-2 mine, rock properties from nearby mines (Esterhuizen et al., 2018) and the rock properties database for U.S underground coal mines (Tulu et al., 2017) were used to initially estimate the rock strength.

In NA-2 mine, various instruments were installed at the monitoring site to monitor the mining-induced ground response. The location of the instrumentation site was in the middle entry of the three entry gateroad and the layout of the instrumentation are shown in Zhang et al. (2018). There were: (i) four cable bolt load cells, (ii) three six-channel extensometers, and (iii) six Borehole Pressure Cells (BPCs). Roof sag and cable bolt loads were monitored and recorded.

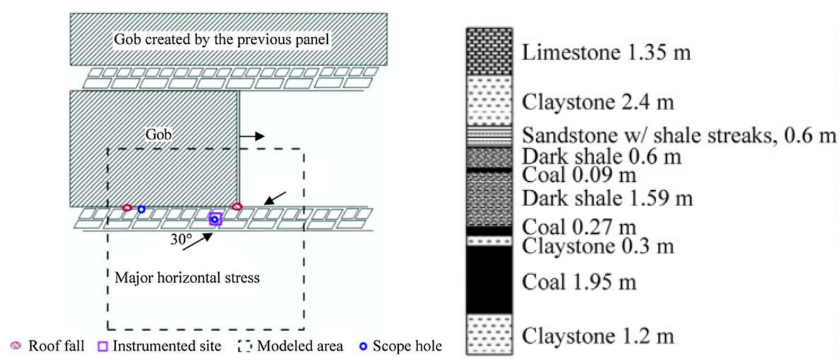

Figure 4.16. *Panel layout and the instrumentation site, and scope hole at the instrumentation site (after, Zhang et al., 2018).*

For Mine NA-2, rock strata behaviors, including roof rock deformation and cable bolt loading, were re-evaluated by the calibrated model and compared with field measurements. Figure 4.17-left shows the roof rock deformation calculated by the model when the longwall face reached the study site, and Figure 4.17-right shows the cable bolt loads calculated by model and measured on the field. It can be observed that the model approximated roof rock deformation and bolt loads fairly accurately.

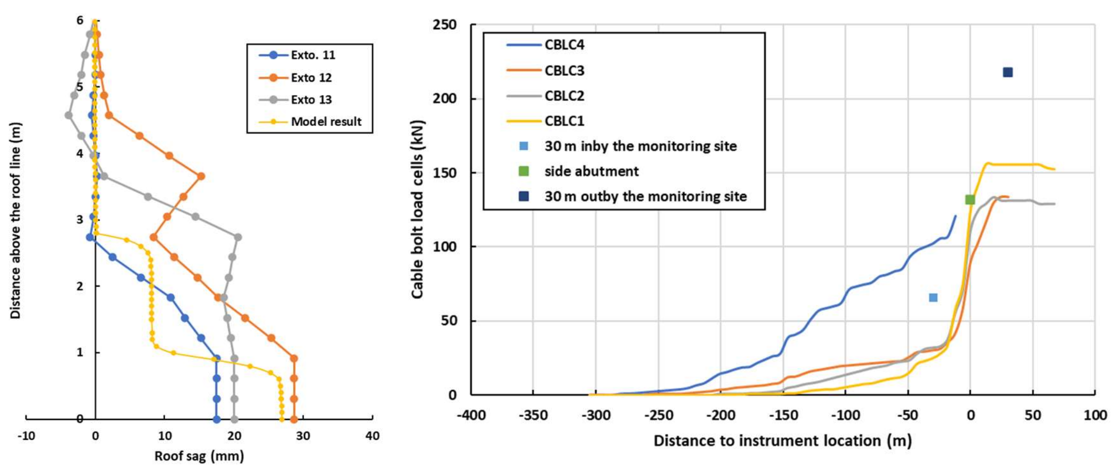

Figure 4.17. *Comparison between model calculated roof deformation and cable bolt loads with field measurements in NA-2 mine (after, Gearhart et al., 2017 and Zhang et al., 2018).*

The ground reaction curve that was developed for multiple stress states is shown in Figure 4.18. Since no standing support was used in this middle entry application, the performance of the roof bolts associated with the measured roof deformation were used to aid in the validation of the GRC.

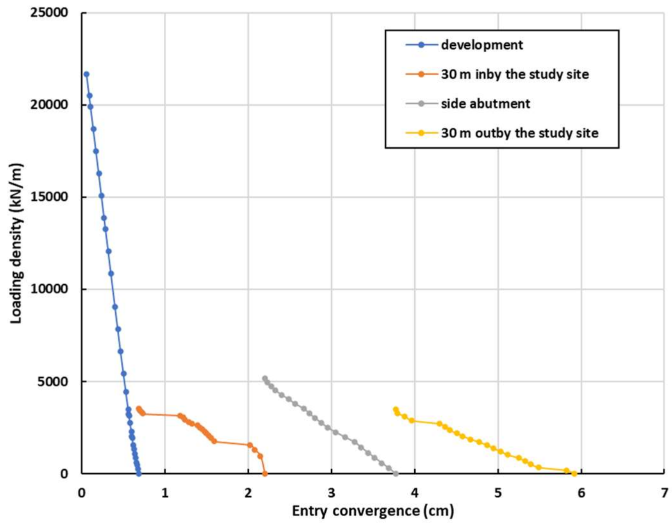

Figure 4.18. *Ground reaction curves under various stress states in NA-2 mine (Zhao, 2022).*

<u>*Case study 3 – NA-6 Mine:*</u> NA-6 is in Greene Country of Southwestern Pennsylvania and extracted the Pittsburgh coal bed. The average overburden depth of NA-6 is approximately 200 m. Detailed discussions of the field instrumentation and monitoring results at NA-6 mine can be found in Gale et al., (2004) and Oyler et al., (2004). Entries in NA-6 were approximately 2.1- 2.4 m high and 4.9 m wide. The selected study area was part of a three-entry gateroad system (Figure 4.19-left). Oyler et al., (2004) and Gale et al., (2004) collected most of the ground response information from B array and C array (Figure 4.19-right). B array, which is located at the adjacent crosscut between panel 10 North and panel 11 North, was selected in this study.

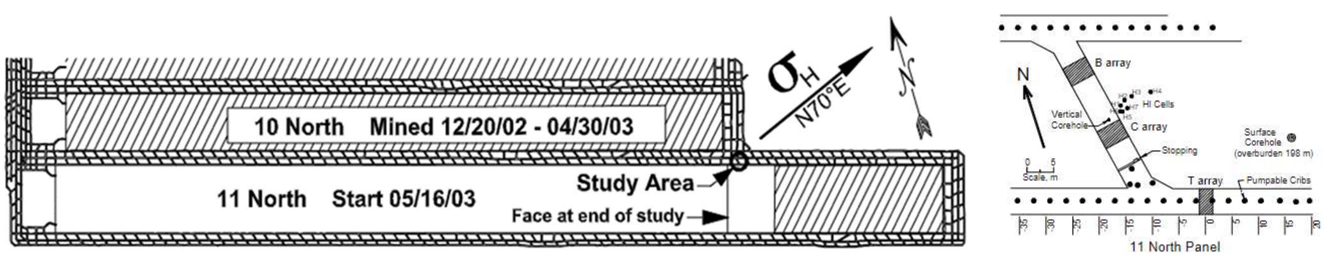

Figure 4.19. *Layout of NA-6 mine and view of the monitoring sites (Oyler et al., 2004).*

A vertical core hole was drilled at the study site to analyze the immediate roof geology (Oyler et al., 2004). The core hole is approximately 6 m long and located between B array and C array (4.20-right). A geologic column of the immediate roof at the study site was mapped based on the information from the drilled core hole (Oyler et al., 2004; Barczak et al., 2003). The immediate roof of the study site can be roughly divided into three different units (Oyler et al., 2004): (1) a sequence of coals and weak black and gray shales in the lowest 2.7 m, (2) a slightly stronger claystone and fireclay sequence from 2.7 to 5.4 m, and (c) a significantly stronger limestone layer above 5.4 m from roof line (Figure 4.20-left). The vertical core hole at the study site barely reached the limestone rock layers, and the nearby surface core holes indicated that the immediate roof limestone layer may be interbedded with some weak shale layers. The thickness of the whole limestone layer was estimated to be greater than 30 m (Barczak et al., 2007). Since the laboratory rock test data are not available, immediate roof rock mass properties were estimated based on the recorded rock type and rock strata condition. Rock properties database, which was constructed by Tulu et al., (2017) for U.S underground coal mines, was utilized to estimate the rock mass strength.

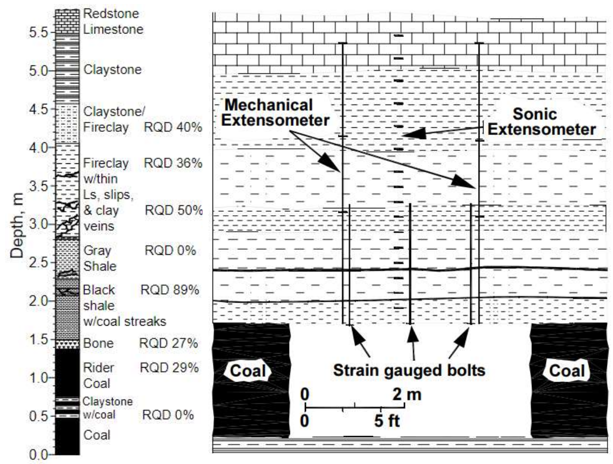

Figure 4.20. *Core log from the study site and locations of extensometers at array B in NA-6 mine (after, Oyler et al., 2004).*

Vertical stress and horizontal stress change were measured and recorded by seven CSIRO Hollow Inclusion (HI) cells, which were installed over pillar (Oyler et al., 2004). The HI cells were installed in a fan pattern. The most comprehensive roof movement measurement was provided by multi-point sonic extensometer (Figure 4.20-right). Roof sag was measured approximately every 0.3 m up to 5.8 m above the gateroad roofline. However, the sonic extensometer can only be manually read at that time (Oyler et al., 2004). Loads on the lower unrouted portions of the combined bolts were measured during the longwall panel retreat process (Figure 4.20-right) (Oyler et al., 2004). The Field Report indicated roof sag measurement was stopped when the longwall face reached 26 m from the study site, because the deteriorating roof conditions affected the reading activities (Gale et al., 2004).

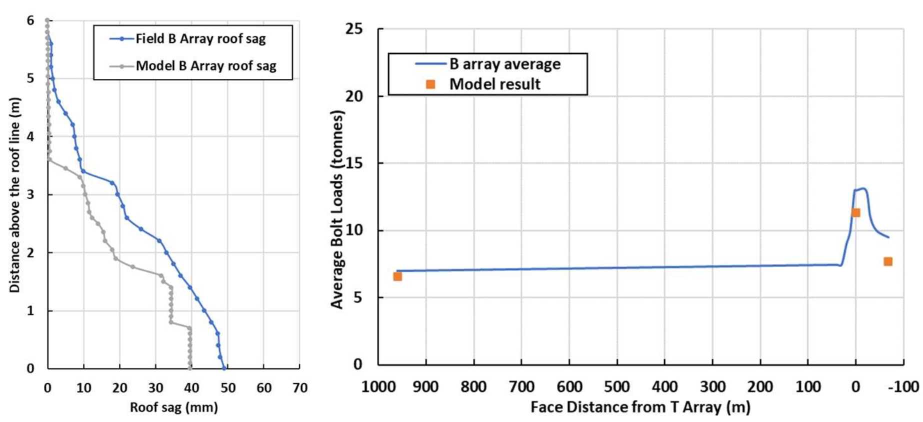

Figure 4.21. *Comparison between model calculated roof deformation, bolt loads and field measurements (after, Zhao, 2022).*

Roof strata response, including cable bolt load and roof rock deformation, were re-evaluated by the calibrated model and compared with the filed measurements (Figure 4.21). It can be seen that the model approximated roof rock deformation and bolt loads close to field measurements. For NA-6 mine, two stress states were used for developing the ground reaction curves (Figure 4.22). Without a standing support in this area, the roof bolting and roof deformation information was used for the validation on the local GRC.

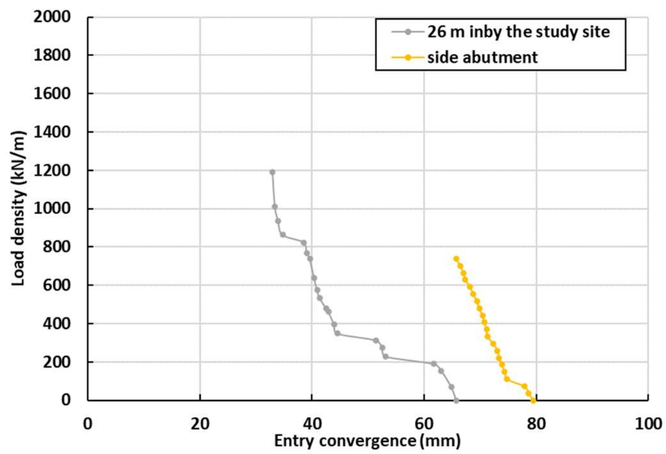

Figure 4.22. *Ground reaction curve under two stress states (Zhao, 2022).*

<u>*Case study 4 – CA-1 Mine:*</u> CA-1 is from the southwest corner of Virginia and extracts the Pennsylvanian Age Pocahontas No.3 coal seam. The overburden depth ranges from 410 m to 730 m. The strike and dip of the Pocahontas No.3 coal seam are N38E and 0.5°, respectively. Detailed discussions of the monitoring results and background information can be also found in Esterhuizen et al., (2018), Klemetti et al., (2019), and Su et al., (2014). The longwall panels in CA-1 mine are approximately 214 m wide, and the length of the panels are about 3050 m long. CA-1 mine employs a four-entry gateroad system, which is comprised of a yield-abutment-yield pillar system (Figure 4.23-left).

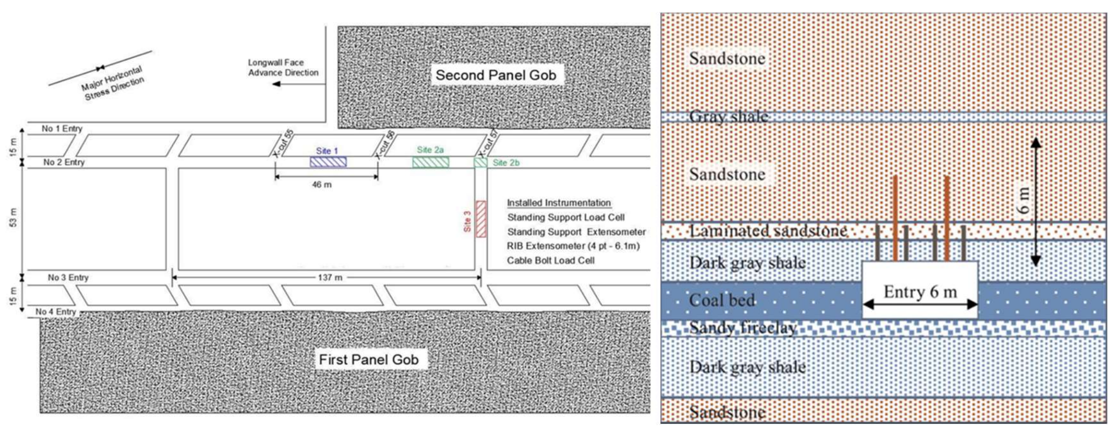

Figure 4.23. *Mine layout and geologic profile of roof and floor strata at the monitoring site (After, Klemetti et al., 2019 and Esterhuizen et al., 2018).*

The typical immediate roof at the study site consists of various types of shales and sandstones. The Pocahontas No.4 coal seam is usually 0-60 cm thick, and normally 15 m above the Pocahontas No.3 seam (Esterhuizen et al., 2018; Su et al., 2014). Rock layers between the gateroad roof line and bolted horizon are some silty dark gray shale layers that vary from 0 to 2.4 m thick. Above these dark gray shale layers, there is thinly to thickly laminated sandstone, which contains mica and coal streaks. This sandstone is approximately 0 to 11 m thick and was named sandstone 1 by CA-1 mine. Above the sandstone 1 rock layer, there is a gray shale layer. The thickness of this gray shale layer ranges from 0 to 1.7 m. Above this gray shale, another strong sandstone layer was observed, which was named sandstone 2 by CA-1 mine. In some locations, sandstone 1 can combine with sandstone 2, if there is no gray shale was observed between these two sandstone layers (Esterhuizen et al., 2018; Klemetti et al., 2019). Figure 4.23-right shows the visualization of local geology determined by borescope observations in an inspection hole at the monitoring site. Tests were performed on the cores taken from the vertical holes in gateroad entry's roof and floor. The summary of material properties of the immediate roof/floor rock are presented in Appendices, Table A.2 (Esterhuizen et al., 2018).

Several instruments were installed to monitor the behavior of the pillar, roof, and ribs of the No.2 gateroad entry. There were: (i) four, six, and eight-point roof extensometers, (ii) borehole pressure cells (BPC), (iii) bi-axial stress meters, (iv) Hollow Inclusion Stress cells (HI-Cells), (v) multipoint rib extensometers – four points, (vi) standing support load cells (J-Packs), (vii) standing support convergence monitors (string pots), (viii) cable bolt load cells, and (iiv) rib bolt load cells (Klemetti et al., 2019).

There is no report clear mentioning of the time when pumpable supports were installed in CA-1. In this study, it was assumed that the pumpable supports were installed after the side abutment loading step. The ground reaction curve under the tailgate stress state was developed (Figure 24).

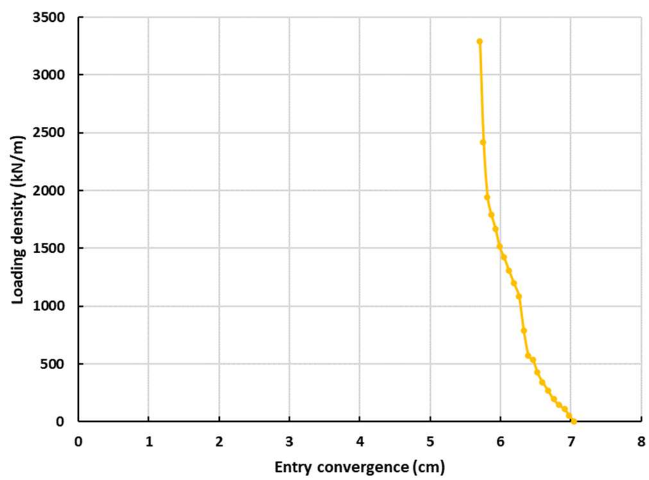

Figure 4.24. *Tailgate GRC developed for tailgate stress state (after, Zhao, 2022).*

<u>*GRC Modeling Approach Verification Test Cases*</u>

In this section, two verification case studies (a successful and an unsuccessful standing supports designs), which are from CA-1 mine, were used for verification of the modelling methodology. This verification study is aimed to validate the modeling methodology and demonstrate that the ground reaction curve (GRC), which is derived from the entry-scale model, can be used to assess the performance of standing supports.

<u>*Verification Case Study 1-Successful Design:*</u> In verification case 1, a bleeder entry from CA-1 mine was selected to validate the proposed modeling methodology. At the study site, a double row of pumpable

supports with 1.58 m spacing at bleeder entries successfully support the entry roof. Figure 4.25 presents the layout and location of the study site. The average overburden depth at the study site is about 610 m. The longwall panels in these districts are 213 m wide and 3048-3505 m long. The bleeder entries are approximately 120 m away from the startup room, separated by barrier pillars. The bleeder system consists of a set of four entries on 30.5 m centers with crosscut spacing varying from 35-52 m (Klemetti et al., 2017).

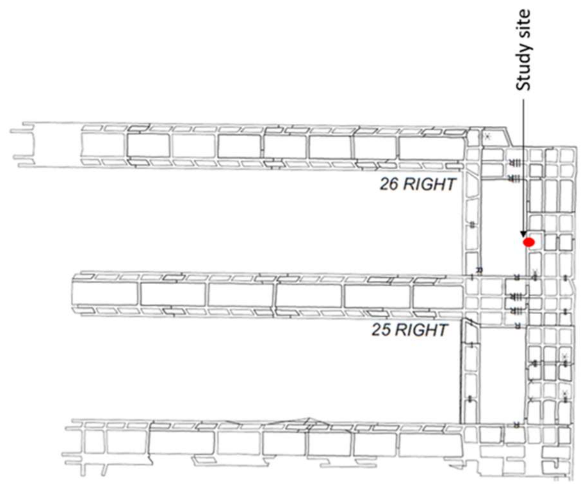

Figure 4.25. *Location and layout of the verification case 1 (After, Klemetti et al., 2017).*

Stress change along the bleeder system was fully analyzed by a panel-scale model from Klemetti et al., (2017). Klemetti et al. analyzed two loading conditions: development and second panel loading conditions. The development phase represents the time when the bleeder entries were fully excavated, and the second panel phase refers to the stage when both "Panel 25 Right" and "Panel 26 Right" had been completely mined.

Table A.3, in appendices, summarizes lithology in the immediate roof and floor. Immediate roof and floor rock mass information was gathered from nearby core logs (Esterhuizen et al., 2017 & Klemetti et al., 2017).

Figure 4.26-left shows the developed ground reaction curves for two loading conditions. Because of the strong roof rock in the immediate roof strata, only minor roof sag was measured at the study site. Klemetti et al., (2017) indicated that a double row of 61-cm diameter pumpable supports was installed at the study site. It was also reported that the designed standing support can successfully controlled the bleeder entry roof condition when panel 26 Right was completely mined. The loading of a double row of pumpable supports as a function of convergence as determined from tests in the MRS is plotted against the ground reaction curve. Only an average of 0.3 cm pumpable support convergence was observed at gateroad roof. The intersection of the ground reaction curve and support response curve is close to the field measurement providing verification of the methodology and results. It is also noted that the support loading at which equilibrium is achieved is far less than the pumpable support yield point and the resultant support convergence.

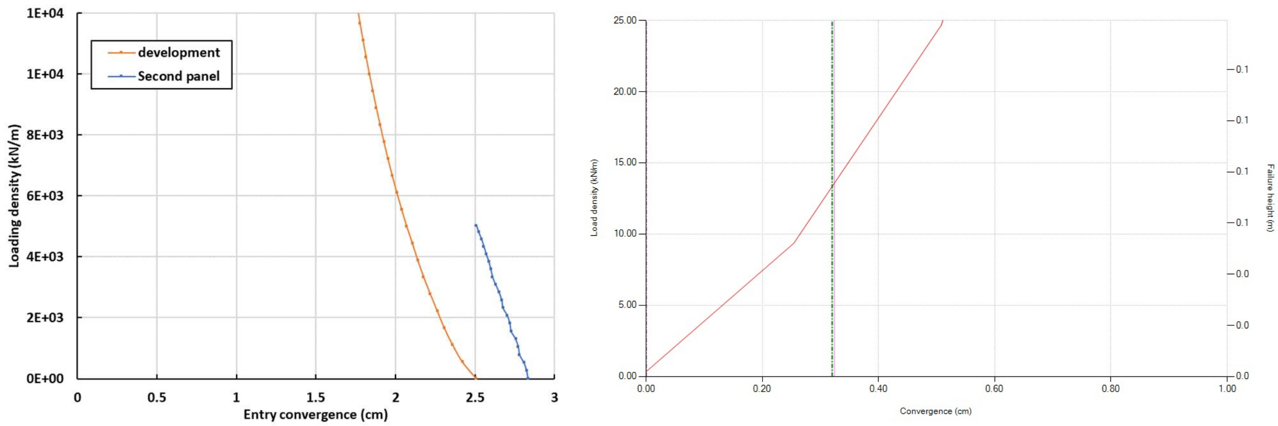

Figure 4.26. *Ground reaction curve under various stress states and STOP approximated standing support performance (after, Zhao, 2022).*

<u>*Verification Case Study 2-Unsuccessful Design:*</u> Figure 4.27 shows the layout and location of the second verification case study site. The study site is located between two longwall panels and the average overburden depth is about 610 m. A four-entry gateroad system, which is comprised of a yield-abutment-yield pillar system, was employed between panel 1 East Dev and panel 2 East Dev. The typical mining height at the study site is about 2.7 m. Table A.4, in appendices, presents the immediate roof/floor rock mass lithology.

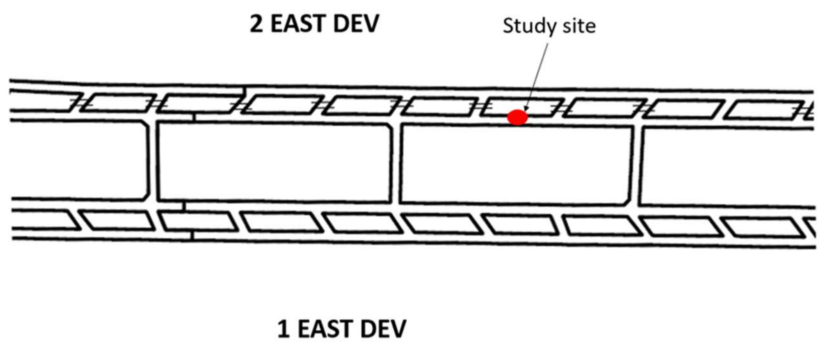

***Figure 4.27**. Gateroad layout and study side (after, Zhao, 2022).*

Ground reaction curves under development and tailgate stress states were developed (Figure 4.28-left). Batcher et al., (2021) indicated that a double row of 76-cm diameter pumpable support was installed at the study site and failed to control the entry roof when the nearby panels approached the study site. To reproduce this unsuccessful support plan and validate the modeling methodology, the model-derived ground reaction curve under the tailgate stress state was applied in STOP. A double row of 76-cm diameter pumpable support with 160 cm center-to-center spacing was utilized in STOP.

Figure 4.28-right shows the model approximated pumpable support performance. The pink line represents the ground reaction curve under the tailgate stress state and the red line represents the pumpable support response curve. As observed, the required support loading density is much larger than the pumpable support capacity. Therefore, it is concluded that a double row of pumpable supports would fail to control the roof in this condition.

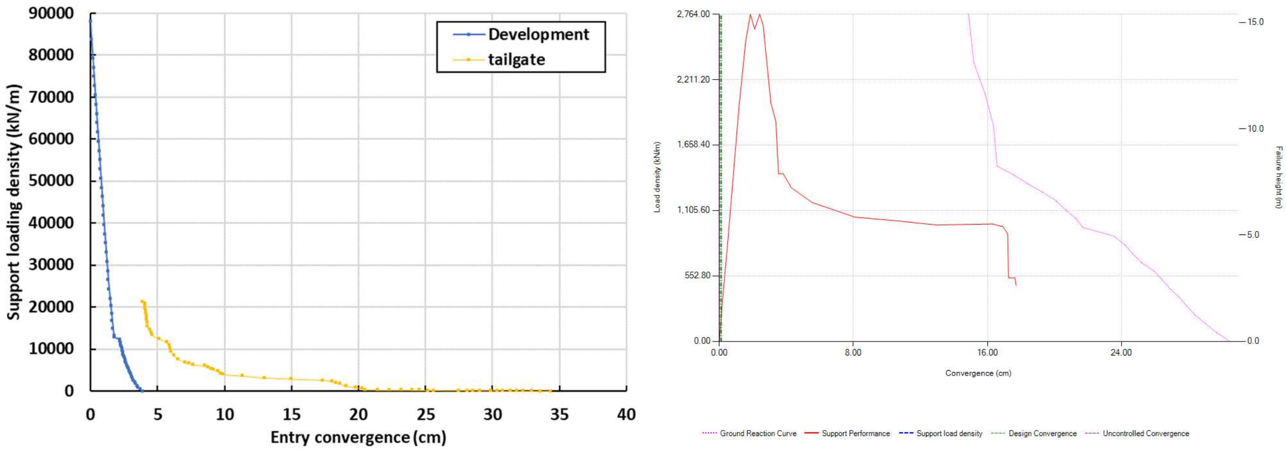

Figure 4.28. *Ground response curve under various stress states and STOP approximated pumpable support performance(after, Zhao, 2022).*

<u>Application of the STOP Program Using the Ground Reaction Curve</u>

The Support Technology Optimization Program (STOP) provides an engineering foundation for support application and a means to examine and compare new support technologies. The fundamental goal of the program is to determine the amount of support necessary to provide equilibrium of a mine entry at a designated convergence. This can be achieved by using the ground reaction curve as the design criteria for the support system. STOP Disclaimer – The STOP software is currently undergoing interface updates, and a tutorial for the use of STOP can be found in the new vesion whan it is published on a designated platform.

The ground reaction data can be entered into the STOP program through an Excel spreadsheet. The four ground reaction curves developed in this project are listed in the appendix. It should be noted that the ground reaction curves are unique to a set of mining conditions but can be used to examine support design under any similar conditions.

<u>Example 1</u>

As an example, we will repeat the analysis of Unsuccessful Design in Verification Case Study 2 using the STOP program and analyze alternative (more successful) support system options. First, the ground reaction curve from the Excel spreadsheet (Table A4 in Appendix A) for this case study is loaded into the STOP program. The methodology to insert a new ground reaction curve will be available in the STOPP program when the new version is published. The design convergence is selected and inputted, which creates a computed support load density associated with the ground reaction curve. It is recalled from the discussion on page 31, that included in the ground reaction information is the uncontrollable convergence and the maximum allowable convergence parameters. The uncontrollable convergence is a measure of the overburden and yielding pillar loading that cannot be fully controlled by a standing roof support system. The maximum allowable convergence is a measure of the onset of failure of the roof above the bolted horizon. For this example, the design convergence of 2.12 inches is chosen which is also the maximum allowable convergence indicating this is the minimum amount of support necessary. The program calculates that the associated support the density is equal to 170.5 tons/ft (see Figure 4.29). This deep cover mine has a weak roof condition, which coupled with a yield pillar situation, makes roof support challenging. As noted in the case study example above, the current pumpable roof support system was not working well.

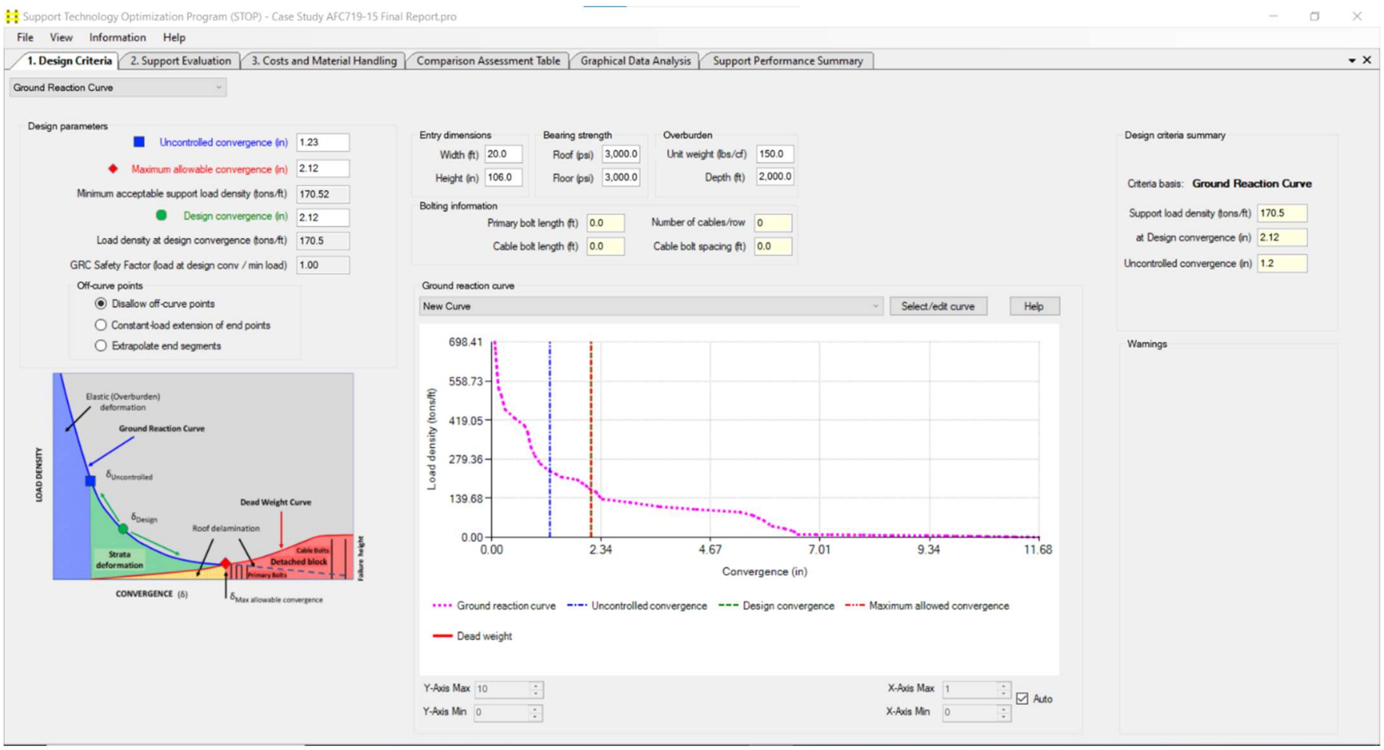

Figure 4.29. STOP ground reaction curve for Example 1 mine.

Next, the support system is selected for analysis. In this case study, the mine used a double row of 30-in diameter pumpable supports placed on a center-to-center spacing of 8 ft. The load-displacement response of the support system is then plotted on the graph. Visually, it is clear that this support system intersects the ground reaction curve near the end of its loading capability and far beyond the design convergence of 2.12 inches, indicating that the support system is inadequate to confidently achieve equilibrium of the mine entry (see Figure 4.30). Clearly this type of support system does not have the yield capability to perform in a high yield environment associated with a yield pillar gate road design.

Next several alternative support systems are considered for analysis including a higher capacity modern-day pumpable support, a Can support, and a Link-N-Lock wood crib. A double row of supports is used in each application. The program calculates the required support spacing necessary to achieve the designated load density of 170.5 tons/ft at the design convergence of 2.12 inches. results are shown in the three figures below and are summarized as follows:

- Modern high-capacity pumpable support – 33.7 in spacing (Figure 4.31)
- 30-in Can support – 27.5 in spacing (Figure 4.32)
- 60-in Link-N-Lock wood crib – 30.7 in spacing (Figure 4.33)

This extremely high density of support is uncommon and is an indication of a challenging situation for conditions in this particular mining area. It would be suggested that alternative (cable) bolting application to be considered. In terms of the standing support options, the Link-N-Lock wood crib has the highest yielding capacity followed by the Can Support. Both would likely provide better support than the current pumpable support system.

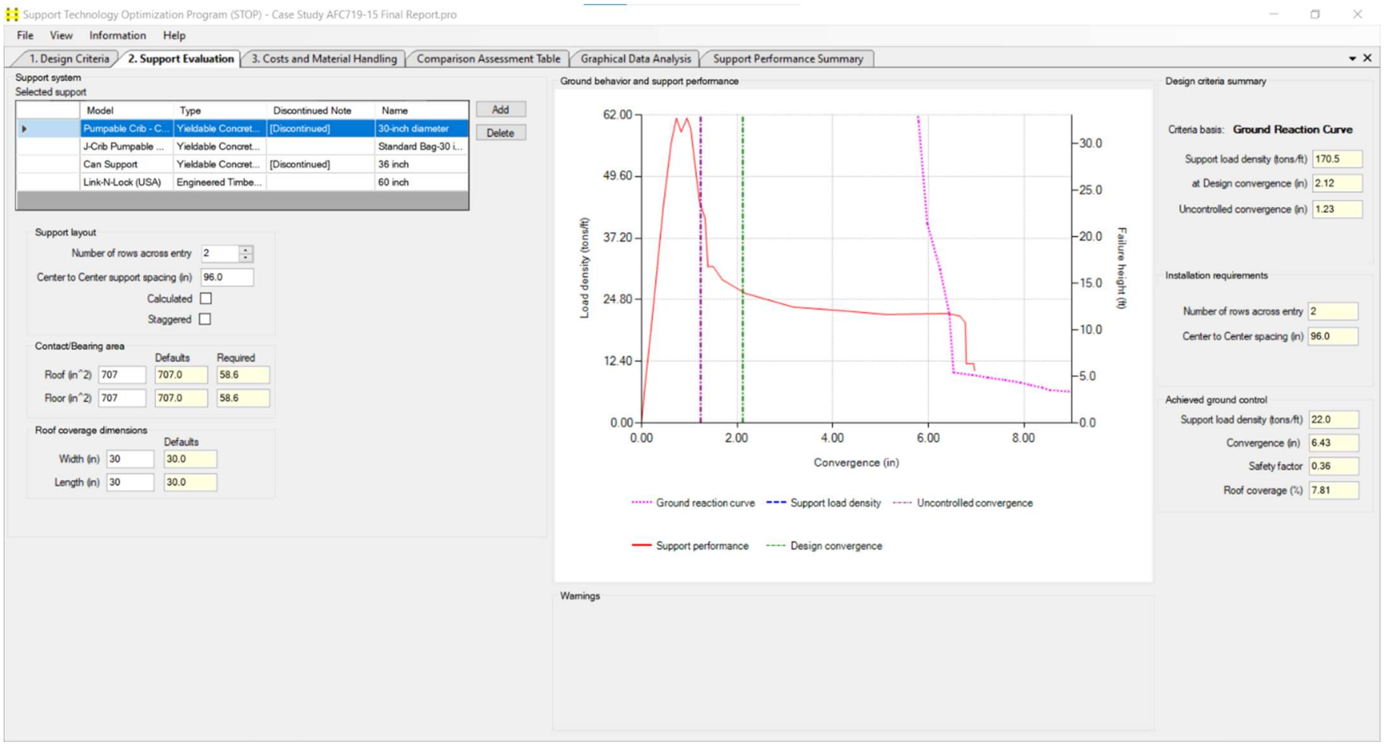

Figure 4.30. *Current pumpable support application for Example* 1 that fails to provide the necessary support load density to achieve equilibrium at the design convergence associated with the ground reaction curve.

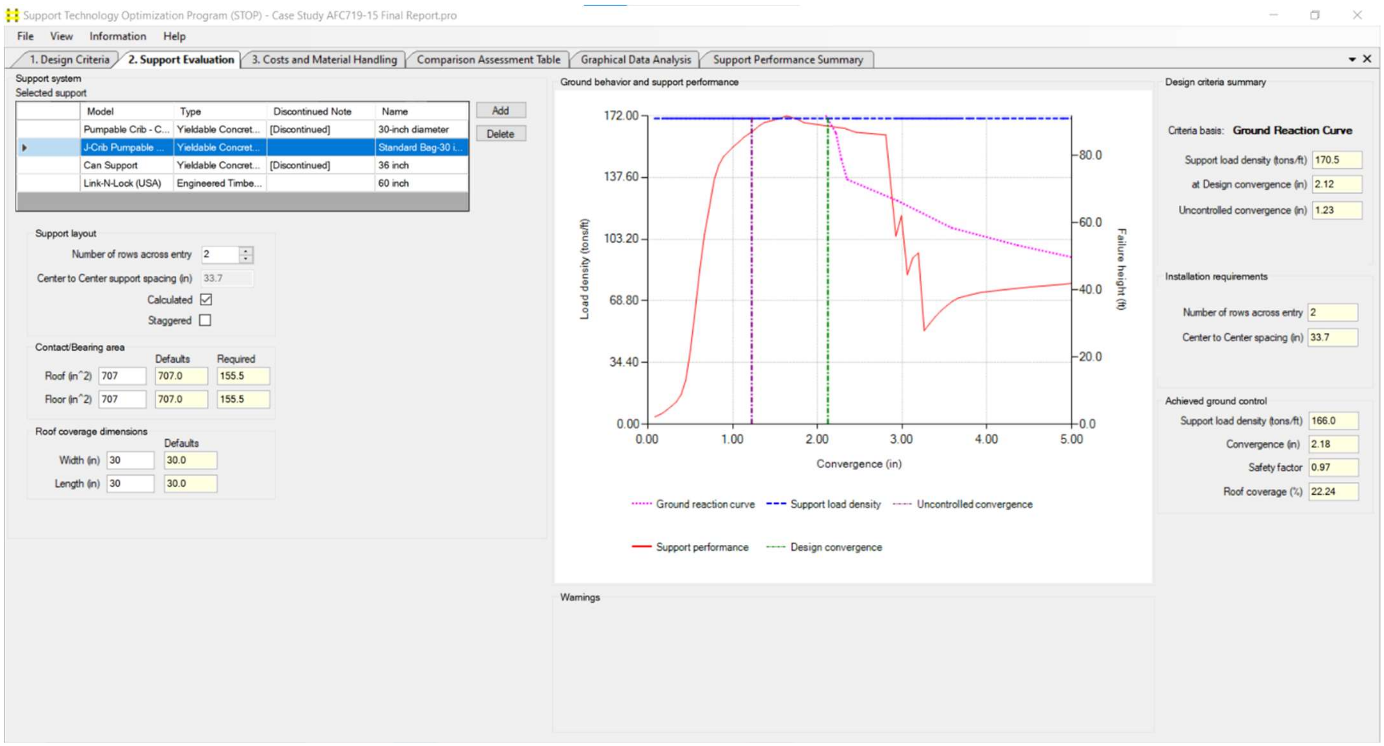

Figure 4.31. Modern pumpable support system option that can provide the necessary support load density to achieve equilibrium at the design convergence.

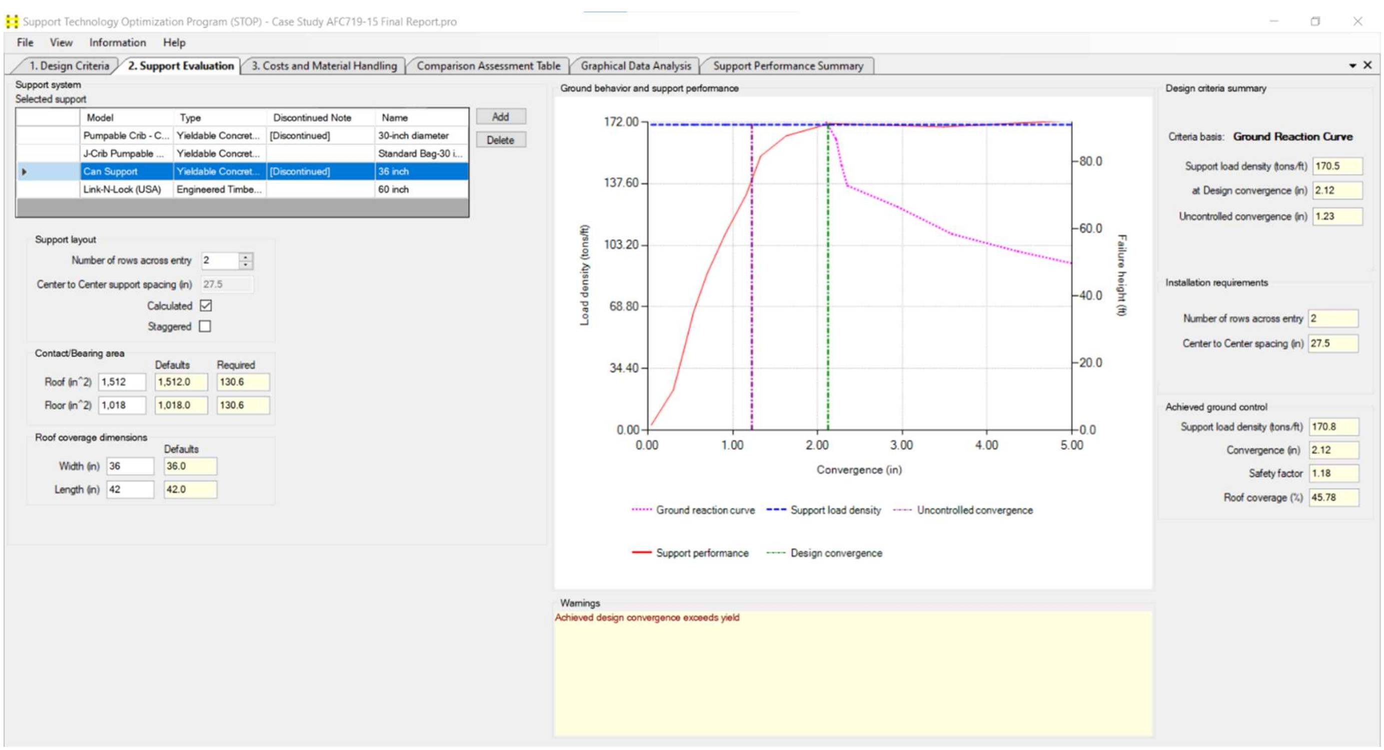

Figure 4.32. Can support application is another support option that can provide the necessary support load density to achieve equilibrium at the design convergence.

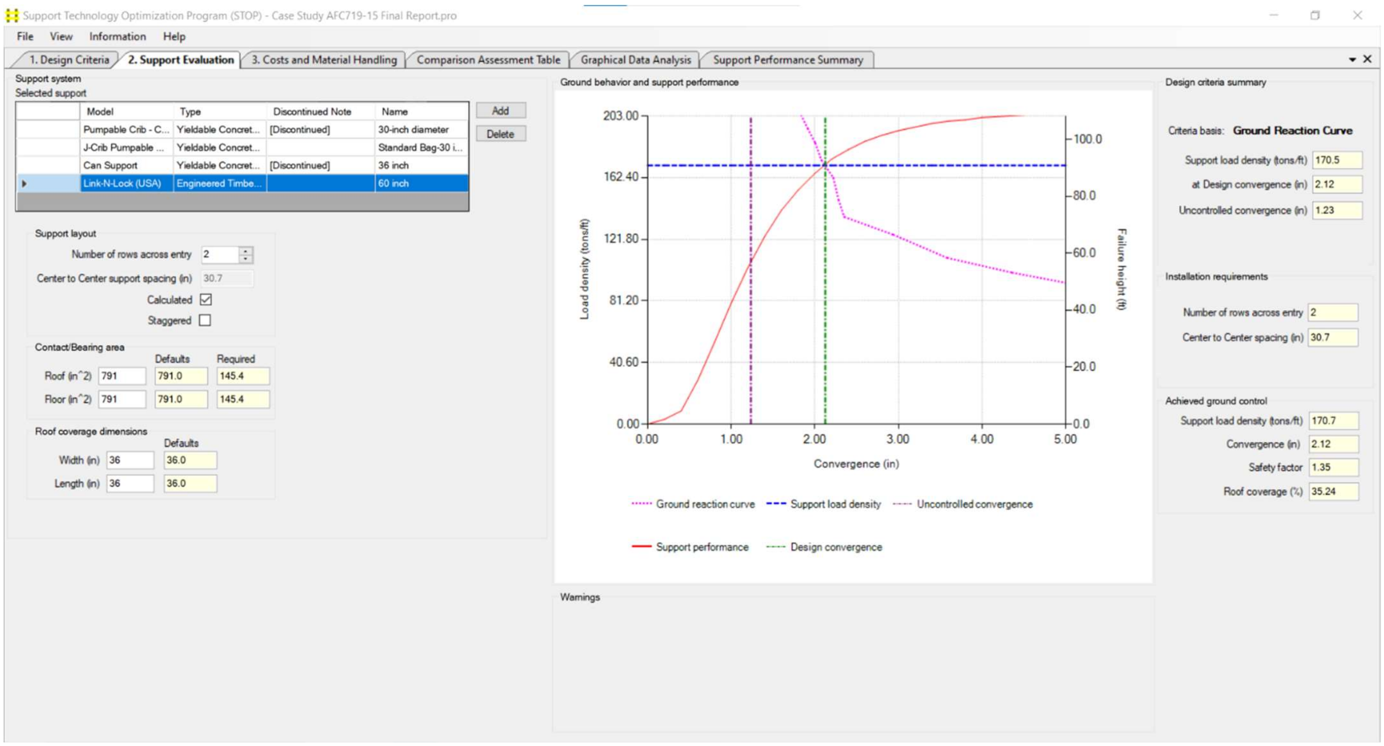

Figure 4.33. Link-N-Lock support application is another support option that can provide the necessary support load density to achieve equilibrium at the design convergence.

<u>Example 2 – The NA-3 mine</u>

The NA-3 mine is another good example of the value of the ground reaction curve in support analysis. The ground reaction curve is shown in Figure 4.34 (Table A5 in Appendix A). The most notable feature on the curve is that it is fairly linear throughout its range. This suggests that the immediate strata are remaining largely intact with relatively little separations. The design convergence is set at 1 inch which is slightly less than the convergence of the wood crib mine measurements. The uncontrollable convergence is set at 0.11 inches using the formulation for this parameter discussed in the ground reaction methodology.

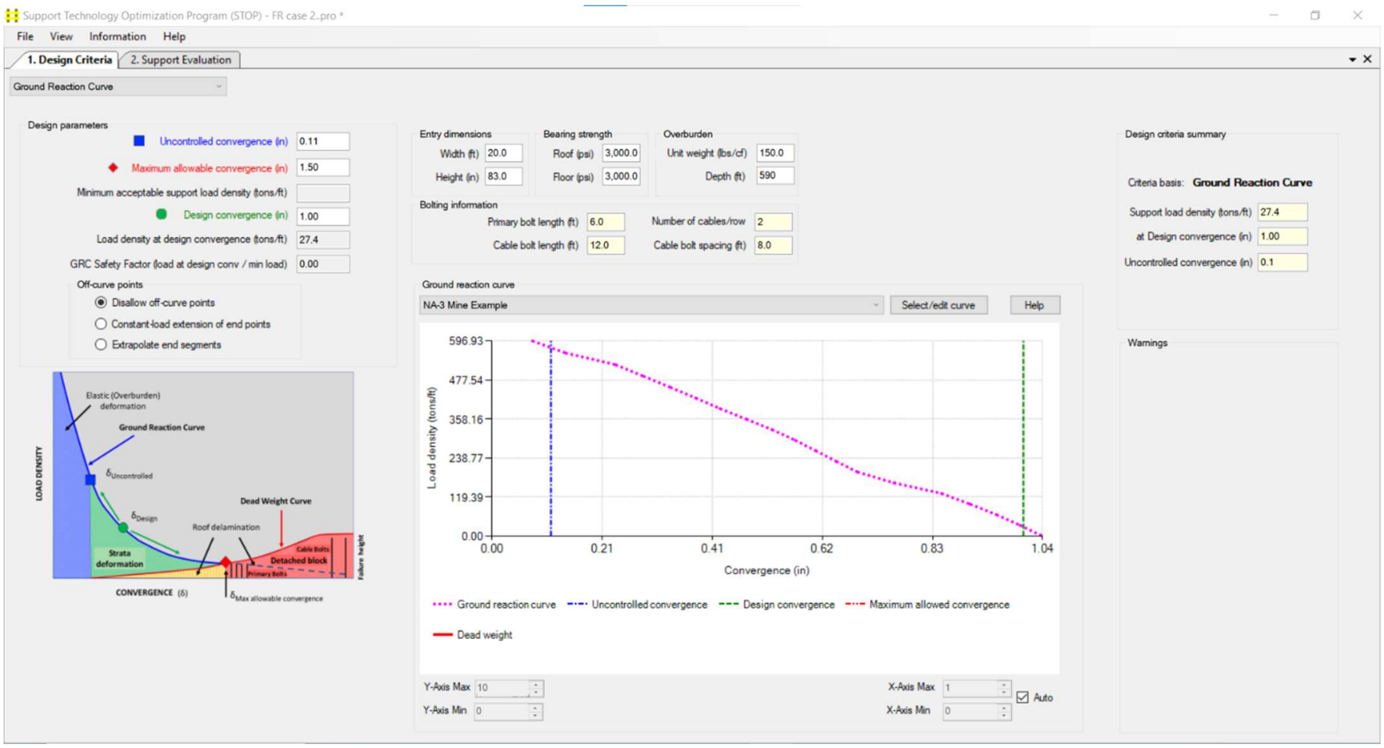

Figure 4.34. STOP ground reaction curve for Example 2 mine

As mentioned in the previous analysis, the wood crib used in the mine was constructed with poor quality timber. In order to simulate this behavior in the STOP program, the conventional wood crib material properties had to be altered (weakened). The simulated 9-point wood crib support system consisting of two rows of wood cribs on a 4 foot center-to-center spacing plotted against the ground reaction curve is shown in Figure 4.35 . The figure shows that this simulated wood crib support system used in the mine achieved a low density of 14 tons per foot at the design convergence, which closely matches the field data shown in Figure 4.15.

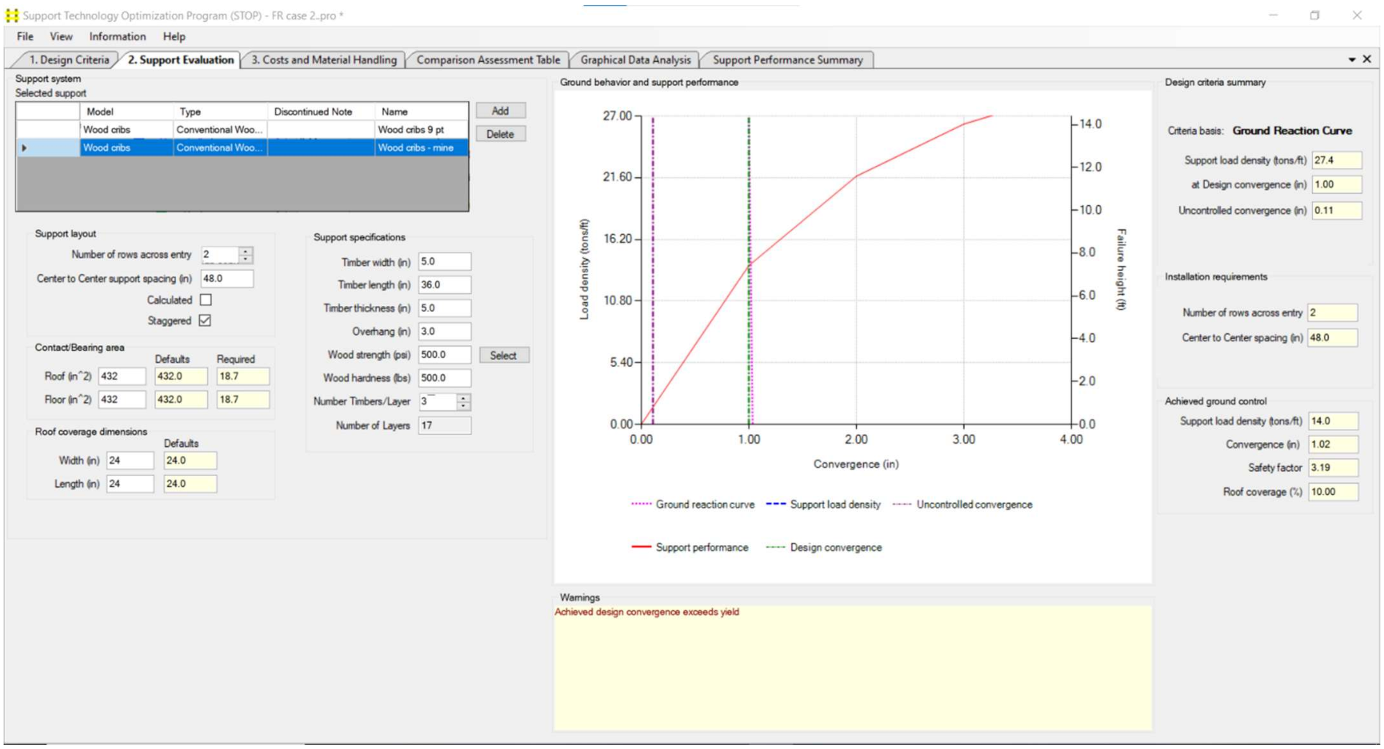

Figure 4.35. Current 9-point wood crib application for Example 2 that provides 14 tons/ft of support capacity sufficient to achieve roof control at 1.02 inches of convergence.

Figure 4.36 shows that a well-constructed nine point crib made a good quality timber would provide about twice the capacity of the mine crib. While moving up the ground reaction curve is always advantageous, the improvement in roof control would likely be minimal if the conditions remain the same, but it would provide in insurance in case the conditions worsened.

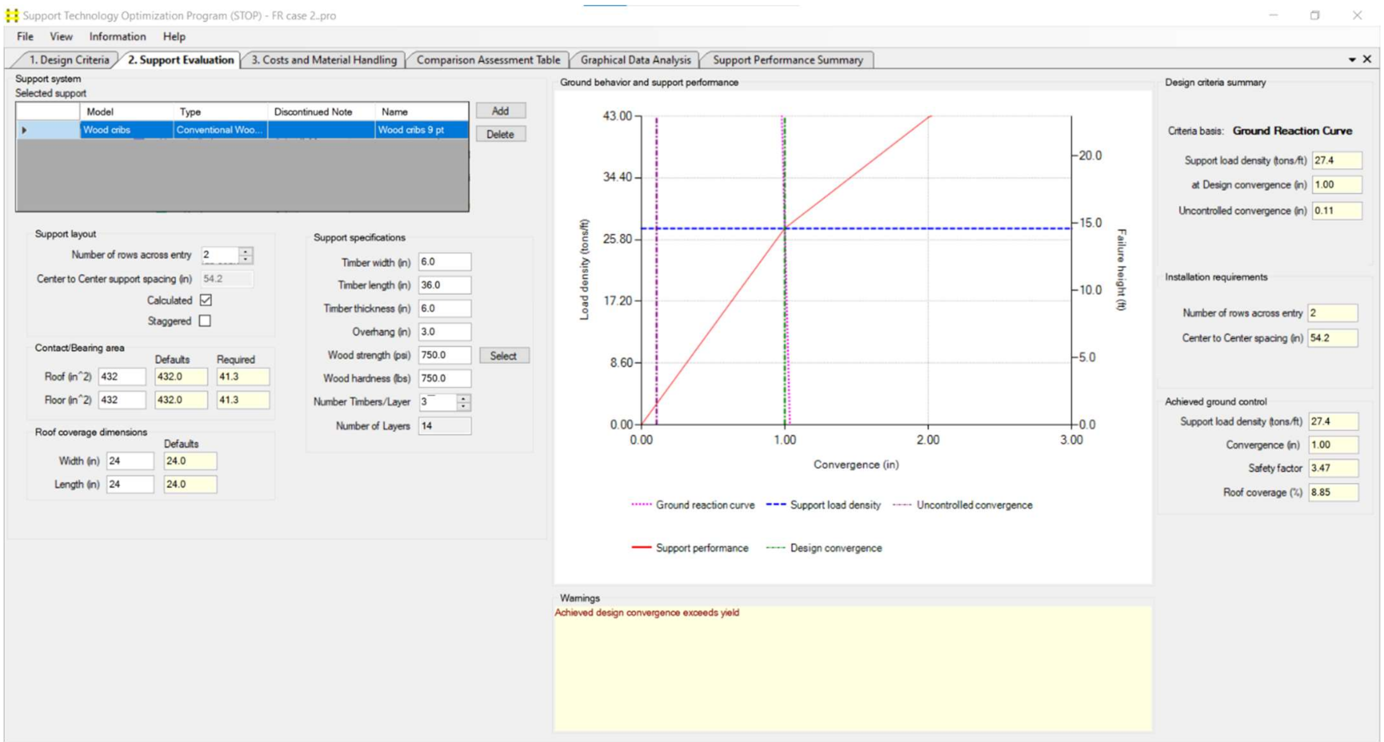

Figure 4.36. Well-constructed 9-point wood crib application made from quality timber for Example 2 that provides twice the load densisty of the mine crib.

<u>Example 3</u>

In this example, we look at the previous case study where the longwall face goes inby to create what is called an isolated condition where there is gob on one side of the entry. The ground reaction curve for this condition is shown in Figure 4.37 (Table A6 in Appendix A). It is noticed that the ground reaction curve starts out fairly linear, followed by an increase in convergence starting at 1.27 inches. Based on field observations, it is believed that the cable bolts broke at this point causing the increase in roof deformation. In order to determine the amount of support necessary to prevent this condition (i.e. cable bolt failure), the design convergence was set at 1.27 inches.

It is seen in Figure 4.38 that a double row of a modern pumpable support system on a tight spacing of approximately 30 inches could conceivably provide the necessary support to prevent the cable bolt failure. However, it is likely that the gob instability would also put this system at risk.

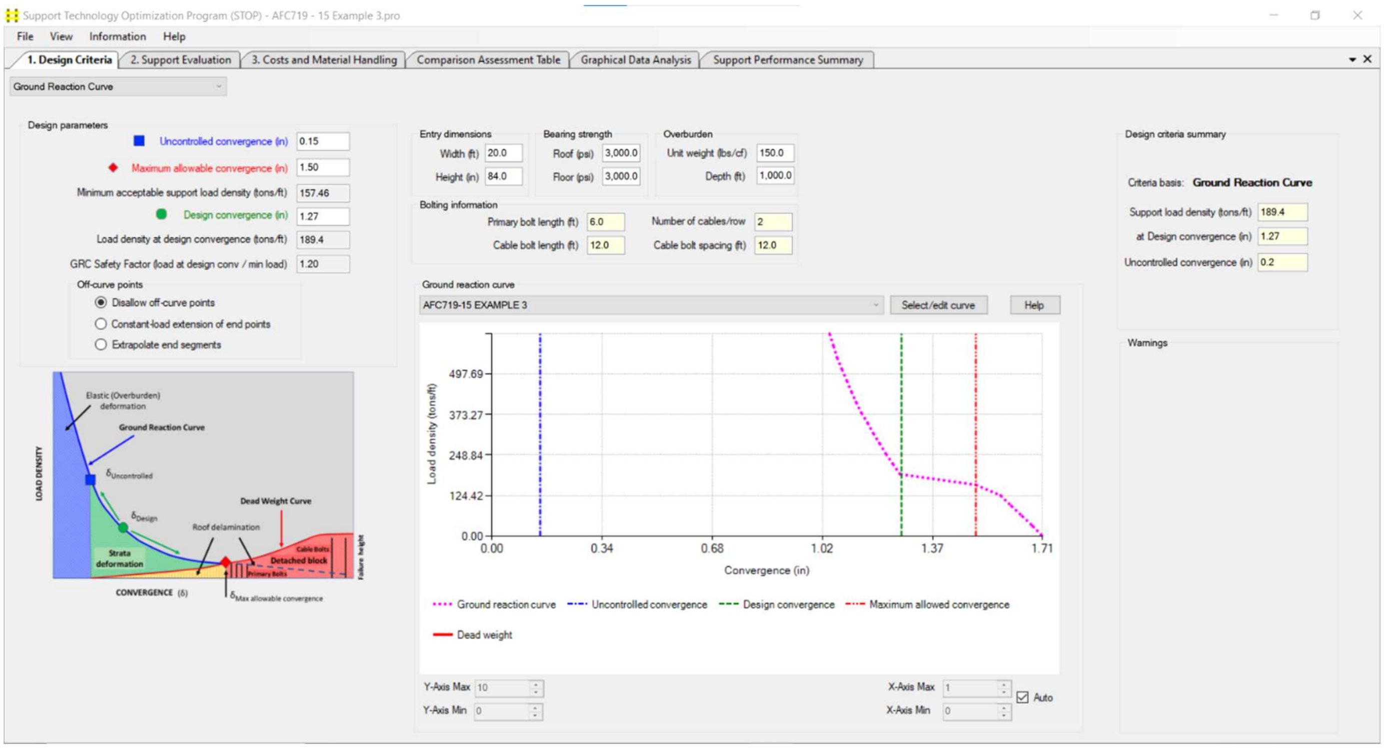

Figure 4.37. STOP ground reaction curve for Example 3 mine.

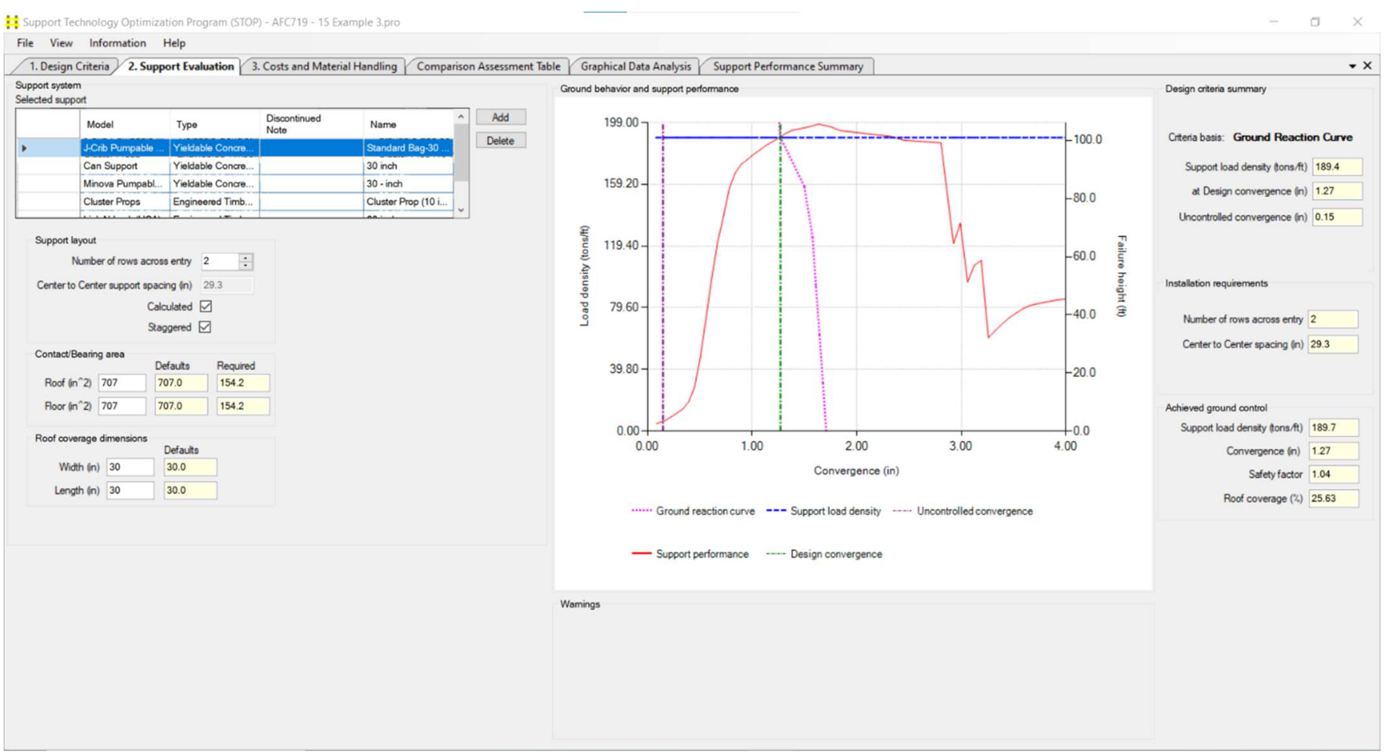

Figure 4.38. Modern pumpable support system on a tight spacing of approximately 30 inches could conceivably provide the necessary support to prevent the cable bolt failure.

STOP Disclaimer – The STOP software is currently undergoing interface updates illustrated in the report and is transitioning to a new venue. It may be unavailable on the NIOSH website during this transition.

Summary Discussion

The ground reaction curve provides a lot of insight into the roof behavior and the necessary support requirements to control it. From the examples shown, a steep linear curve suggests that the immediate roof is largely remaining intact while converging at a slow rate. For this condition, supplemental standing support will have relatively little influence on the roof deformation, provided the deformation does not increase to the point of failure above the bolted horizon. On the contrary, a nonlinear response suggests that the roof strata are separating while deforming. It is this type of ground reaction response that support will have the most impact with increasing support capacity and generally support stiffness providing improved roof control. Finally, any drastic change in the shape of the ground reaction curve can indicate failure of the primary support or failure above the bolted horizon.

5.0 Publication Record and Dissemination Efforts:

1. Tuncay, D., **Tulu, I.B.** & Zhao, H. Geology-Oriented Load Estimation Approach for Underground Coal Mines. *Mining, Metallurgy & Exploration* (2022). https://doi.org/10.1007/s42461-022-00658-1
2. Tuncay, D., **Tulu, I.B.** & Klemetti, T. Re-analysis of Abutment Angle Method for Moderate and Deep Cover Retreat Room and Pillar Mines and Investigation of Loading Mechanics Using Finite Volume Modeling. *Rock Mechanics and Rock Engineering* (2021). https://doi.org/10.1007/s00603-020-02336-4
3. Tuncay, D., **Tulu, I.B.** & Klemetti, T. Verification of 3D Numerical Modeling Approach for Longwall Mines with a Case Study Mine from the Northern Appalachian Coal Fields. *Mining, Metallurgy & Exploration 38, 447–456* (2021). https://doi.org/10.1007/s42461-020-00312-8
4. Tuncay, D., **Tulu, I.B.** & Klemetti, T. Investigating different methods used for approximating pillar loads in longwall coal mines. *International Journal of Mining Science and Technology (IJMST)*, Issue 1, January 2021. https://doi.org/10.1016/j.ijmst.2020.12.007
5. Zhao, G., **Tulu, I.B** & Peng, S. "Characteristics of Abutment Pressures and Bolt Loads in Longwall System: A Review on Stress/Load Measurements." *41st International Conference on Ground Control in Mining*, Canonsburg, PA, July, 2022.
6. Tuncay D, **Tulu I.B.** "Introduction of Hard Rock Influence Factor (HRIF) into Abutment Load Estimation for Underground Coal Mines." *40th International Conference on Ground Control in Mining*, Virtual, 2021.
7. Zhao, H., **Tulu I.B.** "Application of Local Geology Dependent Ground Reaction Curve for Evaluating Standing Support Performance in Gateroad Entries." *40th International Conference on Ground Control in Mining*, Virtual, 2021
8. Batchler, T, Tulu I.B., Zhao, H., Mathews, T. "Evaluation of Standing Supports for Longwall Tailgate Entry Using NIOSH STOP." 40th International Conference on Ground Control in Mining, Virtual, 2021.
9. D. Tuncay, I. Tulu and H. Zhao. "Geology Oriented Abutment Load Estimation Approach for Underground Coal Mines." SME Annual Conference and Expo, Salt Lake City, UT, March 01, 2022.
10. M. Ates, D. Tuncay and I. Tulu. "Implementing a Laminated Overburden Model to ALPS." SME Annual Conference and Expo, Salt Lake City, UT, March 01, 2022.
11. Tuncay, Deniz, "Geology Oriented Loading Approach for Underground Coal Mines" (2021). Graduate Theses, Dissertations, and Problem Reports. 10337.https://researchrepository.wvu.edu/etd/10337
12. Zhao, Haochen, "Development of an Entry-Scale Modeling Methodology to Provide Ground Reaction Curves for Longwall Gateroad Support Evaluation" (2022). Graduate Theses, Dissertations, and Problem Reports. 11376. https://researchrepository.wvu.edu/etd/11376

6.0 Conclusions and Impact Assessment:

The research presented here has several significant results that will undoubtedly improve the quality of the ground control design and safety of mine workers in the United States in the future, particularly for underground coal mining sector. During this research study, (i) a practical mine-specific, geology-dependent global overburden loading model, (ii) a python script program of ALPS-LAM and (iii) local geology-dependent Ground Reaction Curve (GRC) for STOP were developed.

The mine-specific, geology-dependent, global loading model was developed from back analysis of 12 case studies conducted in 11 different longwall coal mines. A total of 36 different numerical models were used for statistical analysis, to determine a way to better estimate the percentage of load carried by the gob, by including simplified geology data. To include the effect of overburden geology, a new parameter called the total strong layer thickness (t_{str}) is derived that considers the critical span (S_i) of the overburden layers together with the panel width and overburden depth. It is calculated as the sum of all layers with S_i/pw values larger than 0.1. The t_{str} parameter can then be used to estimate the gob load percentage using a statistical model for single panel configurations and for the consecutive panel mining. The new methodology was compared against the empirical estimates for the field study mines, and the new methodology was found to give closer results to the field measurements. Following the verification of the new methodology, the next step was the implementation of the new method of gob load estimation into a practical design tool. LaModel software was selected for this purpose due to its ability to model complex geometries in addition to its practicality. To check the applicability of introducing the new method into LaModel, an additional three verification field case studies were analyzed. The loads on the pillars and the adjacent coal were calculated from the LaModel results and compared to the field measurements and the new loading model was found to estimate the loads close to the measurements. Finally, the same loads were calculated using the default LaModel calibration method and it was observed that the new methodology improved the results.

The local geology-dependent Ground Reaction Curve (GRC) methodology was developed and verified by six field measurement case studies from four underground coal mines in Eastern U.S. The entry-scale model at the study sites also provided realistic approximations of the loading path of the bolt load and the ground response around the underground openings. Following the model re-evaluation section, ground response curves under various stress states were derived from model results. Then, the STOP was utilized to evaluate the performance of the installed standing support and the alternative standing support based on the applied support type and spacing. This new methodology was verified with successful and unsuccessful standing support designs from the Central Appalachian longwall mine. Results of the verification case studies demonstrated that the ground reaction curves derived from the approach detailed in this research can approximate the standing support performance within the range of the field measurements and observations.

Finally, the practical loading models, design tool and GRC approach developed during this research are immediately available to the mining industry, Mine Safety and Health Administration (MSHA), National Institute for Occupational Safety and Health (NIOSH), and State agencies to evaluate and consider for application in the ground control design process.

7.0 Recommendations for Future Work:

The following research are recommended for future work based on the findings from this research project where a practical mine-specific, geology-dependent global overburden loading model, a python script program of ALPS-LAM and local geology-dependent Ground Reaction Curve (GRC) for STOP were developed:

- A practical mine-specific, geology-dependent global overburden loading model used case studies from underground coal mines to develop the new load estimation methodology. Different longwall mines were also used for the verification of this methodology. However, the findings of this study are also applicable for retreat room-and-pillar mines where similar overburden mechanisms are involved. ARMPS software has an extensive database of case studies from room and pillar coal mines and the cases with detailed geological information can be used to further verify the new methodology. ARMPS-LAM software can also help batch-run these cases after the information about the overburden geology is introduced.
- A python script program of ALPS-LAM can be programmed as more user-friendly Windows application, like ARMPS-LAM.
- The Ground Reaction Concept in the STOP provides a mechanistic approach to standing support design by correlating the support resistance to the overall ground deformation culminating in convergence of the mine entry. The ground reaction concept can be expanded to include intrinsic support by developing a local roof conceptual model formulated by roof strata reaction curves (RSRCs) that would allow the evaluation and selection of the most effective primary and secondary roof bolt system and enhance the STOP platform to provide a unified support design tool for both standing and intrinsic support.

8.0 References:

1. Agioutantis, Z., & Karmis, M. (2017). Quick Reference Guide and Working Examples, SDPS for Windows v6.2J.
2. Barcazk, T.M., Esterhuizen, G.S., Ellenberger, J., (2008). A first step in developing standing roof support design criteria based on ground reaction data for Pittsburgh seam longwall tailgate support. In: Proceedings of the 27th International Conference on Ground Control in Mining, pp. 347 – 357.
3. Barczak, T. M. (August 2000). Optimizing Secondary Roof Support with the NIOSH Support Technology Optimization Program (STOP). In proceedings of the 19th International Conference on Ground Control in Mining, S.S. Peng et al., editors. West Virginia University, Morgantown, WV. pp:74-84.
4. Barczak, T. (2020). Support Technology Optimization Program (STOP) Help Manual. The National Institute for Occupational Safety and Health (NIOSH).Batchler, T.J., Matthews, T.J.,
5. Tulu, I.B. and Zhao, H. (August 2021). Evaluation of Standing Supports for Longwall Tailgate Entry Using NIOSH Support Technology Optimization Program (STOP). In proceedings of the 40th International Conference on Ground Control in Mining. West Virginia University, Morgantown, WV.
6. Dolinar, Dennis R. "Variation of horizontal stresses and strains in mines in bedded deposits in the eastern and midwestern United States." (2003).
7. Esterhuizen, G. S. and Barczak, T. M. (2006). Development of ground response curves for longwall tailgate support design. In Golden Rocks 2006, The 41st U.S. Symposium on Rock Mechanics (USRMS): 50 Years of Rock Mechanics — Landmarks and Future Challenges. Yale, D. P. ed., Paper 06-935, (Golden, Colorado: June 17–21, 2006) Curran Associates, Inc., p. 10 pp.
8. Esterhuizen, G., Mark, C., & Murphy, M. (2010). Numerical model calibration for simulating coal pillars, gob and overburden response. Proceedings of the 29th International Conference on Ground Control in Mining, (pp. 1-12). Morgantown WV.
9. Esterhuizen, G.S., Tulu, I.B. and Bajpayee, T.S. (June 2017). Application of a Brittle Failure Model to Assess Roof Stability in Coal Mine Entries. In proceedings of the 51st US Rock Mechanics / Geomechanics Symposium held in San Francisco, California, USA, pp: 25-28.
10. Esterhuizen, G. S., Gearhart, D. F., and Tulu, I. B. (2018). Analysis of monitored ground support and rock mass response in a longwall tailgate entry. International Journal of Mining Science and Technology, 28(1): pp: 43–51.
11. Esterhuizen, G. S., Tulu, I B., Gearhart, D F., Dougherty, H., Dyke, M. (2020). Assessing support alternatives for longwall gateroads subject to changing stress. International Journal of Mining Science and Technology. International Journal of Mining Science and Technology, Volume 31, Issue 1, Pages 103-110.
12. Esterhuizen, G.S., Klemetti, T., Sears, M.M., Zhang, P., Dyke, M.V, Dougherty, H. and Tulu, I.B. (2021). Assessing Longwall Gateroad Ground Response and Support Alternative. Mining, Metallurgy and Exploration.
13. Esterhuizen, G. S (2021). Personal communication.
14. Galvin, J. (1981). The mining of South African thick coal seams: rock mechanics and mining considerations. Ph.D. Dissertation: University of the Witwatersrand.
15. Gearhart, D. F., Tulu, I. B., and Esterhuizen, G. S. (2017). Changes in stress and displacement caused by longwall panel retreats. In Proceedings, 36th International Conference on Ground Control in Mining. Mishra, B., et al., eds. (Morgantown, WV: July 25–27, 2017) Englewood, CO: Society for Mining, Metallurgy, and Exploration, Inc., pp. 313-–320.

16. Hill, D., Stone, R., Suchowerska, A., & Trueman, R. (2015). Pillar abutment loading – New concepts for coal mining industry. Proceedings of the 15th Coal Operators' Conference (pp. 204-211). University of Wollongong: The Australasian Institute of Mining and Metallurgy and Mine Managers Association of Australia.
17. Hoek, E. and Brown, E.T. (1980). Underground Excavations in Rock. London: Institution of Mining and Metallurgy.
18. Jun, L., Ray, A., Morsy, K. and Peng, S. (2008). Effects of Rock/Coal Interface Property on Coal Pillar Strength. In proceedings: 27th International Conference on Ground Control in Mining. Morgantown, West Virginia
19. Kaiser, P. K. and Kim, B. (2008). Rock Mechanics Advances of Underground Construction and Mining. Keynote Lecture. In Proceedings of Korea Rock Mechanics Symposium., Seoul, South Korea, October 2008, Korean Society for Rock Mechanics, pp: 1-16.
20. Karmis, M., Jarosz, A., & Agioutantis, Z. (1989). Predicting subsidence with a computer. Coal, 54-61.
21. Klemetti, T., Tulu, I., & Van Dyke, M. (2018). Deep cover bleeder entry performance and support loading; a case study. International Journal of Mining Science and Technology, 85-93.
22. Klemetti, T., Van Dyke, M., Tulu, I., & Tuncay, D. (2019b). A Case Study of the Stability of a Non-typical Bleeder Entry System at a U.S. Longwall Mine. Proceedings of the 38th International Conference on Ground Control in Mining. Morgantown WV.
23. Klemetti, T., Van Dyke, M., Tulu, I., Tuncay, D., Wickline, J., & Compton, C. (2019a). Longwall Gateroad Yield Pillar Response and Model Verification - A Case Study. 53rd US Rock Mechanics/Geomechanics Symposium. New York City.
24. Luo, Y. (1989). An integrated computer model for predicting surface subsidence due to underground coal mining: "CISPM". Ph.D. Dissertation. West Virginia University.
25. Luo, Y., & Qiu, B. (2012). CISPM-MS: a Tool to Predict Surface Subsidence and to Study Interactions Associated with Multi–Seam Mining Operations. Proceedings of 31st International Conference on Ground Control in Mining.Luo and Qiu, 2012
26. Mark, C. (1987). Analysis of longwall pillar stability. PhD Dissertation: The Pennsylvania State University.
27. Mark, C. (1990). Pillar design methods for longwall mining IC 9247. U.S. Bureau of Mines.
28. Mark, C. (1992). Analysis of Longwall Pillar Stability (ALPS): an update. Proceedings of the Workshop on Coal Pillar Mechanics and Design (pp. 238-249). U.S. Bureau of Mines.
29. Mark, C. (1999). Empirical Methods For Coal Pillar Design. Proceedings of the Second International Workshop on Coal Pillar Mechanics and Design (pp. 145-154). Pittsburgh, PA: NIOSH.
30. Mark, C., Compton, C.S., Oyler, D.C. and Dolinar, D.R. (2002). Anchorage Pull Testing for Fully Grouted Roof Bolts. In proceedings of 21st International Conference on Ground Control in Mining. Morgantown, West Virginia: West Virginia University, August; pp:105-113.
31. Mark, C. (2006). The evolution of intelligent coal pillar design: 1981-2006. Proceedings of the 25th International Conference on Ground Control in Mining, (pp. 325-334).
32. Mark, C. (2010). ARMPS 2010: Pillar design for deep cover retreat mining. Proceedings of the Third International Workshop on Coal Pillar Mechanics and Design. Pittsburgh, PA: Department of Health and Human Services, Public Health Service, Centers for Disease Control and Prevention, National Institute for Occupational Safety and Health (NIOSH).
33. Mark, C., & Agioutantis, Z. (2019). Analysis of Coal Pillar Stability (ACPS): A New Generation of Pillar Design Software. International Journal of Mining Science and Technology, 29(1), 87-91.

34. Mark, C., and Agioutantis, Z.G. (2020). Analysis of Mine Roof Support (AMRS) for US coal Mines. Mining Metallurgy & Exploration. DOI: 10.1007/s42461-020-00301-x.
35. MSHA. (2020a). Mine Data Retreival System. Retrieved from https://www.msha.gov/mine-data-retriecal-system
36. MSHA. (2020b, March). Accident Injuries Data Set. Retrieved from https://arlweb.msha.gov/OpenGovernmentData/OGIMSHA.asp
37. Peng, S. (2008). Coal Mine Ground Control (3rd Ed.). Morgantown: Department of Mining Engineering, West Virginia University.
38. Serbousek, M.O. and Signer, S.P. (1987). Linear Load-Transfer Mechanics of Fully Grouted Roof Bolts. Report of Investigations 9135.
39. Salamon, M., Oravecz, K., & Hardman, D. (1972). Rock mechanics problems associated with longwall trials in South Africa. Proceedings of 5th International Strata Control Conference, (pp. 1-21).
40. Sears, M., Esterhuizen, G. S., and Tulu, I. 2019. Overview of current US longwall gateroad support practices: An update. Mining Metallurgy & Exploration, 36(6): 1137–1144, https://doi.org/10.1007/s42461-019-0077-3.
41. Su, D. W. H. (1991). Finite element modeling of subsidence induced by underground coal mining: The influence of material nonlinearity and shearing along existing planes of weakness. In Proceedings: 10th International Conference on Ground Control in Mining. Peng, S. S. ed., (Morgantown, WV: June 10–12, 1991) Morgantown, WV: West Virginia University, pp. 287–300.
42. Tadolini, S.C. (August 2012). The Next Generation of Cable Bolts for Improved Ground Support. In proceedings of 31st International Conference on Ground Control in Mining. Morgantown, West Virginia: West Virginia University,
43. Tulu, I. B., Esterhuizen, G.S., Heasly, K.A. (2012). Calibration of FLAC3D to Simulate the Shear Resistance of Fully Grounted Rock Bolts. 46th US Rock Mechanics / Geomechanics Symposium held in Chicago, IL, USA, 24-27 June 2012.
44. Tulu, I., & Heasley, K. (2012). Investigating abutment load. Proceedings of the 31st International Conference on Ground Control in Mining, (pp. 28-37). Morgantown, WV.
45. Tulu, I., Esterhuizen, G., Gearhart, D., Klemetti, T., Mohamed, K., & Su, D. (2018). Analysis of global and local stress changes in a longwall gateroad. International Journal of Mining Science and Technology, 127-135.
46. Tulu, I., Esterhuizen, G., Mohamed, K., & Klemetti, T. (2017). Verification of a calibrated longwall model with field measurements. Proceedings of the 51st US Rock Mechanics / Geomechanics Symposium. San Francisco, CA.Tuncay et al. (2021, 2022)
47. Tuncay, D., Tulu, I., & Klemetti, T. (2020). Analysis of ARMPS2010 database with LaModel and an updated abutment angle equation. International Journal of Mining Science and Technology, 111-118.
48. Tuncay, Deniz, "Geology Oriented Loading Approach for Underground Coal Mines" (2021). Graduate Theses, Dissertations, and Problem Reports. 10337. https://researchrepository.wvu.edu/etd/10337
49. Tuncay, D., Tulu, I.B. & Zhao, H. Geology-Oriented Load Estimation Approach for Underground Coal Mines. Mining, Metallurgy & Exploration (2022). https://doi.org/10.1007/s42461-022-00658-1
50. Tuncay, D., Tulu, I.B. & Klemetti, T. Re-analysis of Abutment Angle Method for Moderate and Deep Cover Retreat Room and Pillar Mines and Investigation of Loading Mechanics Using Finite Volume Modeling. Rock Mechanics and Rock Engineering (2021). https://doi.org/10.1007/s00603-020-02336-4

51. Tuncay, D., Tulu, I.B. & Klemetti, T. Verification of 3D Numerical Modeling Approach for Longwall Mines with a Case Study Mine from the Northern Appalachian Coal Fields. Mining, Metallurgy & Exploration 38, 447–456 (2021). https://doi.org/10.1007/s42461-020-00312-8
52. Tuncay, D., Tulu, I.B. & Klemetti, T. Investigating different methods used for approximating pillar loads in longwall coal mines. International Journal of Mining Science and Technology (IJMST), Issue 1, January 2021. https://doi.org/10.1016/j.ijmst.2020.12.007
53. Van Dyke, M., Klemetti, T., Tulu, I., & Tuncay, D. (2020). Moderate cover bleeder entry and standing support performance in a longwall mine: a case study. Proceedings of 2020 SME annual meeting and exhibit. Phoenix, AZ: Society for Mining, Metallurgy, and Exploration.Van Dyke et al., 2021.\
54. Zhao, Haochen, "Development of an Entry-Scale Modeling Methodology to Provide Ground Reaction Curves for Longwall Gateroad Support Evaluation" (2022). Graduate Theses, Dissertations, and Problem Reports. 11376. https://researchrepository.wvu.edu/etd/11376

9.0 Appendix

Table A.1. *Material properties of roof rock mass at study area in NA-3 coal mine, loosely correlated top-down (after Esterhuizen et al., 2017 & Esterhuizen et al., 2018).*

Rock type	**Uniaxial compressive strength (MPa)**	**Elastic modulus (GPa)**	**Poisson's ratio**	**Internal Friction Angle (°)**	**Residual Friction Angle (°)**	**Strength anisotropy ratio**
Dark gray shale	85.3	16.7	0.15	24.00	56.00	N/A
Black shale	22.7	N/A	N/A	N/A	N/A	N/A
Shaley sandstone	144	40.8	0.25	19.20	40.5	0.8
Gray clay shale	80.8	15.5	0.26	N/A	34.4	0.4
Limestone	265	78.6	0.3	33.10	N/A	0.9
Claystone (calcareous nodulus)	103.6	22.3	0.14	18.10	42.4	0.4
Clay shale	43.8	14.1	0.22	31	39.3	0.2
Carbonaceous shale	23	6.9	N/A	25	N/A	0.1
Gray silty shale	58.5	10.8	0.21	26.40	35.2	N/A
Coalbed being mined	N/A	N/A	N/A	N/A	N/A	N/A
Dark-gray shale with coal streaks	59.0	9.4	0.28	7.65	54.7	N/A
Dark-gray shale with sandstone streaks	60.7	16.0	0.14	14.30	41.4	N/A

Table A.2. *Key material properties of rock mass at CA-1 mine (Esterhuizen et al., 2018)*

Rock type	**Uniaxial compressive strength (MPa)**	**Elastic modulus (MPa)**	**Friction angle (°)**	**Strength anisotropy ratio**
Strong sandstone	145	35.9	38	1.0
Laminated sandstone	117	29.0	35	0.7
Dark gray shale (slickensides)	69	16.6	28	0.2
Gray shale	83	20.0	25	0.4
Sandy fireclay	50	12.4	28	0.8

Table A.3. *Immediate roof/floor rock mass condition at verification case 1 (After Esterhuizen et al., 2017 &Klemetti et al., 2017).*

Rock type	**Thickness (m)**
Sandstone 2	10
Shale parting	1
Sandstone-dark, thickly bedded, fine grain, few mic (Sandstone 1)	5.5
Laminated Standstone	0.3
Shale-light, silty, thinly bedded	1.1
Shale-dark, silty, plant, fossils, thinly bedded	0.34
Bleeder entry	

Fireclay	0.5
Dark gray shale	2
Unnamed sandstone	5

Table A.4. *Roof and floor rock mass condition (after, Batcher et al., 2021).*

Roof rock		**Floor rock**	
Rock type	**Thickness (m)**	**Rock type**	**Thickness(m)**
Sandstone-Strong	4.89	*Shale Gray*	1.96
Laminated Sandstone	1.71	*Shale Gray*	1.96
Dark Grey shale	0.98	*Shale Gray*	4.89
Dark Grey shale	0.98	*Sandstone-Strong*	9.78
Dark Grey shale	0.98		

Table A.4. *GRC input for STOP program application - Example 1.*

Load (Tons/ft)	Convergence (inch)	Load (Tons/ft)	Convergence (inch)	Load (Tons/ft)	Convergence (inch)
729.94	0.00	174.01	2.08	4.06	10.21
716.16	0.05	162.36	2.22	3.55	10.40
698.41	0.06	147.92	2.28	3.04	10.58
677.80	0.07	136.55	2.35	2.54	10.81
660.44	0.08	124.84	2.94	2.03	10.98
635.49	0.09	109.59	3.58	1.52	11.17
611.19	0.10	99.83	4.36	1.01	11.42
584.75	0.11	90.17	5.28	0.51	11.68
559.23	0.12	78.59	5.57	0.00	11.98
532.47	0.14	69.63	5.67		
506.00	0.20	60.62	5.79		
481.10	0.24	40.12	5.97		
457.54	0.28	30.94	6.24		
426.64	0.48	21.84	6.44		
399.22	0.70	10.15	6.52		
373.64	0.76	10.15	6.52		
347.82	0.80	9.64	6.91		
323.25	0.83	9.13	7.23		
291.59	0.91	8.63	7.60		
262.98	1.03	8.12	7.92		
236.21	1.23	7.61	8.13		
236.21	1.23	7.10	8.37		
226.95	1.35	6.60	8.54		
215.74	1.48	6.09	9.27		
206.04	1.81	5.58	9.52		
195.01	1.91	5.07	9.70		
185.24	2.00	4.57	9.91		

Table A.5. *GRC input for STOP program application - Example 2.*

Load (Tons/ft)	Convergence (inch)
668.21	0.00
636.42	0.04
596.93	0.08
560.20	0.14
524.10	0.23
489.18	0.28
455.17	0.33
422.54	0.38
390.00	0.43
357.84	0.48
325.87	0.53
293.40	0.57
261.57	0.61
228.81	0.65
196.18	0.69
162.89	0.76
130.62	0.84
97.71	0.90
65.65	0.95
33.46	0.99
0.00	1.04

Table A.6. *GRC input for STOP program application - Example 3.*

Load (Tons/ft)	Convergence (inch)
654.46	1.04
622.11	1.05
584.18	1.06
548.28	1.07
512.62	1.08
477.86	1.10
443.87	1.11
411.92	1.13
378.96	1.15
348.37	1.16
316.29	1.18
285.86	1.20
253.25	1.22
222.38	1.24
189.98	1.27

157.73	1.50
125.16	1.58
93.22	1.61
62.12	1.64
30.98	1.68
0.00	1.71